Final Report 1998-18

MINNESOTA DEPARTMENT OF TRANSPORTATION

PaveCool

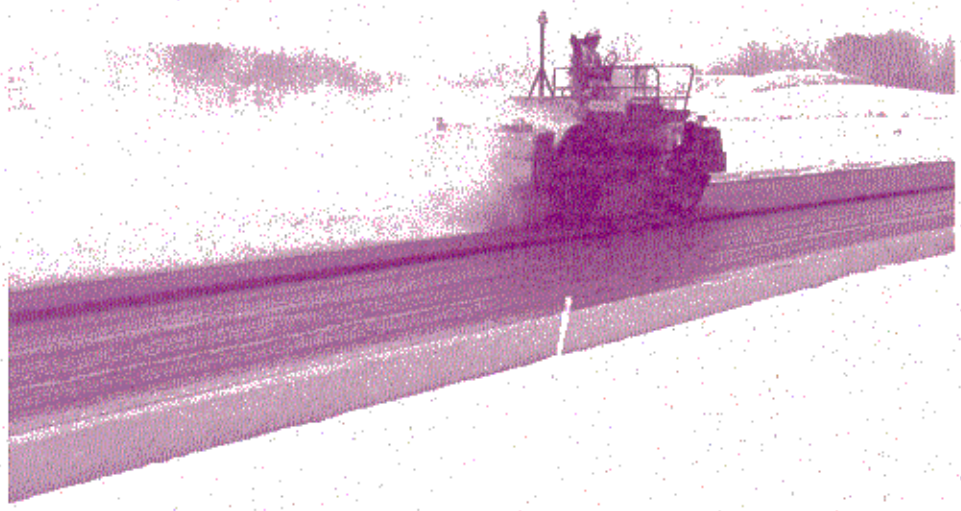

An Asphalt Paving Tool For Adverse Conditions

Download PaveCool software:

http://www.dot.state.mn.us/app/pavecool

Technical Report Documentation Page

1. Report No.	2.	3. Recipient's Accession No.
MN/RC - 1998- 18		

4. Title and Subtitle	5. Report Date
AN ASPHALT PAVING TOOL FOR ADVERSE CONDITIONS	June 1998
	6.

7. Author(s)	8. Performing Organization Report No.
Bruce A. Chadboum, Rachel A. DeSombre, David E. Newcomb, James A. Luoma, Vaughan R. Voller, David H. Timm	

9. Performing Organization Name and Address	10. Project/Task/Work Unit No.
University of Minnesota Department of Civil Engineering 500 Pillsbury Drive, S.E. Minneapolis, Minnesota 55455-0116	11. Contract (C) or Grant (G) No. (C) 72632 TOC # 165

12. Sponsoring Organization Name and Address	13. Type of Report and Period Covered
Minnesota Department of Transportation 395 John Ireland Boulevard Mail Stop 330 St. Paul, Minnesota 55155	Final Report - 1995 to 1998
	14. Sponsoring Agency Code

15. Supplementary Notes

16. Abstract (Limit: 200 words)

Poor compaction can lead to early deterioration of an asphalt pavement. It often happens when paving occurs during adverse weather conditions. Yet, in Minnesota, paving must often occur under adverse conditions.

A new tool now simulates the cooling of an asphalt mat behind the paver under a variety of environmental conditions. The software, PaveCool Version 2.0, offers users insights into how adverse climate conditions will affect their ability to produce a durable, quality road surface. Users input the type of existing surface, type of asphalt mix, and weather conditions. The output shows a cooling curve with recommended compaction starting and stopping times. Field tests confirm the value of this program as an aid to cold weather paving. A Windows program, PaveCool 2.0 runs on laptop computers (Windows 95,98, or NT required).

This report documents the study of thermal properties and compactibility of hot-mix asphalt, related laboratory tests on the thermal diffusivity and thermal conductivity of hot-mix asphalt at typical compaction temperatures, a literature review, and testing results. It also includes a copy of the PaveCool Version 2.0 software.

17. Document Analysis/Descriptors	18. Availability Statement
asphalt paving, cold weather construction, bituminous paving, asphalt compaction	No restrictions. Document available from: National Technical Information Services, Springfield, Virginia 22 16 1

19. Security Class (this report)	20. Security Class (this page)	21. No. of Pages	22. Price
Unclassified	Unclassified	145	

AN ASPHALT PAVING TOOL FOR ADVERSE CONDITIONS

Final Report

Prepared by:

Bruce A. Chadbourn
David E. Newcomb
Vaughan R. Voller
Rachel A. De Sombre
James A. Luoma
David H. Timm

University of Minnesota
Department of Civil Engineering
500 Pillsbury Dr. SE
Minneapolis, MN 55455-0116

June 1998

Prepared for

Minnesota Department of Transportation

TABLE OF CONTENTS

LIST OF TABLES

LIST OF FIGURES

EXECUTIVE SUMMARY

The problems associated with asphalt paving during cold weather conditions are well known and the practice is avoided when possible. However, paving during adverse weather conditions is often necessary, especially in northern regions. In order to minimize the uncertainty associated with cold weather paving, a study was undertaken to evaluate the thermal properties and compactibility of hot-mix asphalt. Laboratory tests were performed to determine the thermal diffusivity and thermal conductivity of hot-mix asphalt at typical compaction temperatures. A gyratory compactor capable of measuring shear stress in the sample during compaction was used to analyze the compaction characteristics of various mixtures.

A computer program was developed to simulate the cooling of an asphalt mat behind the paver under a variety of environmental conditions. An extensive literature review was conducted to determine the thermal properties of various paving materials and identify appropriate thermal testing procedures for hot-mix asphalt. Methods of estimating the contribution of solar energy and wind to the pavement cooling problem were located. Thermal diffusivity and thermal conductivity tests were adapted to suit the needs of this study. The results of compaction studies provided recommended starting compaction temperatures based on binder grade.

This information was incorporated into a Windows program that can be run on laptop computers in the field. Inputs include the type of existing surface, type of asphalt mix, and various environmental conditions that are easily measured or obtained from local weather reports. The output is a graphical display showing a cooling curve with recommended compaction starting and stopping times.

The field verification portion of this study consisted of temperature measurements taken from a variety of paving projects over a period of three years. The results have confirmed the value of this program as an aid to cold weather paving.

CHAPTER 1
INTRODUCTION

BACKGROUND

The quality of asphalt concrete pavement layers constructed during the mid to late fall of the year is of great concern in northern tier states. As ambient temperatures steadily decrease, the uncertainties surrounding the performance of such structures increase. This is because time constraints on the mixing, transport, laydown and compaction of the asphalt mixture become more critical. Any condition leading to a cooling of the material below the proper compaction temperature prior to the completion of rolling may result in an under-densified pavement layer. Such material may exhibit:

1. Increased susceptibility to fatigue and thermal cracking due low tensile strength
2. Rutting due to consolidation
3. Raveling on the pavement surface
4. Sensitivity to moisture

In an effort to avoid these types of distress from occurring prematurely, most northern agencies have placed limitations on asphalt paving when ambient temperatures are not favorable for achieving the desired level of compaction.

There are numerous reasons for asphalt paving to take place under less-than-desirable conditions. The letting and awarding of construction contracts may have been delayed for administrative and fiscal purposes, or construction may have been delayed due to inclement weather, scheduling or contract problems. The owner of the pavement facility may not be willing to wait for the next construction season to place the asphalt concrete layers in order to have a finished surface for winter use, or so that the pavement will withstand the next thaw weakening period.

Regardless of the reason, agencies and contractors are frequently faced with this problem and the results of having an under-compacted asphalt pavement in service can be cost-prohibitive. For agencies, the consequences of premature pavement distress include increased maintenance costs and incurring rehabilitation costs before planned. Contractors face the prospect of payment

penalties for low density in the short term as well as reduced competitiveness with other types of pavement surfacing in the long term. The whole industry suffers diminished public opinion when maintenance and rehabilitation occur more frequently than what is considered reasonable by the public. In the end, the costs associated with traffic delays during maintenance and rehabilitation are borne by motorists.

Given that late-season asphalt paving cannot be completely avoided, the issue is whether the construction process might be improved to avoid problems associated with low in-place hot mix asphalt density. One approach to this improvement is providing construction personnel with information to help them make decisions concerning the timing and condition of construction operations. With this in mind, a computer tool was conceived which would allow agency inspectors, paving supervisors and other interested parties to use simple input concerning weather conditions, mixture type and temperature, and paving lift thickness to compute the time window for beginning and finishing hot mix compaction.

OBJECTIVES

The purpose of the research was to develop a computational tool to aid in identifying possible strategies for placing asphalt concrete under adverse conditions. Particular emphasis was placed on strategies for late fall or night paving, when cool temperatures shorten the time available for compaction of the lifts.

SCOPE

This project entailed a combination of model development, laboratory experiments, field verifications and computer tool refinement. Specifically, the following were accomplished:

1. Initial Model Development – A one-dimensional heat-flow model was constructed to compute the rate of cooling for the asphalt layer. This model accounted for atmospheric conditions, the temperature and thickness of the material being placed and the type and condition of the layer which is underneath the paving.
2. Laboratory Thermal Properties – An experimental program was executed to measure the thermal properties (conductivity and diffusivity) of asphalt concrete. Special

innovation was required to prepare samples and test the materials. Of particular interest was the change in the thermal properties with the change in temperature.

3. Laboratory Compaction Properties – The compaction characteristics of asphalt mixtures were assessed using a gyratory compactor. In this program, the power to compact samples and the shear force generated during compaction were measured. It was possible to identify an effective range of compaction temperature as well as relate the grade of asphalt binder to the temperature at which compaction should start.
4. Field Verification – The rate of cooling in several field projects was monitored and compared to the predicted rate of cooling calculated by the model. This comparison validated the model and provided a correlation to the laboratory compaction data for suggesting starting and ending times for field compaction.
5. Final Refinement – The computer tool was configured to maximize its ease of use. The input screen is the same as the output screen. The calculation time is very fast, and there are a variety of advisory screens that appear when the appropriate conditions exist. The help file contains the users manual, and it is indexed for convenience.

CHAPTER 2
LITERATURE REVIEW

COMPACTION OF HOT-MIX ASPHALT PAVEMENT

The compaction process has a great effect on the strength and durability of hot-mix asphalt pavement. The main objective of pavement compaction is to achieve an optimum compacted density. This helps to ensure that the pavement will have the necessary bearing capacity to support the expected traffic loads and durability to withstand weathering.

Mechanics of Compaction

Most of the work in the compaction of particles has been done in geotechnical engineering, and soil compaction can be examined to illustrate some of the basic principles of asphalt mixture compaction. The addition of asphalt binder, a viscoelastic, temperature dependent material, to a granular soil complicates the problem.

Sowers and Sowers [1] described three means of soil or particle densification:

1. Reorientation of particles
2. Fracture of the grains or bonds between particles
3. Bending or distortion of particles and their adsorbed layers

Densification of cohesive materials is accomplished through the distortion and reorientation of the particles. The cohesion of the material resists the rearrangement of the particles. In soils, increasing the water content reduces the cohesion between the particles resulting in easier compaction.

According to Sowers and Sowers [1], cohesionless materials such as crushed rock are densified primarily through reorientation of the aggregate and particle fracture at points of contact. It is friction which resists the reorientation of the particles, and increasing angularity leads to increased internal friction and more difficulty in compaction. Moisture content of cohesionless soils also plays a part in the compaction. As moisture content increases, the friction between

particles decreases, reducing the capillary tension between particles, making the soil easier to compact.

The cohesion and internal friction both influence the shear strength of the soil. This shear strength must be overcome in order to compact the material. Figure 2.1 shows the parameters influencing the strength of a material, and Coulomb's equation is used to define shear stress:

$$\tau = c + \sigma \tan \phi \tag{2.1}$$

Where:

τ = shear stress

c = cohesion

σ = confining pressure

ϕ = angle of internal friction

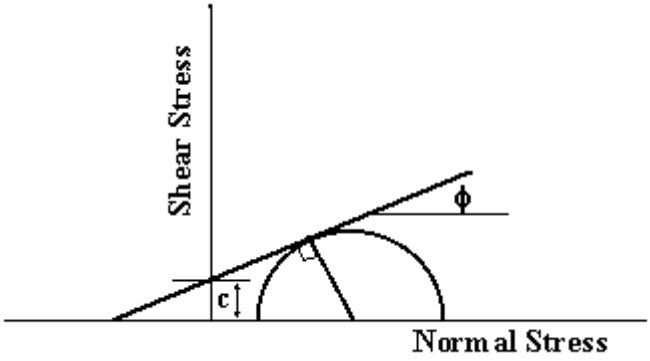

Figure 2.1 Mohr's Circle

Compaction of Asphalt Mixtures

The compaction of an asphalt mixture can be considered to behave somewhere between a cohesive and non-cohesive soil. Kari [2] defined it as "a process where the mix under compaction changes from a loose, plastic, non-cohesive state into a coherent mass possessing a high degree of tensile strength." Asphalt compaction occurs through distortion and reorientation much like a cohesive soil. As the binder viscosity decreases, cohesion decreases making the mixture easier to compact. Asphalt mixtures also behave like non-cohesive soils in that the reorientation of the particles is resisted by friction between aggregate particles. Mixtures that contain less angular aggregate are easier to compact than mixtures with very angular aggregate.

Given that asphalt mixtures behave in the same fashion as soils do, Coulomb's equation can be used to indicate the amount of shear strength in an asphalt mixture. Schmidt et al. [3] stated that the cohesion of the mix is influenced by the amount of binder and filler used, the temperature of the mix, and the nature of the asphalt. The angle of internal friction is influenced by aggregate properties and by the temperature and asphalt content of the mixture. When the cohesion and angle of internal friction are minimized, the shear stress is minimized, and the asphalt mixture can be adequately compacted with a minimum amount of effort.

In the field, the compaction of hot mix asphalt is accomplished through the use of rollers. Kari [2], described field compaction of hot mix asphalt as "a dynamic situation under a moving roller" (Figure 2.2). The compactor wheels sink far enough into the hot mixture until the contact area of the wheel is large enough to reduce the pressure to the bearing capacity of the asphalt. Forward motion of the roller creates shear movement of the aggregate causing a zone of minor decompaction in back of the roller, a zone of major decompaction in front of the roller, and compaction directly underneath the roller wheel.

Regardless of material quality, an inadequate pavement will result if the proper degree of compaction is not attained.

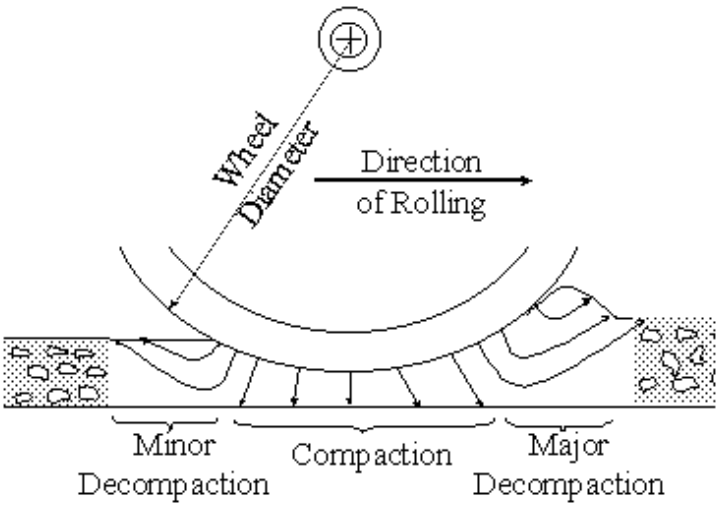

Figure 2.2 Compaction Process (After Kari [2])

Workability of Hot-Mix Asphalt

Cabrera [4] defined workability of hot-mix asphalt as "the property which allows the production, handling, placing, and compaction of a mix with minimum application of energy." Workability has two components: Spreadability (the ability of a loose mix to be spread evenly over the road surface) and compactibility (the ability of the mixture to be compressed into a compact mass).

Kari [2] discussed two conditions in which compaction becomes difficult. These conditions are described as "overstressed" and "understressed". An overstressed mix has low stability and does not support the weight of the roller. The hot mix asphalt will spread out laterally from the roller or crack with further rolling. There is no effective increase in density of the mix. An asphalt mixture can also be understressed during rolling when the mix is too stable or the roller is not heavy enough to allow the roller wheels to sink far enough into the hot mixture to create the shear forces essential for compaction. In this case, the roller rides on top of the mat and does not provide a reduction in air voids. The optimal point between the overstressed and understressed conditions varies with workability of the mix, the type of roller, and the number of passes.

The workability of asphalt hot-mix is influenced by the type of aggregate, the grade and percentage of asphalt binder, and the temperature of the mix.. Filler content also plays a role in the compactibility of hot-mix asphalt. There is an optimum level of binder cohesion (determined by the filler-to-asphalt volume ratio) for maximum compaction.

Aggregate Effects

The shape, size, texture, porosity, and gradation of the aggregate all have an effect on the compactibility of asphalt mixtures. A dense-graded mix with small, round particles is more easily compacted than an open-graded mix with large, angular particles. A high-porosity aggregate absorbs more binder than a low-porosity aggregate, causing the mix to be stiffer and more difficult to compact.

The Effect of Binder Viscosity

In asphalt binders, viscosity changes with temperature. McLeod [5] showed that a 1,000-fold increase in asphalt viscosity as the temperature drops from 135 °C to 57 °C. There is also a ten-fold increase in resistance to compaction as mix temperature drops from 135 °C to 63 °C, due

entirely to an increase in binder viscosity. Ideally, the binder viscosity should be great enough to resist the decompactive action of the roller, but not great enough to create an understressed mix. A binder with sufficient viscosity reduces the lateral movement of the mix, allowing it to remain beneath the roller long enough to achieve adequate densification. McLeod [5] conducted research on low and high viscosity binders within the same penetration grade. Mixes containing two types of 60/70 penetration asphalt were tested at a temperature of 135 °C behind the paver. Those containing a low-viscosity (0.219 Pa·s at 135 °C) asphalt had about one-half the stability of a mix containing a high-viscosity (0.523 Pa·s at 135 °C) asphalt. Another study by McLeod [5] involving two 85/100 penetration asphalts indicated that to reach a density of 2355 kg/m^3, the low-viscosity (0.225 Pa·s at 135 °C) asphalt required compaction at 85 °C, while the high-viscosity (0.430 Pa·s at 135 °C) asphalt required compaction at 113 °C.

Temperature Effects

Mix temperature is considered the most important factor in achieving proper pavement compaction. The mix temperature at the time of compaction is affected by conditions at the hot-mix plant, the paving process, thermal properties of the hot-mix, thickness and density of the pavement layer, and environmental conditions (air temperature, base temperature, wind velocity, and solar radiation). If the temperature is too low, the mix will be understressed; if it is too high, the mix will be overstressed. This underscores the importance of determining and maintaining an optimal temperature at which maximum densification can take place.

Parker [6] conducted a Marshall compaction study to determine the effect of compaction temperature on air voids in a mix. In an asphalt mixture compacted at 93.3 °C, the air voids content was 2.4 times that of a mixture compacted at 135 °C. Compaction at 79.4 °C resulted in a mix that had an air voids content four times greater than a mixture compacted at 135 °C (Figure 2.3).

Attention to compaction is especially crucial in cold weather conditions, when air voids after compaction can be as high as 16 percent. McLeod [5] conducted research that indicated pavements with this level of air voids showed signs of deterioration after two years. Cabrera [4] showed that inadequate mix temperature during compaction can reduce tensile strength and resilient moduli of asphalt concrete. Furthermore, McCloud [5] demonstrated that mixtures

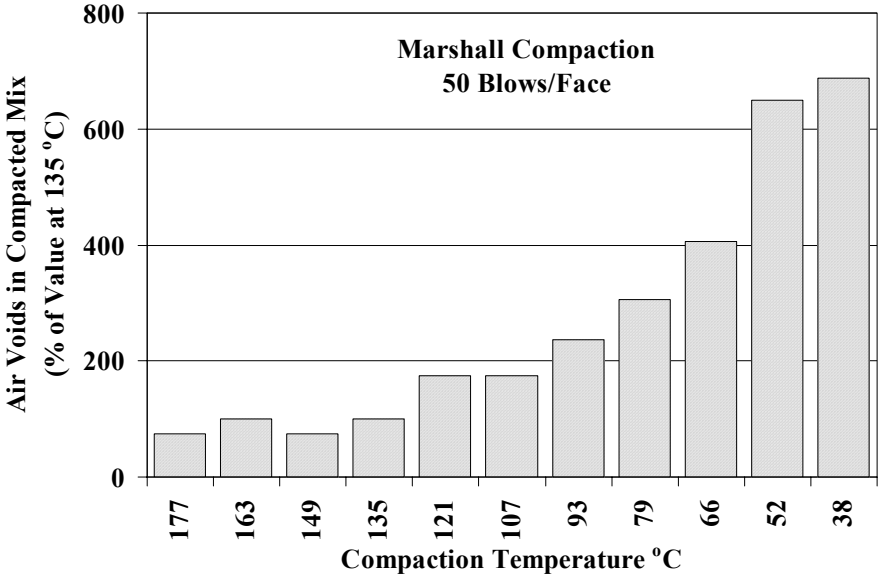

Figure 2.3 Influence of Compaction Temperature on Air Voids (After Parker [6])

compacted to 95 percent of the laboratory-compacted density showed a 77 percent reduction in Marshall stability when compared to those compacted to 100 percent of the laboratory-compacted density.

Filler Effects

Asphalt mixtures have an optimum cohesion where maximum compaction will occur. This cohesion can be affected by the amount of filler used in a mix. Santucci and Schmidt [7] showed that if the binder volume (asphalt + filler) is held constant, there is an optimum filler percentage where maximum compaction can occur.

A study by Heukelom [8] also showed that the amount of filler used in a mix can influence how well a mix is compacted. Figure 2.4 shows that for a given filler type the ease of compaction increases with the percentage of filler in the overall binder content. This proved to be true for limestone, activated marl, and strongly activated marl fillers used in a sand mix.

Control of Hot-Mix Asphalt Compactibility

Hot-mix compactibility is determined by many factors throughout the design and construction process. During the design phase, asphalt binder, aggregate, and filler types and proportions are determined. Once a paving job has begun, temperature control is the principal means of

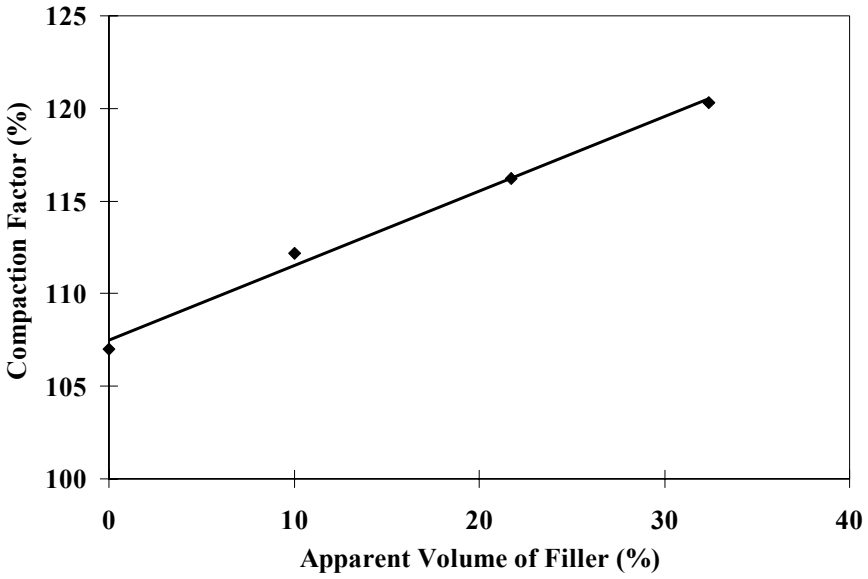

Figure 2.4 Compaction Factor C_F as a Function of the Apparent Volume of Filler (After Heukelom [8])

controlling compactibility. Kari [2] recommended the use of lateral confinement to ensure adequate compaction for an overstressed mix. This is achieved by rolling the edges of the pavement first, providing lateral restraint for the interior portion of the pavement.

Another means of controlling temperature at the time of compaction is by adjusting the lag time between the paver and the roller. There is, however, a limit to the amount the lag time can be reduced. Tegeler and Dempsey [9] reported that in 1971, contractors determined that 10 minutes was the absolute minimum allowable compaction time needed with the present equipment. Cold air and base temperatures can reduce the lag time for a given lift thickness to the point where the mix is understressed by the time the roller arrives.

Kari [2] recommended increasing the lift thickness, which allows the mix to retain heat longer, to improve compaction of an understressed mix. Another aspect of late-season paving that should be considered is the fact that due to low temperatures, very little traffic densification will occur for several months after paving. Therefore, the pavement should be roller-compacted as close as possible to 100 percent of the laboratory-compacted density. According to McLeod [5], this can be achieved by using low viscosity asphalt binders and pneumatic-tire rollers with quickly adjustable tire pressures.

Density and Thickness Changes During Compaction

Assuming density affects pavement thermal properties, a pavement cooling model will require information on how the density and thickness of a hot-mix asphalt lift change with each pass of the roller. Dellert [10] described a conventional rolling pattern using two passes of a three-wheel steel tire roller followed by four passes of a pneumatic tire roller and two passes of a tandem roller. This resulted in the pavement densities (expressed as a percentage of the voidless mix density) shown in Table 2.2. The densities resulting from vibratory compaction varies with the frequency and amplitude of vibration and roller speed. Table 2.1 shows pavement densities as a percent of voidless density for two different vibratory roller speeds. Another variable required by the model is the change in lift thickness with each pass of the roller.

Geller [11] conducted research on steel tire compaction indicating that the maximum compaction depth (reduction in lift height) is reached after the third roller pass. Table 2.3 outlines the amount of compaction accomplished by each of the first three roller passes. Table 2.4 lists several typical ranges of lay-down thicknesses and the expected final lift thicknesses resulting from steel tire rolling.

Table 2.2 Conventional Compaction Densities (After Dellert [10])

Roller Pass	**Percent of Voidless Density**
Paver	80.0
3-Wheel pass 1	90.5
3-Wheel pass 2	92.5
Pneumatic pass 1	93.5
Pneumatic pass 2	94.0
Pneumatic pass 3	95.0
Pneumatic pass 4	95.0
Tandem pass 1	95.5
Tandem pass 2	96.0

Table 2.1 Vibratory Compaction Densities (After Dellert, [10])

Roller Pass	**Percent of Voidless Density**	
Roller Speed	46 m/min.	76 m/min.
Paver	83.0	83.0
1	94.0	92.0
2	95.0	92.7
3	95.9	93.0

Table 2.3 Estimated Compression Depth (After Geller [11])

Roller Pass	Percent of Total Compression Depth
1	60
2	30
3	10

Table 2.4 Typical Lay-Down and Compacted Lift Thicknesses (After Geller [11])

Laydown Thickness (mm)	Compacted Thickness (mm)	Total Compression (mm)
32 to 38	25	6 to 13
51 to 57	38	13 to 19
64 to 79	51	13 to 19
83 to 89	64	19 to 25
102	76	25

Tegeler and Dempsey [9] reported that density changes in hot-mix asphalt have a much greater effect on the thermal conductivity of hot-mix asphalt than temperature changes. A paving mixture will typically leave the spreader at 75 to 80 percent of the laboratory-compacted density. They estimate that thermal conductivity ranges from 1.04 W/m·K immediately behind the paver to 1.56 W/m·K after final compaction.

THERMAL PROPERTIES OF PAVEMENT MATERIALS

Conduction

Heat conduction is described by Fourier's law, which states that the heat flux in a given direction, q_z (W/m^2) is proportional to the temperature gradient, $\partial T/\partial z$ (change in temperature/change in depth) in that direction. The proportionality constant, k (W/m·K) is called the thermal conductivity. One-dimensional steady-state heat conduction is described by the following differential equation:

$$q_z = -k\frac{\partial T}{\partial z} \tag{2.2}$$

There is a negative sign on the right side of the equation because heat flows in the direction of decreasing temperature. This relationship is simplified by assuming constant heat flow:

$$\frac{\partial q_z}{\partial z} = -\frac{\partial}{\partial z}\left(k\frac{\partial T}{\partial z}\right) = 0 \tag{2.3}$$

A further simplification involves assuming constant k:

$$k\frac{\partial^2 T}{\partial z^2} = 0 \tag{2.4}$$

Describing transient heat flow requires two more thermal properties. Specific heat at constant pressure, c, J/kg·K, is a measure of heat storage capacity. Thermal diffusivity, α, m^2/s, is a measure of heat propagation speed. These properties, along with density, ρ, kg/m^3, are related by the following equation:

$$\alpha = \frac{k}{\rho C_p} \tag{2.5}$$

Transient heat flow is represented by the following equation:

$$\frac{\partial}{\partial z}\left(k\frac{\partial T}{\partial z}\right) = \rho c\frac{\partial T}{\partial t} \tag{2.6}$$

This relationship is also simplified by assuming constant thermal conductivity:

$$k\frac{\partial^2 T}{\partial z^2} = \rho c\frac{\partial T}{\partial t} \tag{2.7}$$

Combining Eqs. (2.5) and (2.7) produces the one-dimensional form of the diffusion equation:

$$\frac{\partial^2 T}{\partial z^2} = \frac{1}{\alpha}\frac{\partial T}{\partial t} \tag{2.8}$$

Radial heat flow theory is also used to measure thermal properties. Goldberg and Wang [12] developed a probe to determine *in situ* soil thermal conductivity. Given a cylindrical heat source infinite in length and infinitely small in diameter inside an infinite homogeneous mass, the temperature at time, t and distance, r from the heat source is represented by Eq. (2.9).

$$T(r,t) = \frac{Q/L}{4\pi k}\int_{\frac{r^2}{4\alpha t}}^{\infty}\frac{e^{-u}}{u}du \tag{2.9}$$

Where:

T = temperature, K

Q/L = line heat source strength per unit probe length, W/m

k = thermal conductivity of the medium, W/m·K

r = radial distance from the line heat source, m

t = time, s

α = thermal diffusivity of the medium, m^2/s

The time derivative of Eq. (2.9) is:

$$\frac{\partial T}{\partial(\ln t)} = \frac{Q/L}{4\pi k} e^{\left(\frac{-r^2}{4\alpha t}\right)} \tag{2.10}$$

When $r^2/4\alpha t \rightarrow 0$, the thermal conductivity may be approximated as:

$$k = \frac{Q/L}{4\pi\Delta T} \ln\left(\frac{t_2}{t_1}\right) \tag{2.11}$$

Typical values of thermal conductivity, specific heat, and thermal diffusivity for asphalt pavement are summarized in Table 2.5. Most notable is the wide variation in reported thermal values. Turner and Malloy [13] reported the lowest value of k (0.76 W/m·K) and Kavianipour [14] reported the highest value (2.88 W/m·K). Jordan and Thomas [15], Corlew and Dickson [16], Tegeler and Dempsey [9], Kersten [17], and O'Blenis [14] reported intermediate values. Kavianipour suggested that the wide range of reported values was due to variability of aggregate

Table 2.5 Reported Thermal Properties for Asphalt Concrete

k (W/m·K)	c (J/kg·K)	$\alpha \times 10^6$ (m^2/s)	Source
0.76			Turner and Malloy [13]
0.80-1.06	850-870	0.37-0.53	Jordan and Thomas [15]
1.21	920	0.59	Corlew and Dickson [16]
1.21-1.38	840-1090		Tegeler and Dempsey [9]
1.49			Kersten [17]
0.85- 2.32			O'Blenis (in Kavianipour [14])
2.28-2.88		1.15-1.44	Kavianipour [14]

and binder thermal properties. Reported values of thermal conductivity for limestone varied from 0.7 W/m·K (Turner and Malloy [13]) to 2.2 W/m·K (Raznjevic [18]), while those for granite varied from 2.2 W/m·K (Turner and Malloy [13]) to 4.2 W/m·K (Raznjevic [18]), and thermal conductivity values reported for various asphalt binders ranged from 0.14 W/m·K (Saal [19]) to 0.74 W/m·K (Raznjevik [18]).

Convection

Convection is the process of heat transfer between a solid surface and a fluid. Convection models are divided into two types: Free (or natural) convection takes place when the only fluid motion is due to buoyancy effects caused by thermal gradients. Forced convection occurs when some other force, such as wind, causes the fluid to move relative to the surface. Complex fluid motion makes precise modeling of convection very complicated, but Ozisik [20] stated that for most engineering applications this process can be approximated by defining a heat-transfer coefficient, h (power/area·temperature) to represent the heat transfer between a solid surface and a fluid. Convective heat transfer can now be estimated by the following equation:

$$q = h\left(T_f - T_s\right) \tag{2.12}$$

Where:

T_f = mean fluid temperature

T_s = surface temperature

Radiation

Ozisik [20] described radiation as the transfer of heat between two bodies by either electromagnetic waves or photon particles. As with convection, the process in reality is very complex, involving radiation originating from or penetrating into a certain depth below the surface of a body. Most engineering applications allow the simplifying assumption that the exchange of radiative energy occurs only at the surface of a body.

The amount of energy emitted or absorbed by a body is proportional to the fourth power of the absolute temperature of that body. The proportionality constant for radiation is called the Stefan-Boltzmann constant, σ. The simplest radiation model involves the transfer of heat between two "black bodies" (objects which emit or absorb energy perfectly, that is, without reflecting or

transmitting any energy) where one body is completely enclosed in the other body (Figure 2.5). In this case, the heat flux is represented by the following equation:

$$q = \sigma\left(T_1^4 - T_2^4\right) \tag{2.13}$$

Where:

σ = Stefan-Boltzmann constant (5.669×10^{-8} W/m^2·K^4)

T_1 = Temperature of smaller body (K)

T_2 = Temperature of larger body (K)

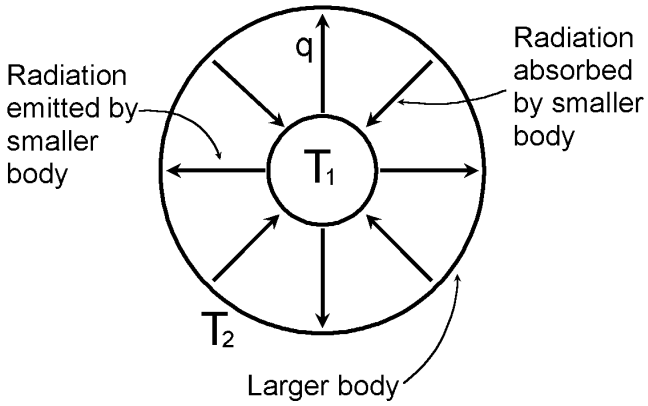

Figure 2.5 Two-Body Radiation Model

In reality, no object absorbs or emits radiation perfectly, so factors representing a materials absorptance (a) and emittance (ε) must be included in radiation models. These factors have values between 0 and unity, and represent the fraction of total radiative energy absorbed and emitted, respectively, by a surface. The energy transmitted by a solid body, such as a pavement structure, to a surrounding media (either the earth's atmosphere or outer space), is represented by a modification of Eq. (2.13):

$$q = \varepsilon\sigma\left(T_1^4 - T_A^4\right) \tag{2.14}$$

Where:

ε = total pavement emittance, reported in Corlew and Dickson [16] as 0.95

T_1 = surface temperature of the first pavement layer (K)

T_A = ambient air temperature (K)

A form of equation 2.12 representing solar energy absorbed by a pavement would be complicated, but this is unnecessary when the net solar flux at the surface, H_s is known. The equation representing solar energy absorbed by a pavement assumes the following form:

$$q = aH_s \tag{2.15}$$

Where:

a = the total pavement absorptance (reported in Corlew and Dickson [16] as 0.85)

A means of estimating H_s for a variety of conditions is outlined in Appendix B.

LABORATORY MIXTURE DESIGN AND COMPACTION METHODS

Mixture Design Methods

One very important aspect of mixture design is the method of compaction used. There are typically three different methods for compaction: Marshall, kneading, and gyratory. All three methods have the same target which is to increase the density of an asphalt sample by changing the orientation of the aggregate particles. The difference between the three methods is in how the increase in density is achieved. The three main mixture design methods are outlined below and the compaction type for each method is discussed.

Marshall mixture design uses a variety of aggregate and asphalt cement tests to determine if the material properties of proposed aggregate and asphalt combination would provide suitable strength and durability during construction and use. Once the materials are chosen, the optimum asphalt content must be determined. This is done based upon volumetric and strength properties of the compacted mixture such as voids in mineral aggregate, percentage of air voids in compacted samples, stability and flow. The properties of a particular mix are then compared to acceptable values that have previously been established based upon the expected amount of traffic for the pavement. The Marshall mixture design uses a standard method of compaction, described in ASTM D 1559-89 as a 4536 g hammer dropped through a 457.2 mm distance onto a 98.4 mm plate which rests on the hot-mix asphalt. The required number of blows depends upon the estimated traffic level of the road for which the mixture is being designed.

Hveem mixture design is similar to Marshall mixture design in that both methods aim to produce compacted aggregate mixtures with sufficient stability to resist traffic and sufficient film

thickness of asphalt on the aggregate particles to resist weathering and moisture susceptibility effects. One major difference between Hveem and Marshall mixture designs is the type of compactor used for preparing laboratory specimens. Instead of using a repeated blow from a hammer, Hveem compaction relies upon a kneading compactor called the California Kneading Compactor. According to Consuegra, et al [21], this type of compactor applies a pressure of 1.7 MPa (for the first 20 blows to semi-form the specimen) to 3.4 MPa over one-third of the area of the free face of the sample. The compactor foot is then rotated to apply forces uniformly around the free face of the sample. The partially free face allows particle to move relative to one another, creating a kneading action that densifies the mixture. A uniform load is applied to the entire face at the end of the procedure.

Superpave mixture design also has provisions for choosing quality aggregates and asphalt. The methods for determining the properties of the material are largely performance based to provide a better relation between field performance and laboratory results. This process differs in that it is based more upon volumetric properties of the compacted laboratory samples than upon the stability of the samples. This type of testing depends largely upon gyratory compactors which are used to better simulate engineering properties of mixtures produced in the field. This type of compaction uses a continuous normal force and a rocking motion, which creates a shearing force, to work the aggregate particles into a denser configuration.

A study by Consuegra et al. [21] found that the gyratory compactor produced mixtures with properties closest to those found in the field. The kneading compactor ranked second to the gyratory compactor because it was able to produce some relative motion of particles during compaction. Marshall compactors were ranked last due to their inability to simulate mixtures produced in the field.

Methods Used to Define Workability and Compactibility

There have been few studies done to define the compactibility and workability of hot mix asphalt. Aggregate properties may vary greatly from mix to mix depending upon the types of materials available. Asphalt properties are also greatly varied, different and changes in asphalt viscosity with temperature make it difficult to quantify workability.

Heukelom [8] proposed a method for determining the workability of hot mix asphalt that includes two characteristics of a mix: spreadability and compactibility. Spreadability is defined as "the ability of a loose mix to be spread over the road surface to achieve an even distribution and pre-arrangement of aggregates," and workability as "the ability of the pre-arranged particles to be forced into their mutual interstices forming a compact mass under the weight of a roller." The compactibility of the mixture was measured by the "compaction factor." Marshall mix design samples were used in computing the compaction factor for different mixes. The compaction factor is defined as:

$$C_F = \frac{\text{volume after 5 blows}}{\text{volume after 100 blows}} \times 100 \tag{2.16}$$

The compaction factor is used as an indication of compactibility. Increasing the amount of filler in a mixture will increase the compaction factor for a mixture because the mixtures will be too stiff to densify under their own weight and will require more blows for compaction. Changing other mixture properties will also affect the compaction factor, providing a basis for comparing different mixes.

Cabrera [22] described how a gyratory testing machine at the University of Leeds was used to define the workability of asphalt mixtures. A gyratory compactor was used for this study because the kneading action of the compactor better simulated the compaction effort of construction equipment than Marshall hammers. Samples were compacted to 30 gyrations using an axial load of 0.7 MPa. Specimen heights were collected at 5-cycle intervals and the weight of the sample was determined after the sample had been extruded from the gyratory mold and cooled. The porosity was calculated at each interval using height and weight data. Porosity (P_i) was plotted against the log of the number of gyrations for each check point (i). A linear relation was determined in the form of:

$$P_i = A - b\left[\log(i)\right] \tag{2.17}$$

Where:

P_i = porosity at point (i)

A, b = constants

The workability index (WI) was equated to the inverse of the constant A, which is the porosity at 0 cycles. Higher WI values indicate that a mixture is easier to compact.

Bissada [23] quantified the compactibility of asphalt mixtures in a different method in 1984. The stiffness of a mixture was related to its resistance to compaction. A mathematical model was used to determine the resistance of different asphalt mixtures. These data were then related to stiffness measurements from creep testing for a method to control permanent deformation in asphalt pavements.

The mathematical model used to determine the resistance to compaction indicates a differential relationship between the rate of change of density of the mix and that of compactive effort applied. The equation is:

$$\frac{d\gamma}{dC} = \frac{1}{R}(\gamma_\infty - \gamma) \tag{2.18}$$

Where:

C = compactive effort (Nm)

R = resistance to compaction (Nm)

γ_∞ = maximum achievable bulk density (g/cm^3)

γ = bulk density (g/cm$^{3)}$ at a certain compaction level

The compactive effort (C) is determined from the number of blows from the Marshall hammer:

$$C = N_B \times 2 \times C_B \tag{2.19}$$

Where:

N_B = number of Marshall hammer blows per side

C_B = compactive effort per blow = 21 Nm

Integration of Eq. (2.18) results in:

$$\gamma_C = \gamma_\infty - (\gamma_\infty - \gamma_0)e^{-C/R} \tag{2.20}$$

Where:

γ_C = bulk density (g/cm$^{3)}$ at a given compaction level C

γ_0 = bulk density at the start of the compaction process (g/cm^3)

Experimentally determined bulk density values are used in the equation to determine the resistance to compaction. Resistance to compaction is then plotted against the mix stiffness determined from creep testing to measure the performance of a mix with respect to permanent deformation.

Marvillet, et al [24] described a means of measuring workability using a mixer equipped with a device to measure the torque required for mixing. The inverse of the resistance moment was used as the workability value. This measurement of workability was proposed based upon the idea that mixes that are difficult to compact will also be difficult to mix.

Superpave Compaction Specifications

Superpave mix design [25] has a provision to account for the compactibility of an asphalt mixture. Limits are set at three checkpoints during mix design for the percentage of maximum density achieved during compaction. The density for a given number of cycles during the compaction process (N_x) is specified for three points: $N_{initial}$, N_{design}, and $N_{maximum}$. Densities at these points are to be less than 89%, equal to 96% and less than 98% of maximum density, respectively. $N_{initial}$ is a checkpoint to ensure that the mixture will not be too tender during construction to support the compactors. N_{design} is used to determine the air void content for the optimum asphalt content, and $N_{maximum}$ is used to determine if there may be potential problems with rutting during service conditions. The number of cycles for each density checkpoint is based upon the expected traffic loading of the pavement and the design high air temperature of the region. These limits are set to ensure that the asphalt mixture is neither too soft nor too stiff for the service conditions of the pavement.

COMPUTATIONAL MODELS

The computational models considered in this thesis are based on a one-dimensional finite difference or finite element approach. A finite difference scheme approximates the temperature at a point by applying thermal calculations to the temperatures at neighboring points. A finite element scheme approximates the temperature in an element of specified volume by applying thermal calculations to the temperatures in neighboring elements. In one-dimensional problems, the finite difference and finite element schemes are essentially identical. In order to predict

pavement cooling rates, both a space-step (Δz) and a time step (Δt) must be considered. In one-dimensional pavement cooling models with constant Δz, it is convenient to label points numerically, beginning with 1 at the uppermost layer, and N at the lowest layer. An unspecified interior point and its neighbors are called "n," "n - 1," and "n + 1." The corresponding temperatures at these points are referred to as "T_n," "T_{n-1}," and "T_{n+1}" (Figure 2.6). A convenient means of identifying points in time in a model with constant Δt is to call a point "t" and the subsequent point "t + Δt." Accordingly, the temperature at a point in time may be labeled "$T_{n,t}$," "$T_{(n+1),(t)}$," "$T_{(n-1),(t+\Delta t)}$," etc.

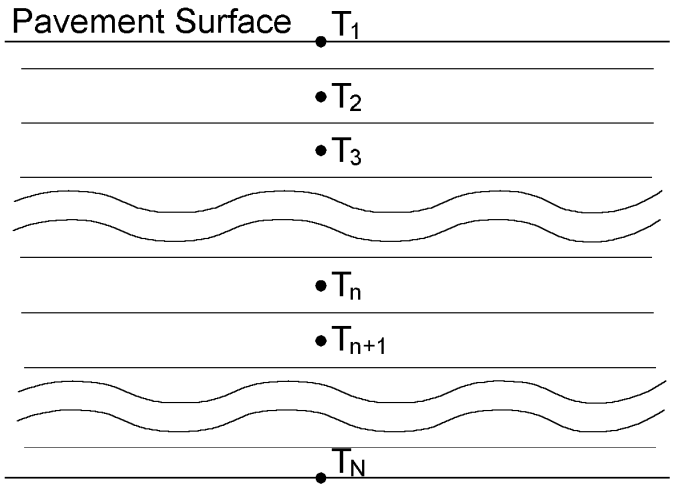

Figure 2.6 Finite Difference Model

A further distinction is made between explicit, implicit and combination schemes. In an explicit scheme, all unknown values required for calculations are taken from the previous time step. Since these values were all calculated in the previous time step, the desired results are reached on the first calculation. In effect, the point of reference for explicit calculations is at the beginning of the time step. In an implicit scheme, an initial estimate is made for values in the current time step, and several iterations of the calculations are made until the values converge, or reach a value that does not change significantly with subsequent iterations. In this case, the point of reference is at the end of the time step. One advantage of the implicit scheme is that it can achieve the same level of accuracy as the explicit scheme while using larger space and time steps. A combination model takes its point of reference at the middle of the time step. This is also an iterative model, but the average of the previous and current time step values are used.

Jordan and Thomas [15] recommended considering the following parameters in a pavement cooling model:

1. Density of pavement layers
2. Thermal conductivity of pavement layers
3. Specific heat
4. Ambient temperature
5. Wind speed
6. Convection coefficient
7. Incident solar radiation
8. Coefficients of emission and absorption of solar radiation for the pavement surface
9. Time and depth increments
10. Initial pavement temperature profiles

Although some of these variables are more important than others, in this case it was assumed that all were required. The first three variables listed can be combined into a thermal diffusivity term by Eq. (2.5). This may be desirable if thermal diffusivity information is more readily available than the other three variables. Ambient temperatures and wind speeds are easily acquired at the site or estimated from local weather reports. The convection coefficient and incident solar radiation are difficult to determine exactly, but an adequate means of estimating the convection coefficient from wind speeds and estimating the incident solar radiation from location, time, and cloud cover information are summarized in Appendix D. The coefficients of emission and absorption for the pavement surface are also difficult to determine exactly. The values assumed by Corlew and Dickson [16] were used in this research. Time and depth increments are determined by the modeler. The optimal increment sizes occur at the point where any further reduction in the size of the increment causes a minimal change in the outcome of the program. The initial temperature profile of the existing structure on which the hot-mix will be placed is generally assumed to be constant, either equal to the ambient air temperature, or to the measured surface temperature. The initial temperature throughout the hot-mix lift is assumed to be the temperature of the mix behind the paver. A summary of previous pavement cooling models is presented in Appendix A.

LABORATORY TESTS FOR DETERMINING ASPHALT PAVEMENT THERMAL PROPERTIES

Although there are many standardized methods for determining thermal properties of materials, asphalt pavement presents problems relating to the specimen dimensions required (an assumption of homogeneity requires that the smallest specimen dimension be several times larger than the largest aggregate particle). Another complication involves the change of the asphalt binder through the temperature range used in the paving process. Once a hot-mix specimen is heated above a certain temperature, it requires a mold or some other form of support to maintain the desired shape. Most of the commercially available thermal property devices were not designed for the standard asphalt specimen sizes or for a loose-mix type of material. Although standard thermal devices can be modified for the purpose of measuring asphalt concrete thermal properties, the cost involved was prohibitive.

The object of most thermal test procedures is to approximate one-dimensional conductive heat flow. In a slab specimen, this is accomplished by insulating the specimen sides or using a sufficiently small height-to-length ratio. This can also be accomplished in a cylindrical specimen if the diameter-to-length ratio is sufficiently small, and a line heat source is located along the central axis of the cylinder. A further simplification involves maintaining either constant heat flow, or constant boundary temperatures.

Thermal Conductivity

Thermal conductivity can be determined by placing a large, flat specimen between a heat source and a heat sink with either constant temperature or constant heat flow and allowing it to reach equilibrium. The thermal conductivity is calculated from the temperatures taken at several depths in the specimen. A method which involves more complicated theory, but requires simpler equipment and less time is the thermal probe method.

Thermal conductivity (k) of hot-mix asphalt can be approximated using American Society for Testing and Materials (ASTM) Designation D 5334 - 92: Standard Test Method for Determination of Thermal Conductivity of Soil and Soft Rock by Thermal Needle Probe Procedure. This procedure involves inserting a probe containing a heating element and a

thermocouple into a cylindrical specimen, applying a constant current, and measuring the temperature change over time.

Specific Heat

Specific heat of solids is often determined by submerging a specimen at a known, constant temperature in a lower-temperature fluid, which is contained in a well-insulated vessel. The specific heat of the solid is calculated from the rise in temperature of the fluid. No direct method of measuring specific heat was used in this research, although the specific heat, c of a material can be calculated if the density, ρ, thermal conductivity, k, and thermal diffusivity, α are known, as indicated in Eq. (2.5).

Thermal Diffusivity

Determination of thermal diffusivity requires measuring a time-temperature relationship, usually utilizing a constant heat flow source, and measuring the temperature at several points in the specimen as a function of time. Most standard thermal diffusivity test methods require very sophisticated heating and temperature measurement equipment. Fwa, et al [26] used a relatively simple transient heat conduction method of estimating the thermal conductivity and thermal diffusivity of asphalt slab specimens. The thermal properties were estimated by analyzing the temperature change at the center of a slab specimen that was cooled by air flowing at a constant velocity. This required estimating the convection coefficient resulting from a constant air flow over the specimen and using plane wall heat conduction theory to determine the thermal conductivity and thermal diffusivity of the slab. A proposed method involves an asphalt slab insulated on the sides and bottom. Thermocouples placed at regular intervals throughout the depth of the slab provide a means of estimating the temperature gradient. The slab is heated to a constant temperature, and then allowed to cool by natural convection and radiation through the top surface. The temperature at four depths in the sample is measured at regular time intervals, and the diffusion equation, Eq. (2.8), is used to estimate the thermal diffusivity.

CHAPTER 3
MODELING OF HEAT TRANSFER DURING ASPHALT PAVING

INTRODUCTION

This chapter describes the development of a heat transfer model for predicting the transient cooling of asphalt concrete layers (lifts) during pavement construction. It is based on previous work done by Luoma, et al [27]. This model is the central part of the computer program for selecting asphalt paving strategies in cold weather conditions, developed in the remainder of this report. The basic elements in the heat transfer model are conduction through the lift with combined radiation and convective cooling at the surface. The proposed model differs from previous asphalt cooling models by Corlew and Dickson [16], Jordan and Thomas [15], and Tegler and Dempsey [9] in two important aspects:

1. Previous models assume a fixed dimension for the lift. In reality the lift is undergoing compaction. The proposed model accounts for the effect of this compaction on the heat transfer by utilizing a deforming space mesh.
2. Previous models assume fixed representative values for the thermal properties. In the actual paving operations, it is expected that the bulk property values of the material will change with : (a) temperature, (b) lift compaction, and (c) asphalt mix. The proposed model takes into account the changing thermal properties; in particular, properties changing with compaction.

THE PAVING PROCESS

The construction of an asphalt pavement starts by combining heated aggregates with liquid asphalt cement at temperatures in the range of 120 to 150 °C. The mixture is then stored in a silo until it is transported by dump trucks to the construction site. At the site, the asphalt concrete may be deposited directly into a paver or placed in a windrow to be picked up and moved through a paver. The paver spreads the material across the pavement in a thickness ranging from 25 to 200 mm, typically 37 to 100 mm, and provides a modest amount of initial compaction. As

the material cools compaction is provided by a series of pneumatic and steel-wheel rollers until the desired density is achieved. If the material cools too rapidly, plastic flow is impeded and improvements in the density cannot be obtained with further passes of the rollers.

Achieving the proper level of compaction during construction is critical to the long-term performance of the pavement. This is difficult when environmental conditions are such that the material loses heat rapidly resulting in a shorter time to work it effectively. The model developed in this research will allow agency and contractor personnel to monitor conditions and estimate the amount of time available to compact the material. This chapter continues the efforts of Corlew and Dickson [16], who first used numerical methods to evaluate asphalt concrete cooling, as well as Jordan and Thomas [15] and Tegler and Dempsey [9].

THE MODEL

Assumptions

A computational model will be developed for tracking the thermal history of the asphalt during the paving process. This model will be based on the following assumptions:

1. The heat transfer in the asphalt lift and ground base is controlled by heat conduction.
2. The heat transfer is one-dimensional through the depth of the lift. This assumption is consistent with Corlew and Dickson [16], Jordan and Thomas [15], and Tegler and Dempsey [9] and is justified on noting that the length scale in the lift, on the order of 0.1 m, is at least an order of magnitude smaller than length dimensions in transverse directions. Areas where two dimensional effects may be important, at the edges of the pavement, are usually in areas that experience low traffic volumes e.g., shoulders and lane markings.
3. In outlining the model, two zones will be considered: (a) the asphalt lift $Z_{top}(t) \geq z \geq Z_{base}$ and (b) the ground base $Z_{base} \geq z \geq 0$ (Figure 3.1). Additional zones, however, e.g., a previously laid lift, are available in the final model.
4. In order to account for compaction the asphalt lift domain can deform in time, this deformation is imposed on prescribing the location of the asphalt lift surface $Z_{top}(t)$ with time.

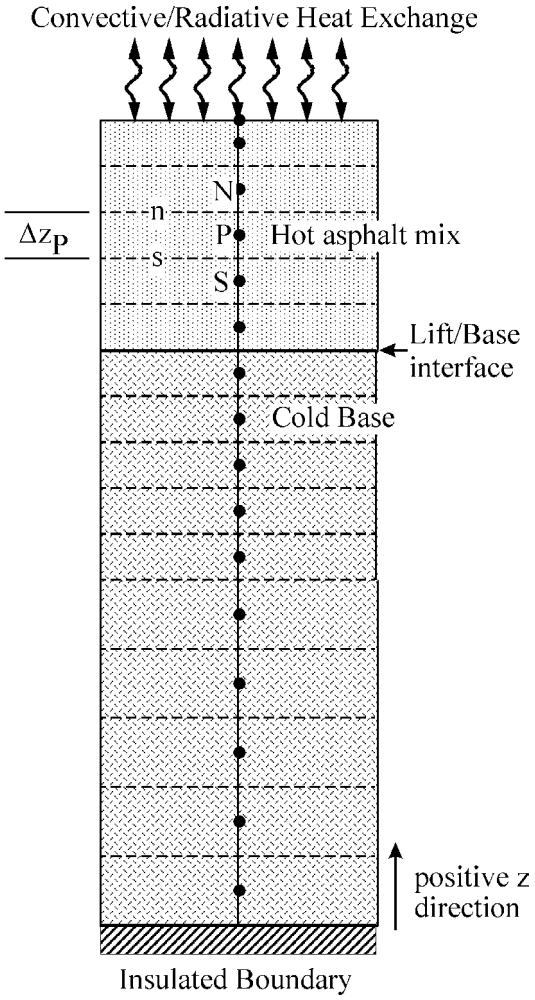

Figure 3.1 Solution Domain for Asphalt Cooling

5. The lower surface in the ground base, z = 0, is assumed to be insulated. Usually this point is chosen far enough away from the hot lift that, in the time scale of the problem, its temperature remains constant throughout the process.
6. The upper surface of the asphalt lift, $z = Z_{top}(t)$ exchanges heat with the surroundings through: (a) convection with the atmosphere, (b) radiation to the surroundings and (c) solar heat absorption. This exchange is accounted for by a net heat flux specified at the surface. In a departure from previous studies, radiation is between the surface temperature and an effective sky temperature (which differs from the air ambient temperature) [28].
7. Thermal properties, in the lift and ground base can be prescribed functions of temperature. In addition the thermal conductivity and density in the lift is also a function of compaction. In this respect, a simple linear compaction model is used.

Governing Equations

With the above assumptions the governing equations are:

Asphalt: $$\rho c \frac{\partial T}{\partial t} = \frac{\partial}{\partial z}\left[k \frac{\partial T}{\partial x} \right] \qquad Z_{top} \geq z \geq Z_{base} \tag{3.1}$$

Base: $$\rho c \frac{\partial T}{\partial t} = \frac{\partial}{\partial z}\left[k \frac{\partial T}{\partial x} \right] \qquad Z_{base} \geq z \geq 0 \tag{3.2}$$

Where:

T = temperature (K)

ρ = density (kg/m^3)

c = specific heat (J/kg·K)

k = thermal conductivity (W/m·K)

At z = 0 (zero flux)

$$k \frac{\partial T}{\partial z} = 0 \tag{3.3}$$

At z = Z_{base} (continuity of flux)

$$\left[k \frac{\partial T}{\partial z} \right]_{base} = \left[k \frac{\partial T}{\partial z} \right]_{asphalt} \tag{3.4}$$

At z = Z_{top} (non-linear convection with convection, radiation and solar input)

$$k \frac{\partial T}{\partial z} = h_c (T - T_{amb}) + \varepsilon \sigma \left(T^4 - T_{sky}^4 \right) - \alpha H_s \tag{3.5}$$

Where:

ε = the total emissivity of the asphalt surface

σ = the Stephan-Boltzman constant (5.67 10^{-8} W/m^2·K^4)

α = the total absorbance of asphalt

T_{amb} = the ambient temperature (K)

T_{sky} = the effective sky temperature (K)

H_s = the incident solar radiation (W/m^2)

h_c = convective heat transfer coefficient ($W/m^2 \cdot K$)

The equation for the calculation of the h_c is adapted from Alford et al [29]:

$$h_c = 7.4 + 6.39\, w^{0.75} \tag{3.6}$$

Where:

w = wind velocity at 2 meters above ground level (m/s)

The initial conditions are a prescribed single temperature value for the lift, T_{lift}, and a prescribed temperature profile in the ground (a constant profile is assumed in the current work).

Numerical Solution

The solution domain is broken up into control volumes, as shown in Figure 3.1. Patankar [30] described a fully implicit formulation is used with 2nd order accuracy treatment of the temperature at the surface node. The discrete equations, related to Eqs. (3.1) and (3.2), have the form

$$a_P T_P = a_N T_N + a_S T_S + b_P \tag{3.7}$$

Where:

a_P, a_N, a_S = coefficients for nodes P, N, and S, respectively (Figure 3.1)

T_P, T_N, T_S = temperatures at nodes P, N, and S, respectively

b_P = source term

In the asphalt, assuming a constant grid spacing, the coefficients at internal points are

$$a_S = \frac{2k_s}{\Delta z_S + \Delta z_P} \qquad a_N = \frac{2k_n}{\Delta z_N + \Delta z_P}$$

$$a_P = a_N + a_S + \frac{\rho_P c_P \Delta z_P}{\Delta t} \quad b_P = \frac{\rho_P c_P \Delta z_P T_P^{OLD}}{\Delta t} \tag{3.8}$$

Where:

Δz = space step

Δt = time step

k_n, k_s = thermal conductivity at interfaces n and s, respectively (Figure 3.1)

The superscript OLD indicates evaluation at the previous time step.

At most interfaces k_n and k_s are evaluated as arithmetic averages of the local nodal conductivity values. On the interface between the asphalt and the ground base a conjugate approach is used, i.e.,

$$k_s = \left[\frac{\Delta z_{asphalt}}{k_{asphalt}} + \frac{\Delta z_{ground}}{k_{ground}} \right]^{-1} \tag{3.9}$$

Within each time step the above equations are solved using a Tri-Diagonal Matrix Algorithm (TDMA) solver described by Patankar [31]. No linearization is employed in treating the radiation boundary conditions and as a result the discrete equations are non-linear and required iteration in a time step (three to four iterations are usually sufficient).

The Deforming Grid

A key feature in the above model is the ability for the asphalt domain to deform. In this way the effects of compaction on the cooling of the lift can be accessed. In the current numerical model deformation is applied instantaneously at a given, specified, instant in time and it is assumed that the rate of compaction is linear and uniform throughout the lift. The compaction procedure is as follows:

The initial uncompacted lift dimension and the amount of deformation required, as a percentage of the lift, to achieve compaction is specified.

Based on the initial, uncompacted lift size a uniform numerical space step is chosen, i.e.,

$$\Delta z_{uncompacted} = \frac{Z_{top}^{initial} - Z_{base}}{n} \tag{3.10}$$

Where:

n = number of control volumes in the asphalt lift

The cooling of the uncompacted lift is calculated on applying the numerical model. The conductivity and the density used in this study are specified in terms of values associated with the final compacted asphalt, i.e., assuming negligible values for air.

$$\rho = (1-g)\rho_{compacted} \qquad k = (1-g)k_{compacted} \tag{3.11}$$

Where:

$$g = \text{compacted volume fraction} = \frac{\%\text{Compaction}}{100}$$

Compaction is applied instantaneously at a specified point in time. In the compaction step a new space step is calculated as

$$\Delta z_{compacted} = \frac{Z_{top}^{compacted} - Z_{base}}{n} \tag{3.12}$$

and subsequent cooling is controlled by the specified compacted thermal values.

Note that since a uniform deformation is assumed no mass enters or leaves the control volumes in the domain during the compaction, as such:

1. Grid convection does not have to be accounted for
2. The mass in a control volume remains fixed
3. The specific heat is not affected by the compaction
4. Nodal temperatures remains constant throughout compaction

The last two conditions are based on the assumptions that the specific heat of air is small and the compaction process does not generate significant heat.

Validation

As an initial verification of the model, input parameters–T_{base} = 12.2 °C, T_{lift} = 132.2 °C, T_{amb} = 12.2 °, h_c = 18.8 W/m^2·K, α = 0.85, H_s = 630 W/m^2, ρ = 2242 kg/m^3, k = 1.211 W/m·K, c = 921 J/kg·K--were chosen to match those used by Corlew and Dickson [16]. The compaction was applied at time t = 0. The predicted cooling curve at a depth of 25 mm in a 37.5 mm lift, is shown in Figure 3.2. For comparison, the results obtained with the Corlew and Dickson model [16] are also shown in Figure 3.2. It is observed that the proposed model is very close to the experimental data; in fact predictions are better than those obtained with the Corlew and Dickson code.

A sensitivity analysis was also performed to ensure that the solution was independent of time and space steps. The temperature profile 900 seconds after laying, predicted with various space and

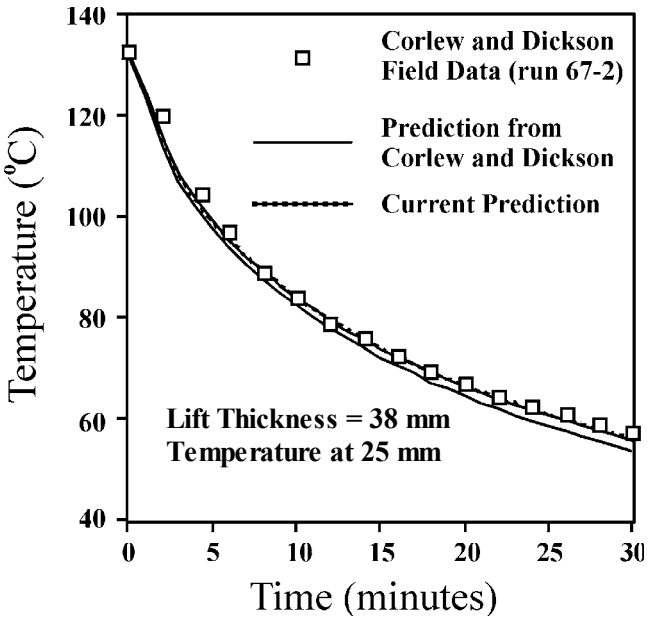

Figure 3.2 Temperature History vs. time

time steps is given in Figure 3.3. These results indicate the robustness of the calculation; a four-fold increase in the grid size results in less than a 2% relative difference in the predicted temperature profile.

THE EFFECTS OF COMPACTION

Previous studies [16], [15], [9] have investigated many aspects of the cooling of asphalt lifts. As noted in the introduction an area that has not been investigated is the effect of the compaction. In order to make such an assessment the current study looks at the question, "How is the cooling of the lift affected by the point at which compaction is applied?" This question is answered by carrying out a number of simulation runs of a 30 minute paving process with the compaction applied at a different time point in each run (t = 0 min. (instantaneous compaction), t = 5 min., 10 min., 15 min., 20 min., 25 min., no compaction). Simulations were carried out for three different lift sizes, each associated with different compaction values:

1. a 0.1 m lift experiencing 5% compaction
2. a 0.15 m lift experiencing 20% compaction
3. a 0.2 m (8 inch) lift experiencing 36% compaction

The first two of these are consistent with common practice. The last represents the worst case of an initial placement process involving loose asphalt [32]. The environmental conditions used in

all the simulations–T_{base} = 2 °C, T_{lift} = 132.2 °C, T_{amb} = 2 °C, h_c = 40.6 W/m^2·K, α = 0.85, H_s = 0.0 W/m^2, ρ = 2200 kg/m^3, k = 1.2 W/m·K), c = 921 J/kg·K--are representative of a cloudy windy fall day in Minnesota.

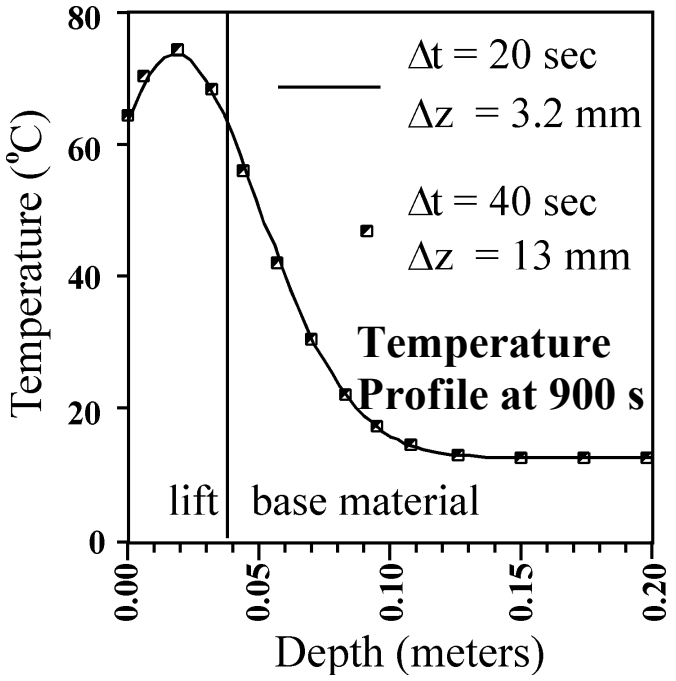

Figure 3.3 Sensitivity of Solution to Time and Space Steps

In presenting the results the cooling of a given lift is expressed in terms of the average heat content (lift volume × c × $T_{average}$) 30 minutes after the initial laying of the asphalt. The heat content value in the case of no compaction is taken as a base and all the results for a given lift thickness are expressed in terms of a normalized heat content, i.e.,

$$HC = \frac{\text{Heat Content (compaction at time t)}}{\text{Heat Content (no compaction)}} \tag{3.13}$$

The results are shown in Figure 3.4. The heat content is clearly a function of when the compaction is applied. With different compaction times there is a monotonic, but non-linear, increase in the heat content between the cases of instantaneous compaction and no compaction. The mechanism for this behavior is the increase in heat transfer after compaction driven by the combination of the increase in thermal conductivity and the decrease in the lift thickness. The cooling of thin to moderate lifts, with small compactions, is relatively insensitive to the

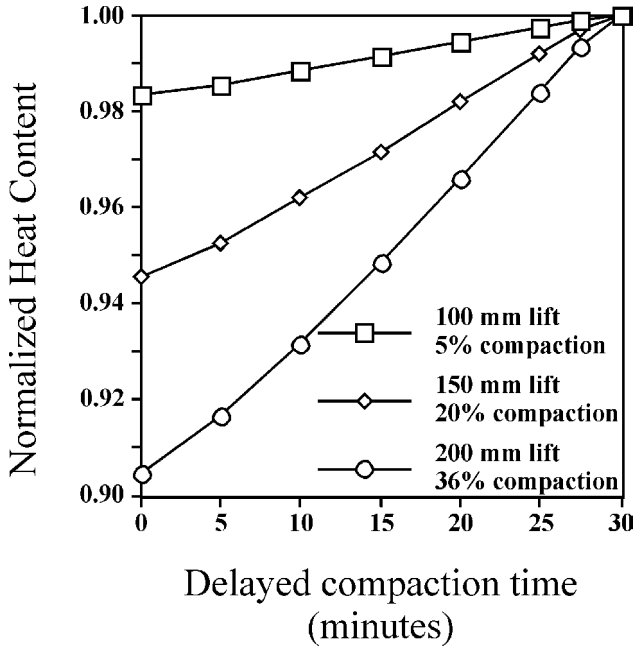

Figure 3.4 Normalized Heat Content of Various Lifts vs. Compaction Time

compaction process. Thick lifts which undergo large deformations, however, show a marked change with the compaction process, up to 10% change for the 0.2 m lift with a 36% compaction.

CONCLUSIONS

A model for describing the cooling of an asphalt pavement has been presented. The underlying numerical approach used in this model represents an improvement over previous asphalt cooling models in that it allows for compaction. Simulations, however, indicate that the effect of the compaction process on the cooling of the lift may only have an effect at the extremes of operating conditions.

Further chapters of this report will present more comprehensive testing of the numerical heat transfer modeling presented above. These chapters will also outline how the heat transfer model is coupled to thermal property measurements and compaction properties with temperature. A linking that leads to a sophisticated tool for scheduling paving operations under adverse conditions.

CHAPTER 4
THERMAL PROPERTIES

INTRODUCTION

Research was conducted to determine the different thermal properties have on hot-mix cooling rates and to investigate the feasibility of using thermal test methods for hot-mix asphalt. This is a continuation of work done by Chadbourn, et al [33]. Future research will provide more complete information on how asphalt thermal properties vary with respect to mix design, temperature, and density.

A model that can predict the cooling rates of many different types of mix designs requires extensive experimental data on the thermal properties of various hot-mix paving materials. This includes information about how hot-mix thermal properties vary with mix type, temperature, and density. A search of the literature revealed a wide range of reported thermal conductivity (k) values for asphalt concrete and limited information on the specific heat (c) and thermal diffusivity (α) of asphalt concrete (Table 2.5). Asphalt thermal properties for different mixture types and test temperatures were rarely reported in the literature.

The model also requires the input of thermal properties of the aggregate base and subgrade soil beneath the asphalt layer, although these properties are less important than those of the asphalt layer. Also, their effect on the cooling properties decreases with increasing distance from the asphalt layer. A literature search produced extensive data on soil and aggregate thermal properties; this research did not include the testing of pavement materials other than hot-mix asphalt.

Other variables which were addressed are the effects of wind velocity and net solar flux on the cooling rate of hot-mix asphalt. A simple method for estimating the convection coefficient between the air and the pavement surface based on wind velocity is presented. The net solar flux varies with latitude, day of the year, time of day, and cloud cover. Two meteorological models were combined to estimate the net solar flux at the surface based on time, location, and cloud cover information.

METHODOLOGY

Overview

A previous section addressed the lack of specific thermal property data on asphalt concrete materials. This section discusses a means of determining whether more specific thermal property information is required to accurately predict pavement cooling rates. A sensitivity analysis was conducted to determine the effects of thermal conductivity, specific heat and, indirectly, thermal diffusivity variations have on the theoretical cooling rates of hot-mix asphalt concrete (Figure 4.1). The results of this sensitivity analysis indicated a need for further analysis of asphalt concrete thermal properties, especially thermal conductivity and thermal diffusivity. This section concludes with a description of two thermal test methods as well as mix design and specimen compaction procedures. Detailed mix design and specimen compaction information is located in Appendix B. A more complete description of the thermal test procedures is provided in Appendix C.

Sensitivity Analysis Of Pavement Thermal Properties

There have been several studies done on asphalt pavement cooling rates in order to determine the best paving methods for various environmental conditions. Heat transfer models require the input of thermal properties such as thermal conductivity (k) and specific heat (c). Little is known about how these properties vary with temperature and type of pavement. Reported values of thermal conductivity for asphalt pavement vary widely in the literature. None of the sources reviewed for this study reported thermal conductivity values of asphalt pavement at temperatures higher than 38 °C, while paving mixtures are typically at temperatures higher than 135 °C. Table 2.5 gives a sample of reported thermal conductivity values. The purpose of this sensitivity analysis was to determine the effect of different pavement thermal conductivity values on the cooling rates of asphalt pavement.

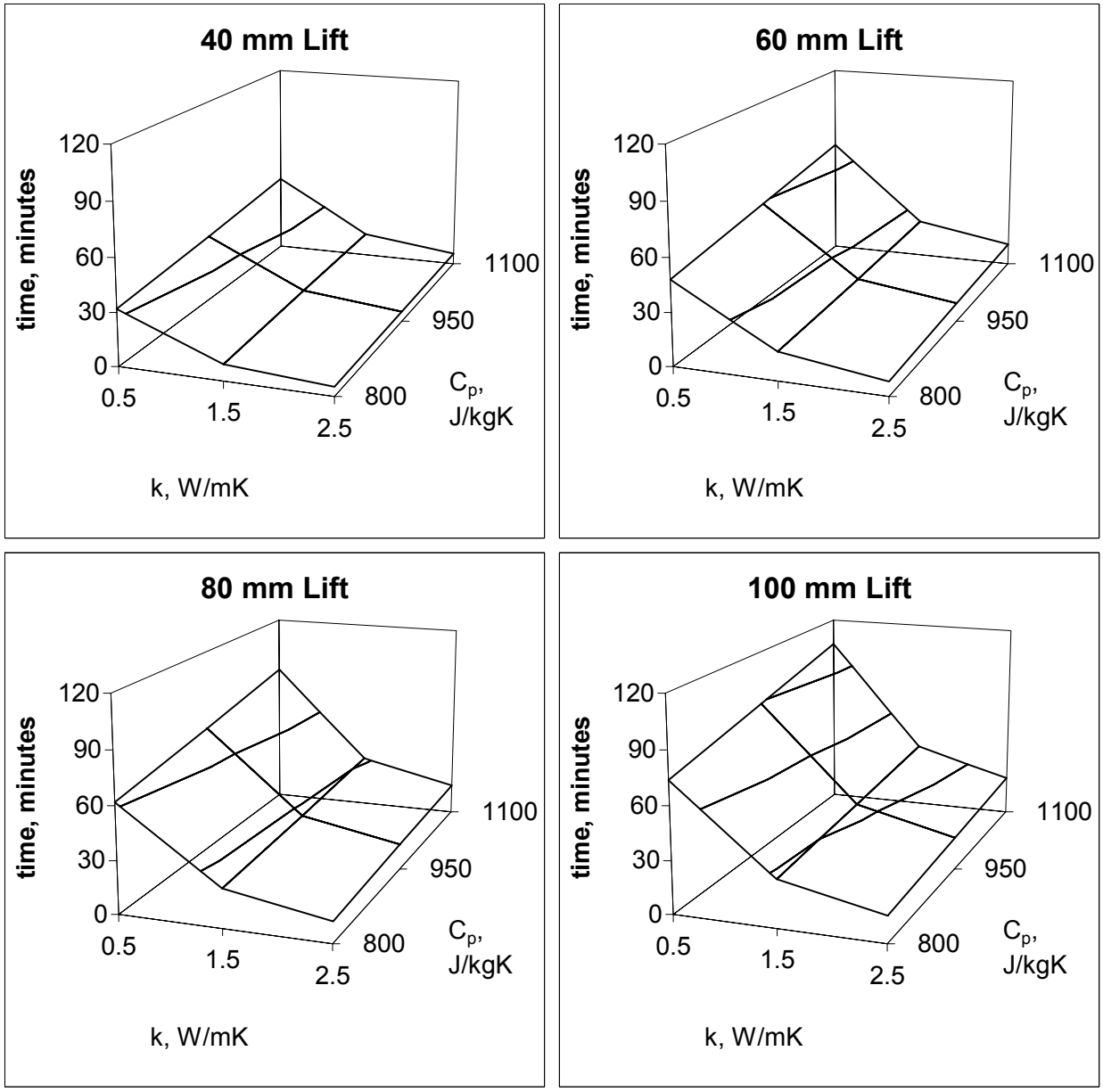

Figure 4.1 Simulated Pavement Cooling Times From 135 to 80 °C

Pavement Cooling Model

An explicit model similar to that developed by Corlew and Dickson [16] was used in a spreadsheet program on a personal computer (Appendix A). Time increment (Δt) and vertical increment (Δz) were chosen close to the values used in the Corlew and Dickson model. Other input values were similar to those used in Corlew and Dickson [16], with the exception of thermal conductivity and specific heat. The thermal conductivity values used in this study were varied from 0.5 to 2.5 W/m·K and the specific heat values were varied from 800 to 1100 J/kg·K

to include the range of reported values. This represents a variation in thermal diffusivity from 0.20 to 1.40 x 10^{-6} m^2/s. The initial mix temperature of 135 °C corresponds to the appropriate recommended compaction temperature for Marshall testing. The target temperature was chosen according to recommended compaction requirements. Tegeler and Dempsey [9] demonstrated that 80 °C is the temperature below which further compaction is impractical.

Simulations were run for pavement thicknesses of 40, 60, 80, and 100 mm. A 13 km wind speed was used. The air temperature and initial base temperature were assumed to be 10 °C.

Results

Figure 4.1 shows the effect of varying thermal conductivity and specific heat on pavement cooling time of a point 12 mm below the surface of the pavement from 135 °C to 80 °C. It is clear that thermal conductivity had the greatest effect on pavement cooling rates. The cooling time increased dramatically as the thermal conductivity approached 0.5 W/m·K. The variation of cooling times within the range of reported pavement specific heat values was not as great, but may warrant further study of this property.

Conclusions

The large effect that thermal conductivity values had on pavement cooling times and temperature profiles indicates a need to obtain thermal conductivity values for different paving materials and at different temperatures. Also of concern is the effect of pavement density on thermal properties, i.e. how cooling rates will be affected during compaction.

One option is to conduct laboratory tests for these thermal properties, use them in the model, and confirm them with field temperature measurements. Since this model requires only thermal diffusivity values rather than separate thermal conductivity and specific heat values, one may only need to measure thermal diffusivity directly with any appropriate transient heat flow method. Another option is to take field temperature measurements for several different paving materials and environmental conditions, and back-calculate the thermal properties.

Determination of Appropriate Thermal Property Testing Procedures

To estimate pavement cooling rates the thermal diffusivity of the pavement materials must be determined. The thermal diffusivity can either be estimated directly using a transient heat flow

method, or calculated from thermal conductivity, specific heat, and density data. A test for thermal diffusivity of asphalt concrete slabs was designed in order to provide the necessary thermal information for a pavement cooling computational model. It involved heating a slab specimen to a constant temperature, and measuring the temperature at several depths over a period of time as the slab cools. An ASTM procedure for determining thermal conductivity was modified for asphalt concrete cylinder specimens so that experimental results could be compared to the thermal conductivity values reported in the literature. The specimen required for this test was a cylinder similar in dimensions to pavement cores used in triaxial testing of asphalt concrete. Specific heat testing procedures were not considered for this thesis because most tests require a hot specimen to be immersed in a fluid. The properties of hot-mix asphalt made this procedure impractical.

Mix Design

Mixtures for this study were selected in order to represent the two types that would be likely to exhibit the most different thermal properties. The mixes selected were a standard dense-graded mix, and a 6.0 mm maximum aggregate size stone matrix asphalt (SMA) mix. The particle size distribution curves are shown in Figure 4.2. The aggregate used consisted of crushed granite for particle sizes of 9.5 mm and greater, and a river gravel for particle sizes of 4.75 mm and less.

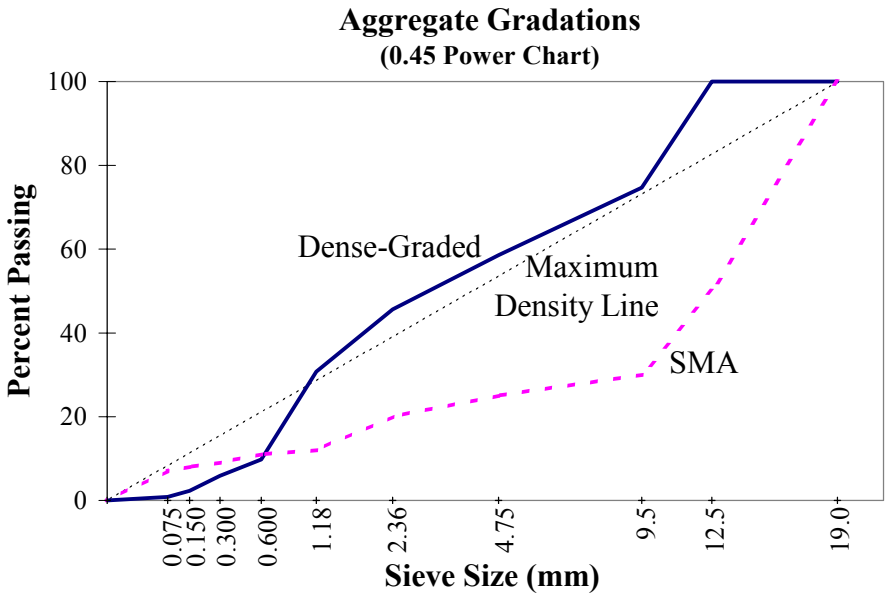

Figure 4.2 Aggregate Gradations Used in Thermal Testing

More detailed material properties are shown in Appendix B. A 120/150 penetration asphalt was used for both mixes.

The asphalt and aggregate were mixed by the Minnesota Department of Transportation (Mn/DOT). Preliminary mixes were aged according to ASTM standards. Enough of each mix was prepared to compact three slabs, two cylinders, and conduct a theoretical maximum specific gravity analysis.

Compaction of Slab Specimens

The compaction procedure was modeled after a process used by Scholz, et al. [34]. The main advantage of rolling wheel compaction related to this study is the ability to compact a slab specimen that approximates an infinite wall, one-dimensional heat transfer condition. The slabs compacted by Scholz, et al [32] were typically 710 x 710 x 100 mm, and were compacted with a motorized steel wheel roller. Scholz, et al [32] reported a typical lateral air void variation of ± 0.6 percent and depth air void variation of ± 1.5 percent.

Slabs of dimensions 380 x 380 x 64 mm were used for this research. The thickness was determined as that of a typical asphalt lift, and the horizontal dimensions were calculated to produce a thickness-to-length ratio less than 0.2. Fwa [26] stated that this is the limiting d/L value for square slabs to ensure that temperature variations at mid-slab can be modeled using one-dimensional plane-wall theory. A smaller version of the ramp and mold system used by Scholz, et al [32] was constructed out of wood. Instead of a motorized, steel-wheel roller, a water-filled 460 mm diameter x 560 mm length lawn roller was used to compact the specimen. The total weight of the roller and water at 25 °C was 115 kg. Ordinarily, in order to best simulate field conditions, the mix would be aged for 3 to 4 hours. However, it was found that aging made both the dense-graded and SMA mixes too harsh for complete compaction with this roller. Since the main objective of this procedure was to compact slab specimens of uniform thickness, the final mixes were not aged prior to compaction. It should be noted that the slab specimens were aged at temperatures between 145 and 150 °C for several hours as a result of the thermal testing procedure.

The roller weight was sufficient to compact a dense-graded mix to approximately 11 percent air voids, but was only able to compact the stone matrix asphalt (SMA) mix to approximately 17 percent air voids (Table 4.1). Although a heavier roller will be required to compact a greater variety of research specimens, the specimens compacted using this roller were of sufficient density to determine the feasibility of thermal property procedures for asphalt concrete and to indicate how asphalt concrete thermal properties vary with temperature and density.

Compaction of Cylindrical Specimens

The thermal probe procedure (ASTM Designation: D 5334 - 92: Standard Test Method for Determination of Thermal Conductivity of Soil and Soft Rock by Thermal Needle Probe Procedure) required a probe consisting of a hollow metal tube, 1.6 mm outside diameter, 1.3 mm inside diameter, a loop of 0.25 mm diameter (No. 30) heating wire, and a 0.25 mm diameter (No. 30) copper-constantan thermocouple. The probe described in the procedure is designed to extend to a depth of 100 mm into the specimen; however, for harder rock specimens that cannot be drilled to that depth can be tested with a probe as short as 25 mm as long as the specimen is at least 100 mm longer than the probe. The heating wire should run the entire length of the probe, with the thermocouple junction located at mid-length. The remaining space inside the probe

Table 4.1 Asphalt Concrete Specimen Air Void Statistics

Specimen	Average Air Voids (percent)	Standard Deviation
Dense-Graded Loose Mix	21.0	0.99
Dense-Graded Mid-Compaction (slab)	14.5	1.17
Dense-Graded Full Compaction (slab)	11.1	1.81
Dense-Graded Full Compaction (cylinder)	4.8	----------
SMA Loose Mix	25.9	1.31
SMA Mid-Compaction (slab)	19.5	2.09
SMA Full Compaction (slab)	16.7	3.60
SMA Full Compaction (cylinder)	8.0	----------

should be occupied by a high thermal conductivity, high temperature epoxy.

The specimens should be cylindrical and at least 100 mm in diameter and 200 mm in height. The specimens used for this study were similar to those used in static and dynamic creep testing, 100 mm in diameter, and approximately 200 mm in height, roughly the equivalent of three Marshall specimens stacked one on top of the other.

The tall cylindrical specimens used in the thermal probe procedure were compacted by a modified Marshall hammer compaction procedure developed at the University of Minnesota. The mold consisted of a steel tube with an inside diameter of 100 mm and a height of 254 mm. The cylinder rested on top of a base plate. The base plate was modified for this research. A steel rod 2.4 mm (3/32 in.) in diameter was fixed to the center of the base plate so that it extended 46 mm into the compacted specimen. This created a hole in one end of the specimen so that a 2.0 mm by 46 mm thermal probe could be inserted. Ideally, the hole in the specimen would have the same diameter as the probe. This was not possible due to unavailability of 2.0 mm steel rod. The discrepancy was compensated for by coating the probe with a high thermal conductivity grease.

The compactor used was a single rotating base Marshall hammer apparatus consisting of a rotating chain with pegs that repeatedly raise and drop a 11.3 kg hammer from a height of 500 mm. It was originally designed to prepare large stone specimens with a diameter of 150 mm. This apparatus was adapted to accommodate a 100 mm diameter by 250 mm mold. The modification involved replacing the 150 mm foot with a 100 mm foot and mounting a new collar on the compactor to secure the top of the mold. The specimens were compacted in three 1300 g lifts. The number of blows for each successive lift was increased in order to equalize the compactive effort received by the three lifts. The number of blows used for the bottom, middle, and top lifts were 20, 35, and 55, respectively.

Asphalt Pavement Thermal Property Measurements

Slab Cooling Method for Thermal Diffusivity of Asphalt Concrete

Given a specimen of dimensions that approximate homogeneity and conditions that approximate one-dimensional conductive heat flow, it is possible to determine the thermal diffusivity from a first-order time-temperature relationship and a second-order space-temperature relationship. Constant heat flow and constant boundary temperatures are not required. This makes thermal diffusivity measurements possible from a very simple test configuration of an asphalt slab, insulated on the sides and bottom, with the top surface exposed to air at a different temperature. Spatial and temporal temperature gradients can be measured with three or four thermocouples at known depths in the specimen, with temperature readings taken at regular time steps (Figure 4.3).

The thermal diffusivity measurement procedure and apparatus were relatively simple. A steel box was welded to support a 25 kg slab. The insulation used was an inexpensive mineral fiber board which was cut to insulate the bottom and sides of the slab and wrapped in heavy paper to

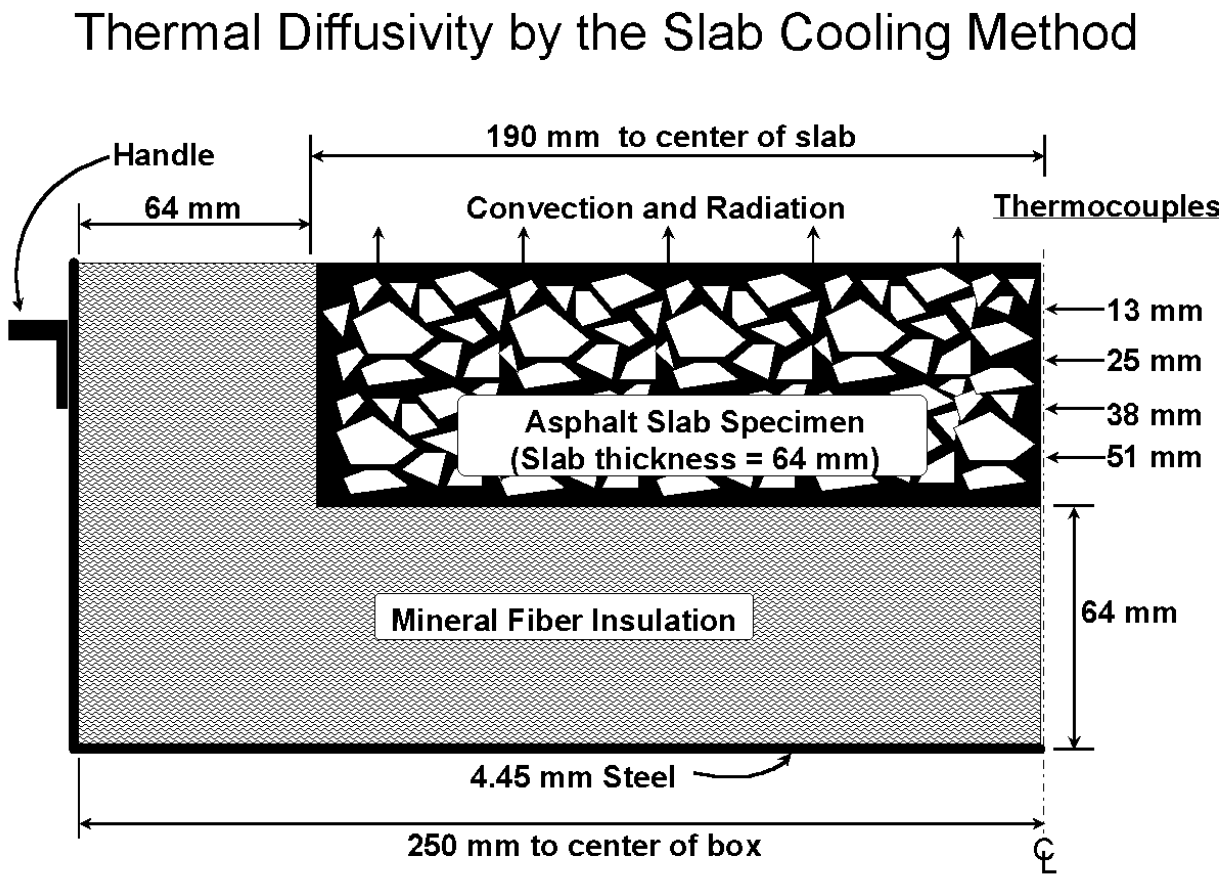

Figure 4.3 Schematic for Thermal Diffusivity by the Slab Cooling Method

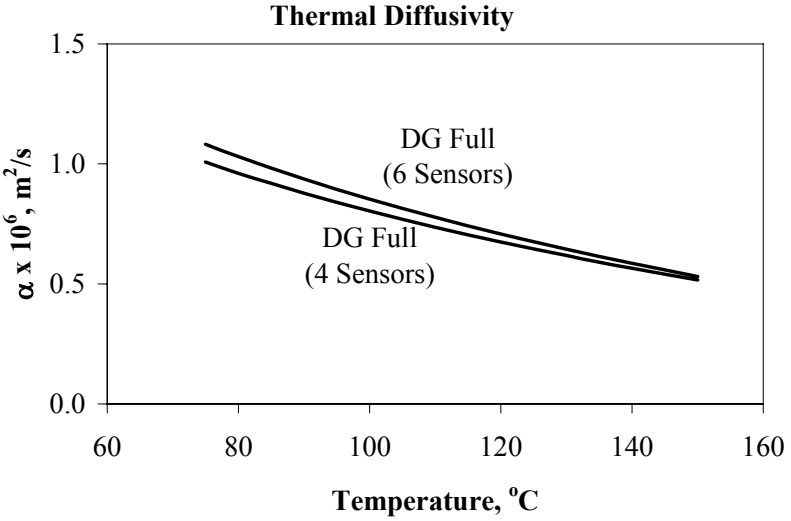

Figure 4.5 Comparison of 6-Sensor and 4-Sensor Methods

prevent the fibers from sticking to the asphalt.

Thermocouples were placed at six locations in the fully-compacted dense-graded slab to test the necessity of using more than four thermocouples. The six thermocouples were placed at depths of 6, 13, 19, 25, 38, and 50 mm. The first and third thermocouple readings were disregarded for the four-thermocouple method. The results of this comparison are shown in Figure 4.5. The effect of using only four thermocouples was a 5 percent decrease in calculated thermal

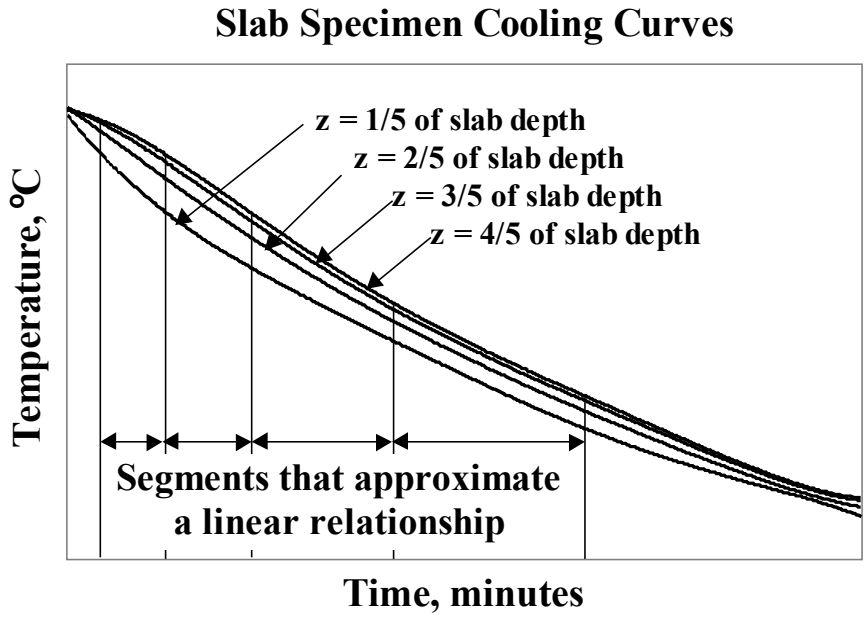

Figure 4.4 Selecting Segments That Approximate a Linear Relationship

diffusivity. This translates into about a 1 percent increase in time required for a pavement to cool from 135 °C to 80 °C (based on simulations). These differences were determined to be of little consequence for the purposes of this study, and the four-thermocouple method was used.

To determine the variation of thermal diffusivity with temperature, select small time intervals

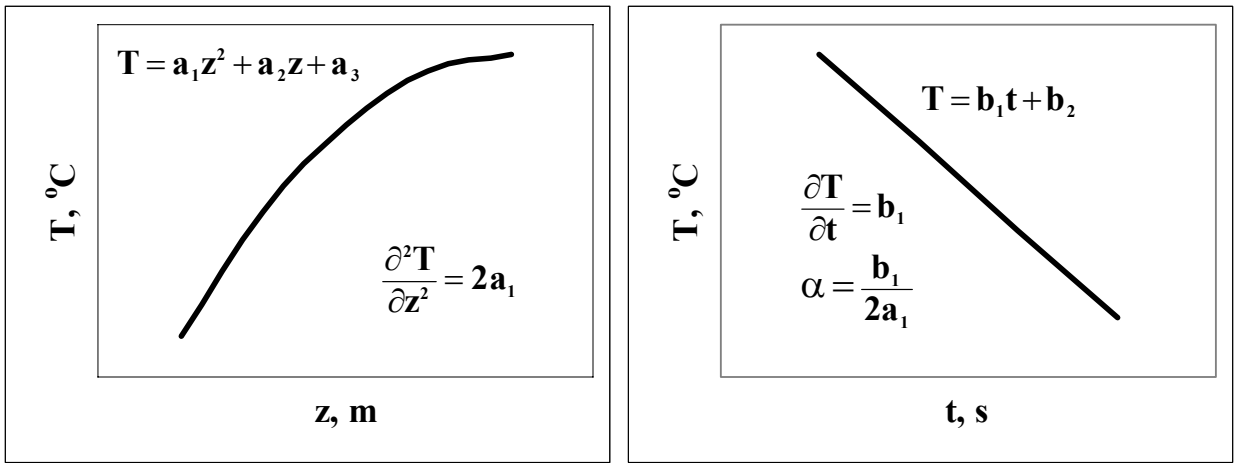

Figure 4.6 Curves and Equations Used to Calculate Thermal Diffusivity

which approximate linear relationships (Figure 4.4). At each time step, plot the average spatial temperature, and fit a linear relationship (Figure 4.6).

$$T = b_1t + b_2 \tag{4.1}$$

To approximate the spatial relationship, average the temperature readings at each depth over each time interval. Plot the average temperature versus time and fit a second-order relationship.

$$T = a_1z^2 + a_2z + a_3 \tag{4.2}$$

Eq. (2.8) can be rearranged to produce the following relationship:

$$\alpha = \frac{\frac{\partial T}{\partial t}}{\frac{\partial^2 T}{\partial z^2}} \tag{4.3}$$

Determine the first derivative of Eq. (4.1) with respect to t.

$$\frac{\partial T}{\partial t} = b_1 \tag{4.4}$$

Determine the second derivative of Eq. (4.2) with respect to z.

$$\frac{\partial^2 T}{\partial z^2} = 2a_1 \tag{4.5}$$

Substitute Eqs. (4.4) and (4.5) into Eq. (4.3) to determine the thermal diffusivity.

$$\alpha = \frac{b_1}{2a_1} \tag{4.6}$$

Plot the thermal diffusivity against the average temperature over the corresponding time interval and note the relationship between thermal diffusivity and temperature. Determine the relationship between thermal diffusivity and density by testing specimens of different densities.

Thermal Probe Method for Thermal Conductivity of Asphalt Concrete

This procedure (ASTM Designation D 5334: Standard Test Method for Determination of Thermal Conductivity of Soil and Soft Rock by Thermal Needle Procedure) required the construction of a thermal probe (Figure 4.7). Little modification was required to measure the thermal conductivity of asphalt concrete. The tall asphalt specimens conformed to the minimum diameter and length requirements. The main difficulty involved the acquisition of a thermal probe. The probe was constructed per the instructions in the test method. The main difficulty involved finding a high-conductivity cement that was workable enough to draw through a 50 mm length of 1.6 mm (1/16 in.) stainless steel tubing. After several attempts, a working probe was constructed using a 2.4 mm (3/32 in.) tube.

The probe was inserted into the end of a cylindrical asphalt specimen (minimum dimensions are 100 mm in diameter by 150 mm in height) and a constant current was applied to the heating wire. The change in temperature with respect to time was then measured and plotted on a semi-log scale, and the thermal conductivity was determined from the linear portion of the curve (Figure 4.8).

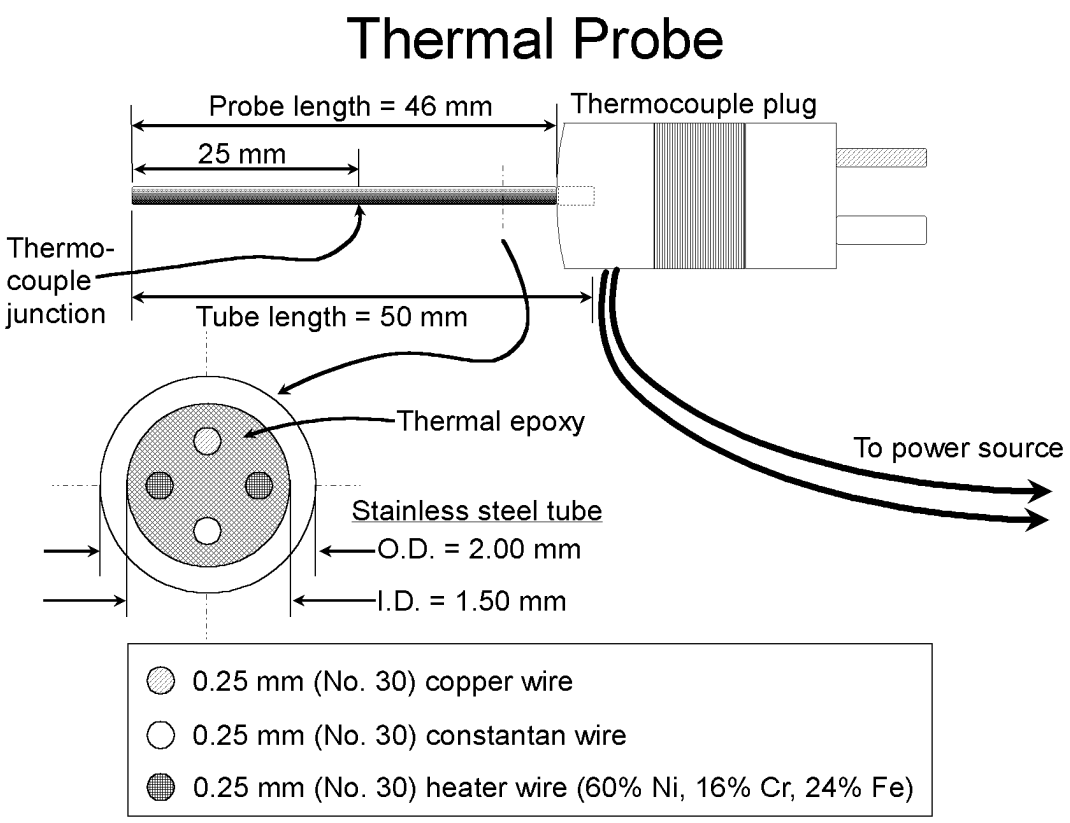

Figure 4.7 Thermal Probe Components

Evaluation of Compaction Processes

After the thermal testing was completed, the specimen air voids were determined. The theoretical maximum specific gravity was determined from loose mix that was set aside after mixing. The test method used is outlined in D 2041 - 91: Standard Test Method for Theoretical Maximum Specific Gravity and Density of Bituminous Paving Mixtures.

The bulk specific gravity of the slab specimens was determined by cutting each slab into nine 125 x 125 x 64 mm sections. The sections from the roller-compacted slabs were also cut horizontally to compare the air voids in the top and bottom halves of the slabs. Each section was labeled according to its position in the slab (see Appendix E, Figure E.1). The bulk specific gravity of the slab sections was determined by the Parafilm-coated specimen method (ASTM D1188-96: Standard Test Method for Bulk Specific Gravity and Density of Compacted Bituminous Mixtures Using Paraffin-Coated Specimens).

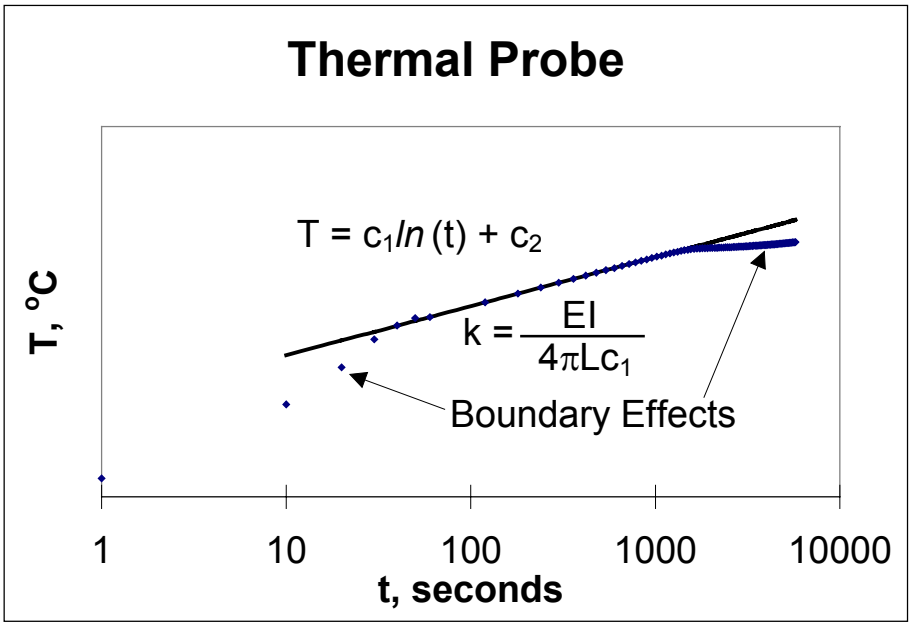

Figure 4.8 Equations Used to Calculate Thermal Conductivity

The bulk specific gravity of the cylindrical specimens was determined according to ASTM D 2726 - 90 Standard Test Method for Bulk Specific Gravity and Density of Compacted Bituminous Mixtures Using Saturated Surface-Dry Specimens.

The air voids of all specimens were calculated according to ASTM D 3203 - 91: Standard Test Method for Percent Air Voids in Compacted Dense and Open Bituminous Paving Mixtures.

RESULTS OF THERMAL TESTING

Density Analysis

Table 4.1 summarizes the slab and cylinder specimen air void data. The air void level of 11.1 percent in the dense-graded full compaction slab specimen exceeded the design air void level of 8.0 percent. The air void level in the SMA full compaction slab specimen was more than twice the design air void level and the compacted specimen exceeded the height of the mold, so it was not used for thermal testing. The SMA mid-compaction specimen was used in place of the full-compaction specimen.

The overall variation in air voids increased with increasing density for both the dense-graded and SMA specimens, as is indicated by the standard deviation values in Table 4.1. The difference between air voids in the top and bottom halves also showed variability increasing with density in

the roller-compacted specimens. In the dense-graded mid-compaction slab, the top half of the slab had an average air void value 0.3 percent greater than that of the bottom half, while the air void level in the top half of the dense-graded full compaction slab was 0.7 percent less than that of the bottom half (see Appendix E, Figure E.2). In the SMA mid-compaction slab, the top half had a 2.0 percent greater air void value than the bottom half, and in the SMA full compaction specimen the top half had a 4.1 percent greater air void value (Figure E.3).

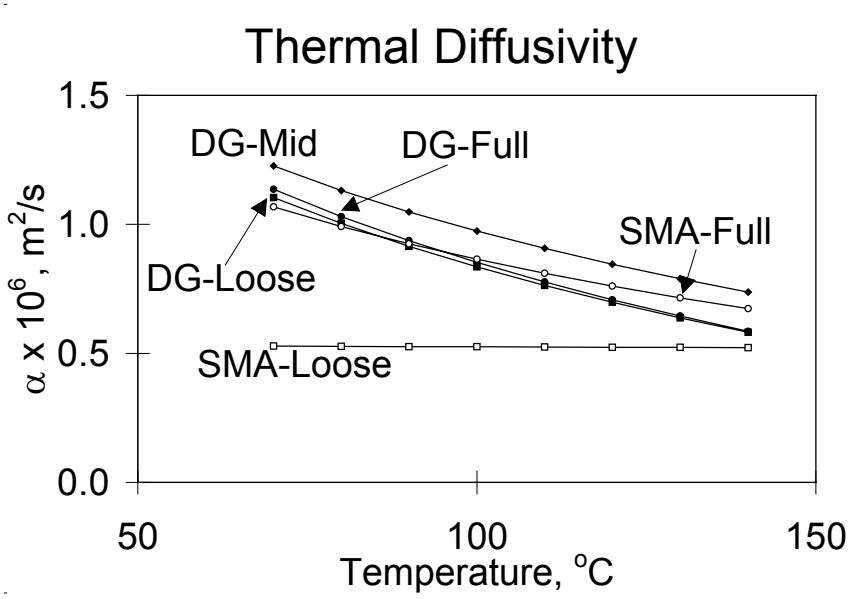

Figure 4.9 Thermal Diffusivity vs. Temperature

Thermal Diffusivity

Figure 4.9 shows the measured thermal diffusivity versus temperature for three dense-graded and two stone matrix asphalt concrete specimens. All except the SMA loose mix specimen exhibited a decrease in thermal diffusivity as the temperature increased. Values ranged from 1.1 x 10^{-6} to 1.3 x 10^{-6} m^2/s at 70 °C to 0.5 x 10^{-6} to 0.7 x 10^{-6} m^2/s at 140 °C. The SMA loose mix displayed very little change, with a value near 0.5 x 10^{-6} m^2/s over the temperature range of the test.

The thermal diffusivity of the dense-graded specimens peaked at a point between the two density extremes (Figure 4.10). The peak was more pronounced at higher temperatures. If a similar trend occurred for SMA specimens, it is not evident in these results, as there were only two data points.

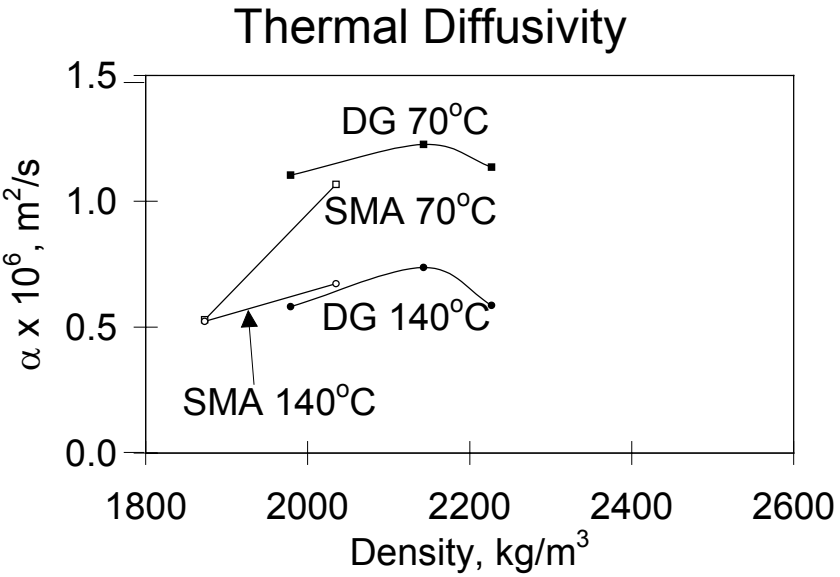

Figure 4.10 Thermal Diffusivity vs. Density

Thermal Conductivity

The thermal conductivity of the two mix types was quite different. The dense-graded mix had values ranging between 2.0 and 2.5 W/m·K, while the SMA values ranged from 0.6 to 1.5 W/m·K (Figure 4.11). All specimens demonstrated similar thermal conductivity behavior with respect to temperature, with a decrease of approximately 0.2 W/m·K as the temperature rose from 25 to 75 °C.

The variation of thermal conductivity with density was also different for the dense-graded and SMA mixes (Figure 4.12). Both mixes exhibited a positive correlation between thermal conductivity and density, but the SMA mix had a much steeper slope.

Effect on Asphalt Pavement Cooling Rates

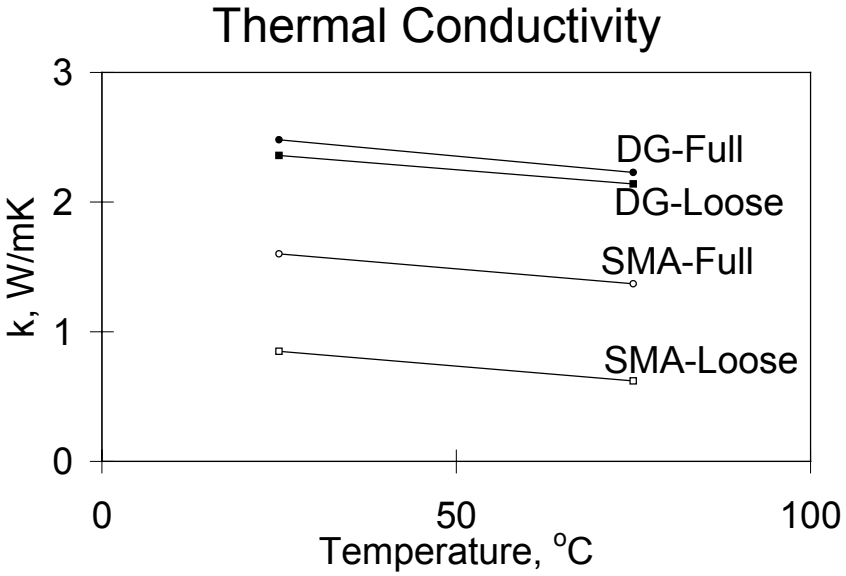

Figure 4.11 Thermal Conductivity vs. Temperature

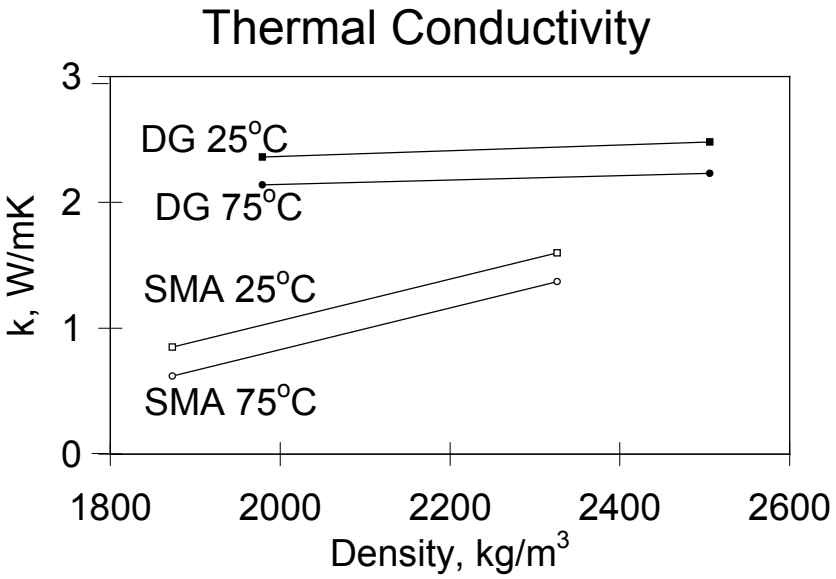

Figure 4.12 Thermal Conductivity vs. Density

Pavement cooling computer simulations were conducted for the thermal diffusivity and thermal conductivity values determined in this study. For the purposes of comparison, the specific heat was held constant at 920 J/kg·K, the value recommended by Corlew and Dickson [16]. The ranges of both the thermal diffusivity (Figure 4.13) and thermal conductivity (Figure 4.14) values represent a tripling of the cooling rate of a 40 mm lift and a quadrupling of the cooling rate of a 100 mm lift.

CONCLUSIONS

Compaction

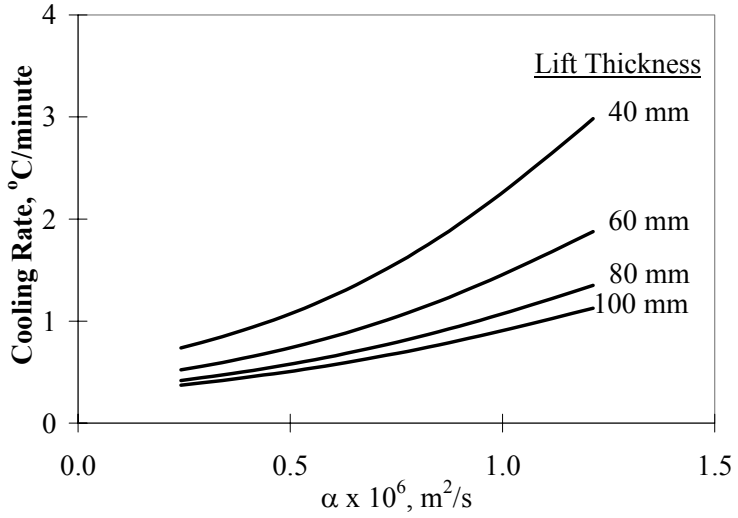

Figure 4.13 Cooling Rate vs. Thermal Diffusivity

The slab compaction procedure developed for this research is relatively simple, but required up to 25 kg of hot-mix asphalt per specimen. The115 kg roller used was not able to compact the

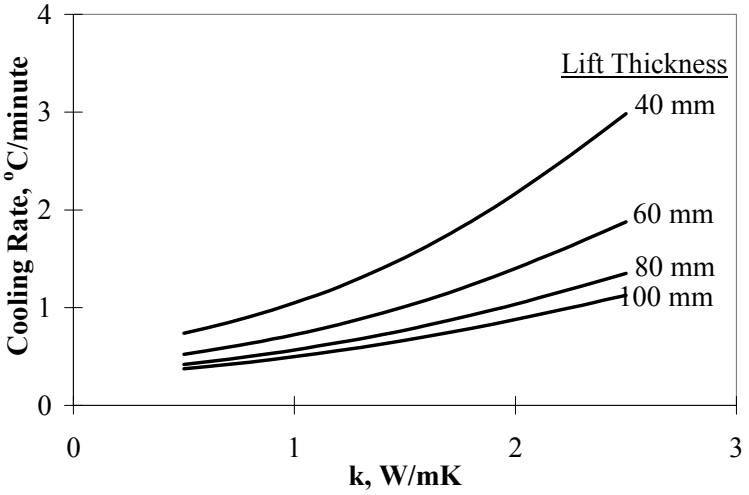

Figure 4.14 Cooling Rate vs. Thermal Conductivity

SMA mix beyond 8 percent air voids. Another difficulty involved placing the loose mix into the mold. Initially, some of the mix spilled out of the mold during compaction, getting between the

edge of the mold (which served as a stop for the roller). This required briefly removing the roller so that the particles could be brushed aside. Five of the six slabs compacted were adequate for thermal testing. The sixth slab, which was to be the fully compacted SMA specimen, could not be compacted to the level of the mold.

The large air void values in dense-graded and SMA slab specimens indicate that the rolling procedure described in this thesis is not adequate for an analysis of fully-compacted asphalt pavement thermal properties. However, the data is useful in terms of analyzing the thermal properties during compaction, which is the goal of this research. Modifications to the roller weight may result in a useful procedure for dense-graded mixtures, but a larger specimen size will most likely be required for large stone specimens.

The three-lift compaction procedure produced specimens of adequate density, although the SMA mix would not compact below the 8 percent air void level. This procedure should be useful for further thermal probe testing, but research to determine the number of blows per lift for a range of specimen densities is required.

Thermal Diffusivity

Due to difficulties acquiring thermal test standards in the desired range of thermal diffusivity and thermal conductivity values and in the proper dimensions, thermal diffusivity and thermal conductivity values were determined by uncalibrated testing procedures. Therefore, the values should be used only to judge the relative effects of mix type, temperature, and density on thermal diffusivity and pavement cooling rates.

The differences in measured thermal diffusivity values for each specimen do not follow a clear pattern. There may be errors associated with the placement of the thermocouples. The theory used in the calculation of thermal diffusivity assumes a homogeneous material, so the size of the aggregate particles may have affected the accuracy of the results. A large, highly conductive aggregate particle located between two thermocouples would cause the thermal diffusivity at that point to greater than that of the mixture. Also, a large void filled with air or asphalt would lower the apparent thermal diffusivity. Another source of error resulted from asphalt drain-down in the SMA specimens, although this occurred during the heating phase, and not during the cooling phase during which the measurements were taken.

The peak thermal diffusivity that occurred in the mid-compaction dense-graded slab was most likely due to errors caused by large aggregate particles between thermocouples. The variation in thermal diffusivity values and their effect on pavement cooling rates indicates the need for further verification of their values and measurements on other types of asphalt concrete.

The range of thermal diffusivity values measured in this study, 0.5 x 10^{-6} m^2/s to 1.3 x 10^{-6} m^2/s, corresponds to a large variation in cooling rates, °C/min., as predicted by the spreadsheet model used in the sensitivity analysis.

The thermal diffusivity values measured represented a two- to three-fold increase in the average cooling rates as the temperature dropped from 140 °C to 70 °C for all but the SMA loose mix specimen. This trend was expected; according to Kersten [17], the thermal conductivity of asphalt concrete decreases with temperature and the specific heat of dry aggregates increases with temperature, and Saal [19] showed that the specific heat of asphalt binders also increases with temperature. A minimal density change within this temperature range is expected, so the thermal diffusivity of asphalt concrete as calculated by Eq. (2.5) would decrease with temperature. The difference in the SMA loose mix specimen may be due to the effect of large air pockets. According to Ozisik [20], the thermal diffusivity of air increases with increasing temperature, which may cancel the temperature effects of the solid components.

The variation in thermal diffusivity with density was more difficult to interpret. The thermal conductivity is expected to increase with density, but increasing the density value in the denominator of Eq. (2.5) reduces the calculated thermal diffusivity value. Also, very little is known about how asphalt specific heat varies with density.

Thermal Conductivity

Tests conducted on the dense-graded specimens resulted in reasonable curves with easily recognizable linear segments on the semi-log plots (See Appendix E, Figure E.6). The SMA specimens presented difficulties as initial large temperature gradients developed between the probe and the specimens. This resulted in plots with short or non-existent linear portions. In addition to the error in calculated thermal conductivity values caused by this gradient, the effective temperature of the test was often ambiguous. The probe temperature was at times

50 °C greater than the initial specimen temperature. As a result, accurate thermal conductivity/temperature relationships were difficult to define. Due to the dramatic increase in probe temperature for these specimens, the elevated temperature test was performed at 75 °C to avoid excessive aging of the asphalt binder.

The thermal conductivity of the SMA specimens is significantly lower than that of the dense-graded specimens, but all specimens show similar temperature-related trends. The temperature range of the thermal conductivity results is 25 to 75 °C, which is significantly lower and somewhat smaller than the temperature range of the thermal diffusivity results, 70 to 140 °C. The model used in the sensitivity analysis indicates that decreasing the temperature from 140 to 70 °C results in a 20 percent increase in the cooling rate for the dense-graded mix, and between a 50 and 80 percent increase in the cooling rate for the SMA mix.

All values fall within the range of reported asphalt pavement thermal conductivity values (Table 2.5) However, since the apparatus was not calibrated with a standard reference material, these results should be used only to identify general trends in thermal conductivity values.

Effect on Asphalt Pavement Cooling Rates

Although the asphalt pavement thermal properties determined by the slab cooling and thermal probe methods have not yet been verified with thermal test standards, the range of cooling rates predicted by this analysis indicate a need for further study of these properties and how they relate to late season hot-mix asphalt paving.

CHAPTER 5
COMPACTION PROPERTIES

INTRODUCTION

The lack of control over the range of field compaction temperatures may cause densities lower than what is specified, leading to pavement distresses. The current method for determining the laboratory compaction temperature of the mix is to plot log-log viscosity versus log temperature, and determine the temperature which corresponds to a viscosity of 1.7 Poise (McLeod [5]). Corlew and Dickson [16] specified a minimum compaction temperature of 80°C in 1968 for use with graphs to determine the time limits for compaction. These guidelines provide an idea of when compaction should begin and end, but they do not provide a temperature range in which compaction can be maximized with the minimum amount of effort. Maximum and minimum compaction temperatures should be based upon mixture type to ensure that density requirements can be met.

Laboratory and field produced asphalt concrete mixtures were tested to determine compaction parameters for different mixture types over a range of temperatures that would be typical of field compaction. Six different laboratory mixtures were created using three different asphalt grades and two different aggregate gradations. Seven different field mixes were also tested. Two of the field mixtures had dense graded aggregate structures typical of pavements constructed in Minnesota, and five mixes were coarse, angular Superpave mixtures. A gyratory compactor was used to prepare all samples. Using the range of temperatures observed in the field during compaction and the amount of shear stress in the sample during compaction, the optimum compaction range was determined. The power required to compact the samples was used as an indicator of the effort required to compact a particular mixture type.

SUMMARY OF MIXTURE TYPES

This study used six different laboratory fabricated mixes and eight mixes sampled from paving projects in the state of Minnesota during the summers of 1996 and 1997. This wide variety of mixes was used to determine the effects of aggregate and asphalt properties on compaction

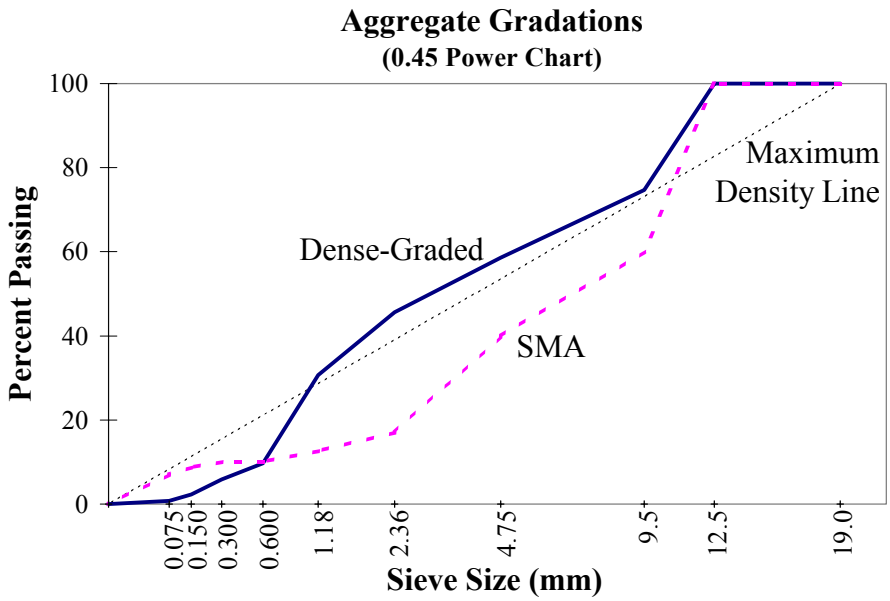

Figure 5.1 Gradations Used in Compaction Testing

properties of asphalt-aggregate mixtures. Laboratory produced mixtures were used because of the control over the proportions of aggregate and asphalt. This allowed for comparison of compaction parameters of mixes with different aggregate gradations and different asphalt types.

Laboratory Mixes

Laboratory mixes were produced using two aggregate gradations and three different asphalt grades for a total of six different mixes. Dense graded and SMA structures (Figure 5.1) were used to investigate the effect of different aggregate structure on compaction requirements. The

Table 5.1 Laboratory Mix Properties

Mix Number	Gradation Type	Asphalt Grade	Asphalt %	Filler %
1	Dense	PG 52-34	5.5	-----
2	Dense	85/100 pen	5.5	-----
3	Dense	PG 58-28	5.5	-----
4	SMA	PG 52-34	6.0	0.3
5	SMA	85/100 pen	6.0	0.3
6	SMA	PG 58-28	6.0	0.3

9.5-mm fraction of each gradation was crushed granite while the remaining portion of the gradation was a more rounded gravel. Material from a bag house was substituted for the 0.075 mm fraction of the gradation due to poor yield of this size material in the gravel. Three different asphalt grades (PG 58-28, PG 52-34 and 85/100 pen) were used to compare viscosity effects on compaction. Cellulose fiber filler was used in all mixes with a SMA gradation to prevent drain down of asphalt during mixing and compacting. Mixture properties are shown in Table 5.1.

Field Mixture Properties

Field mixes were sampled from eight projects in Minnesota during the summers of 1996 and 1997. Table 5.2 shows the project names, year completed, and mixture type. Two of the eight mixes were dense Minnesota mixes. The remaining mixes were designed using Superpave specifications. One of the Superpave gradations had a denser gradation and went through the restricted zone.

FIELD DATA AND SAMPLING

Temperature data collected from various sites were obtained using temperature probes constructed from thermocouple wire and wooden supports. Probes were constructed to lengths of 51 and 76 mm. Each probe could be used at its original length or could be shortened to fit thinner asphalt lifts. Probes were inserted into the mat at either a 45^{o} angle or vertically. Inserting the probe at a 45^{o} angle helped to prevent the wires on the probe from being severed during compaction (Figure 5.2). Temperatures were then recorded every one to five minutes and after every roller pass. The spatial average of the temperatures was determined using the formula:

$$T_{ave} = \frac{\sum_{i=0}^{n} T_i L_i}{\sum_{i=0}^{n} L_i} \qquad (5.1)$$

Table 5.2 Project Names and Dates

Date	Project	Mix Type
8/1/96	Highway 14	Dense Graded
8/27/96	Stearns County Highway 75	Superpave
9/5/96	Highway 8 Blue Earth County	Superpave
9/10/96	I-35 Owatonna	Superpave
10/4/96	Highway 169 Mankato	Dense Graded
8/26/97	Highway 25	Superpave Restricted Zone (Mix B)
8/26/97	Highway 25	Superpave Coarse Mix (Mix A)
8/26/97	Mn/ROAD	Superpave Restricted Zone (Mix B)
8/26/97	Mn/ROAD	Superpave Coarse Mix (Mix A)
9/17/97	I-494	Superpave

Where:

T_i = Temperature at location (i)

L_i = Vertical distance assigned to location (i)

n = Number of thermocouples embedded in the asphalt lift (T_0 represents the infrared surface reading)

$$L_i = \begin{cases} \frac{z_1}{2} & i = 0 \\ \frac{z_{i+1} - z_{i-1}}{2} & 0 < i < n \\ H_T - \frac{z_{n-1} + z_n}{2} & i = n \end{cases} \qquad (5.2)$$

Where:

z_i = Distance from the surface to location (i)

H_T = Lift thickness

The temperature probes were constructed of 30 AWG copper-constantan thermocouple wire attached to wooden slats. Wooden slats were used for their low thermal conductivity. The wire

was chosen because it was fine enough to produce a fast temperature response and had a 260 °C capacity. A schematic of a temperature probe is shown in Figure 5.3.

Mixtures were sampled behind the paver near where temperature data were taken. This ensured that the mix sampled was from the same truckload as the mix where temperature data were taken. The delivery temperature of the mix, air and surface temperatures, and weather conditions were also recorded in addition to cooling data.

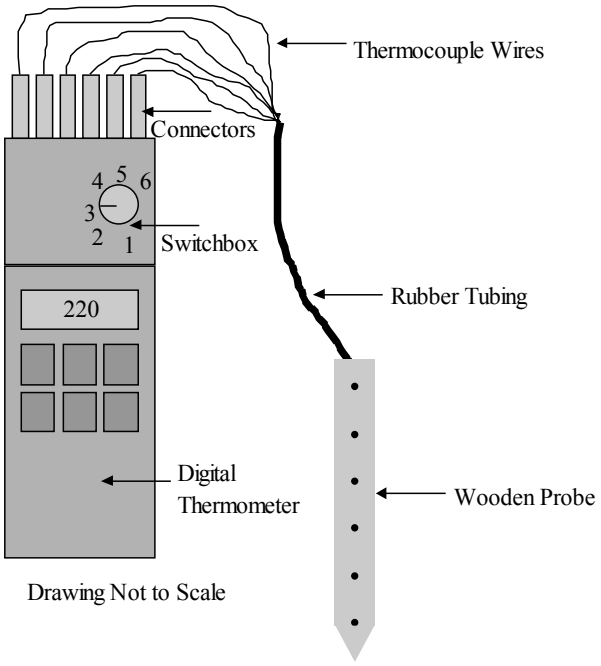

Figure 5.3 Temperature Probe Configuration

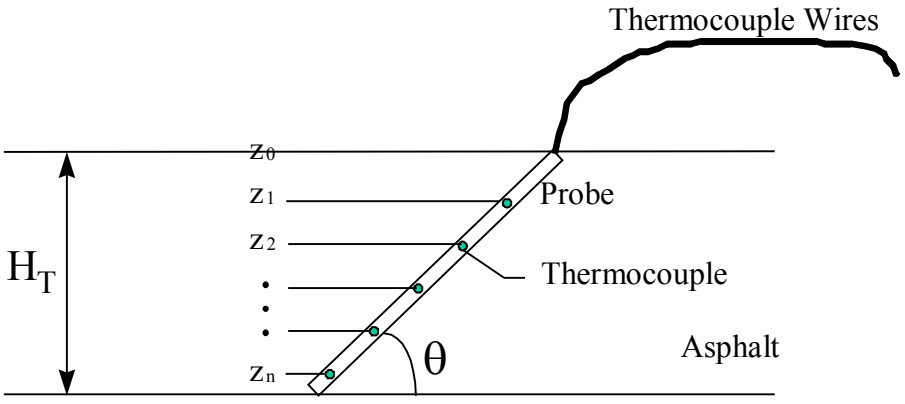

Figure 5.2 Probe Position in Asphalt Mat

Material collected from the field was then brought back to the laboratory and split into the appropriate sample sizes. Material sampled during the summer of 1996 was split into 1300-gram packages to be compacted later. These were then compacted into samples 100 mm in diameter and 64 mm in height. Standard Superpave samples which have a diameter of 15 cm were not used for the first round of testing because the gyratory compactor did not have pressure capacity to compact large samples. Material collected during the summer of 1997 was compacted into standard size 150-mm Superpave samples.

LABORATORY COMPACTION

An Intensive Compaction Tester (ICT) gyratory compactor produced by Invelop Oy of Finland was used to create all laboratory samples. This compactor operates on a "shear-compaction" principle. Compaction with this type of device occurs through two mechanisms: shear displacement and vertical pressure. These two elements allow for the distortion and reorientation of particles, which is necessary for the compaction of a particulate medium. A piston that transmits a force to a plate that rests on top of the asphalt sample applies the vertical pressure. Figure 5.4 shows the set up of the sample during compaction. The gyratory motion of the compactor creates the shear force required for compaction. Figure 5.5 shows a schematic of the

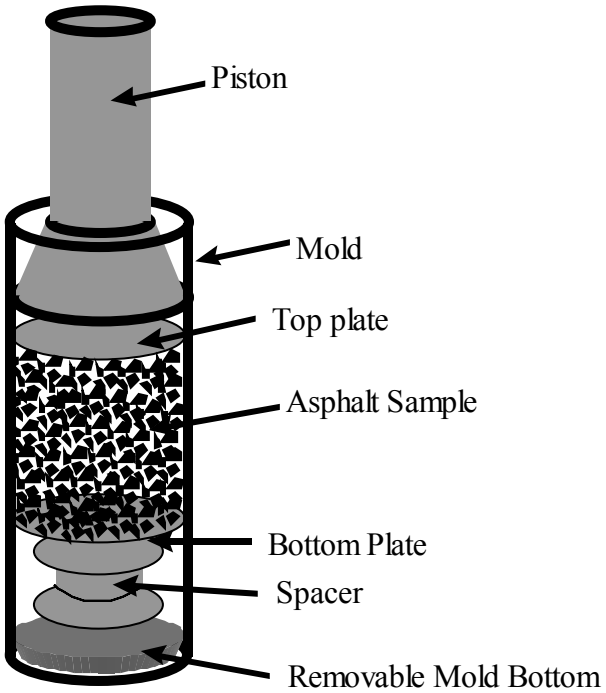

Figure 5.4 Mold Configuration

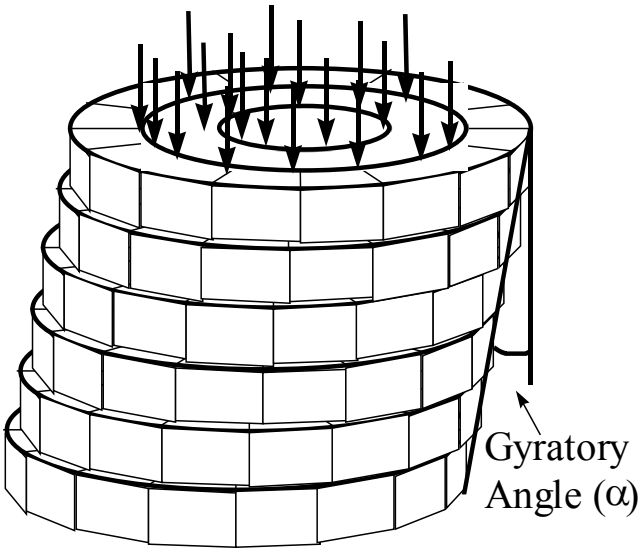

Figure 5.5 Shear Movement in Sample During Compaction

internal shear produced by the gyratory compactor. Aggregate particles in the mixture create shear forces as they slide past one another during compaction.

The change in height of the sample is measured by a linear variable displacement transducer (LVDT) within the ICT gyratory compactor as the sample is compacted. Using the height and weight data of the sample, the density at each cycle is calculated. This allows for two modes of operation. In the first mode, a maximum number of cycles are specified. The compactor will stop when it has reached that number of cycles. This feature can be used for Superpave mix design where the maximum number of cycles is specified based upon the traffic and climatic conditions of the road. In the second mode, a maximum density is specified. In this mode the volumetric density is computed throughout compaction. The machine will stop when it has reached the density value input into the control program or the maximum number of cycles specified.

Compaction Procedure

The same gyratory compaction procedure was used for producing samples from laboratory-designed mixtures and field mixtures sampled during the summer of 1997. Mixtures from projects during the summer of 1996 were compacted with a smaller sample size (100 mm diameter) due to equipment limitations in the laboratory. Samples were made to have a diameter of 150 mm to comply with Superpave standards. Sample heights were approximately 100 mm.

Superpave standards were also used for the compaction pressure and gyratory angle, which were 600 kPa and 1.25°, respectively.

Data Analysis

The type of compactor used in this study allowed for the comparison of the compactibility of different mixtures with respect to temperature and mixture properties. A load cell in the compactor measured the horizontal force needed to create the gyratory motion of the compactor. Using these data along with the sample geometry allowed for the calculation of the shear stress in the sample during compaction. The amount of power required for compaction was also computed using the sample geometry and the pressure used during compaction.

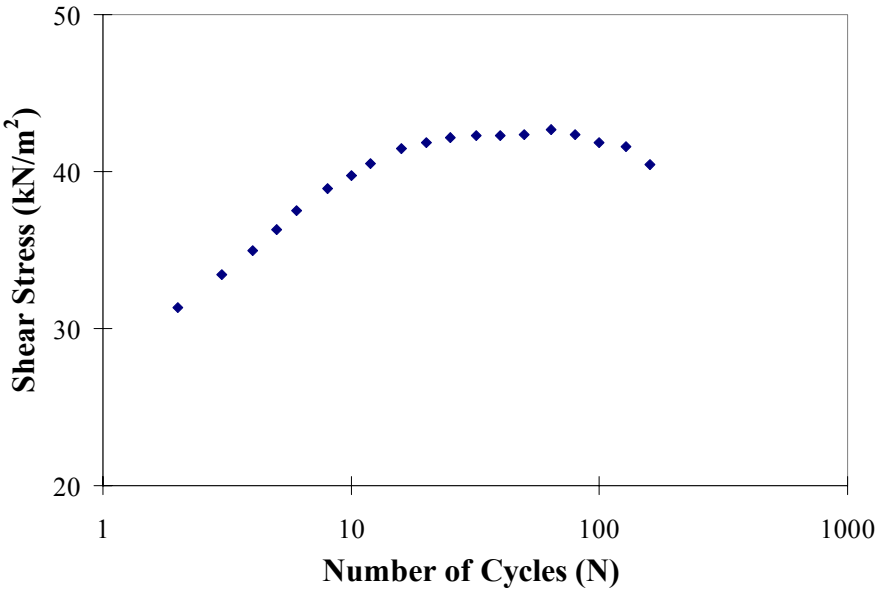

Figure 5.6 Typical Representation of Shear Stress vs. Number of Cycles

A typical plot of shear stress during compaction is shown in Figure 5.6. During the first phase of compaction the slope of the shear stress curve is very steep. The particles in the sample are being reoriented creating an increase in friction due to stone-on-stone contact. When the shear stress curve starts to level off, the density is nearing the specified value. This plot is useful in determining compaction characteristics of asphalt mixes and for comparing relative compaction characteristics between different mixes. If the initial slope of the curve is too flat, the mix may be harsh and problems in achieving a specified density may occur. If the slope of the curve towards the end of compaction is still quite steep, there may be stability problems with the mix.

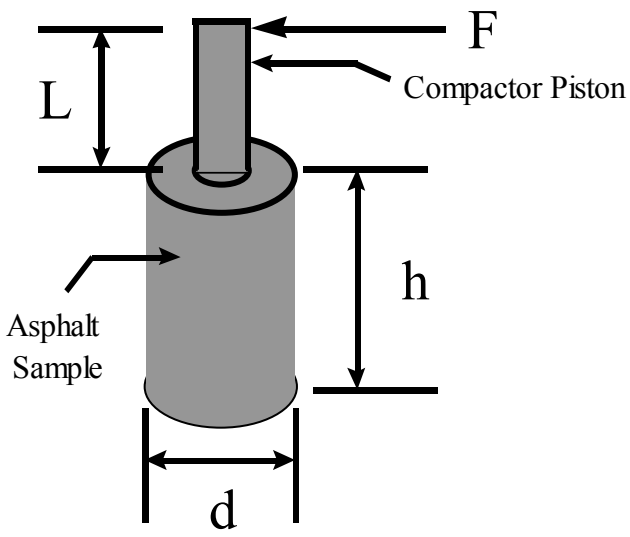

Figure 5.7 Parameters for Calculation of Shear Stress

The moment needed to create the gyration is recorded at each cycle as the sample compacts. A load cell located on the piston of the compactor measures the lateral load needed to create this moment. Using these data in conjunction with the geometry of the sample, the shear stress in the sample can be calculated at any point in time during compaction (Figure 5.7). The shear strength of the mixture must be overcome during compaction in order to meet the required density. The shear strength of the mixture increases as the sample nears its maximum density causing the shear stress measured in the sample to approach a constant value. The shear stress is calculated as:

$$\tau = \frac{2M}{Ah} \tag{5.3}$$

Where:

τ = shear stress

M = gyratory moment = $F \times L$

F = shear force

L = length of piston

A = cross-sectional area of the sample

h = height of sample

The change in height of the sample during compaction can be used to calculate the amount of power required during compaction (Figure 5.8). The power used during compaction represents the rate at which a mix can be compacted under different compaction conditions and mixture properties. The power requirements will increase for larger pressures because the change in height increases. The power requirement will also increase or decrease depending upon mixture characteristics such as aggregate gradation or angularity. These data can be used as comparison of the compactibility of different mix types. Power is calculated with the following equation:

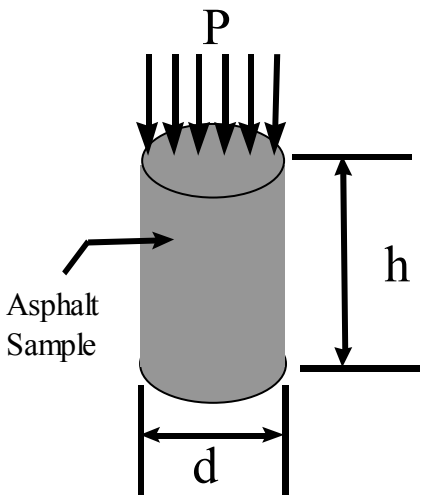

Figure 5.8 Parameters for Calculation of Power

$$Power = \frac{\sum_{i=1}^{n}\left(\Delta h \times P \times \pi d^2/4\right)_i}{t} \tag{5.4}$$

Where:

n = number of cycles

P = pressure in cylinder

Δh = change in height for cycle i

d = diameter of sample

t = time

For laboratory mixes, three samples were compacted at six different temperatures (71, 88, 104, 121, 138, and 149 °C) for each mixture type. The average shear stress and heights of the three samples during compaction were used for the calculation of shear stress and power of a given mix at a given temperature. The average result of three samples was used to help represent the possible variability of mixtures due to sample preparation and material properties. Compactibility parameters for field mixes were calculated using the averaged results of two samples instead of three due to limitations in the amount of mix available for each project. The results of shear stress and power were then plotted against compaction temperature as a means of comparing the effect of different mixture properties on the compactibility of different mixtures.

RESULTS

Shear Stress

Laboratory Mixtures

Using the height and shear stress data computed by the ICT gyratory compactor, the density, shear stress, and power were calculated. These data were then used to make comparisons of mixture compactibility. All results were calculated at an $N_{initial}$ of 8 cycles. This point was chosen to correspond to Superpave requirements for construction and compaction. In the Superpave criteria a limit is placed on the density at $N_{initial}$ to prevent tender mixtures. The shear stress was also determined at $N_{initial}$ over a range of compaction temperatures for each mixture. The minimum shear stress for each mixture was used to estimated the optimum compaction temperature for each mixture.

Figure 5.9 indicates that mixtures with a coarse, angular aggregate structure will not have as much initial compaction as a dense graded mixture. The higher percentage of angular aggregate increases the amount of internal friction between the particles, decreasing the amount of compaction that initially can be seen. This results in a steeper compaction curve because the mixture has a larger volume of voids to reduce over the duration of the compaction. The dense graded mixture undergoes a large amount of initial compaction due to the mixture's initially low internal friction. This results in higher densities than those seen in the SMA mixture. This higher density increases the amount of internal friction in the dense graded mixture. This becomes important when examining the shear stress of the two different mixture types.

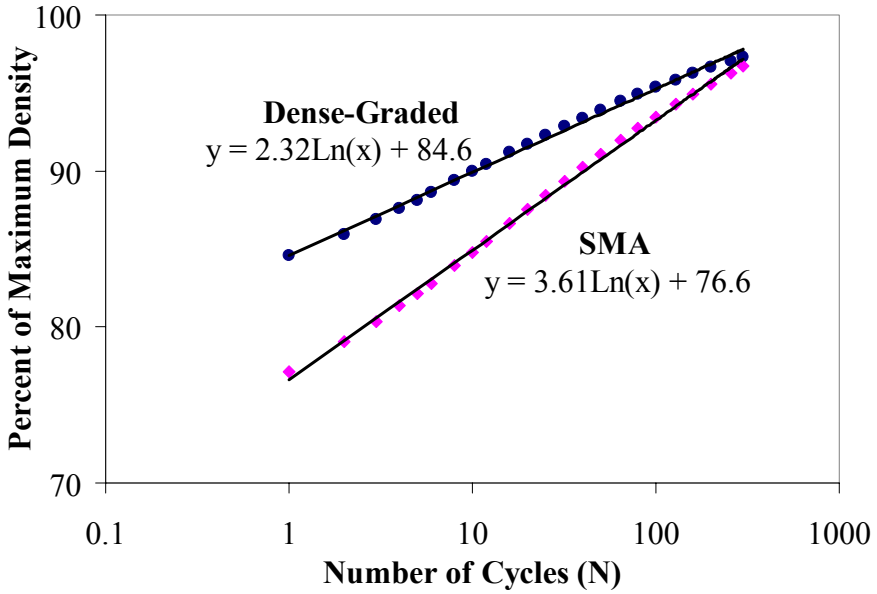

Figure 5.9 Percent of Maximum Density vs. Number of Cycles for PG 52-34 Lab Mixtures

Figure 5.10 indicates that the SMA mixture has a lower shear stress than the dense graded mixture. Since most of the reduction in voids for the dense graded mixture occurred during the first few cycles of compaction, the mixture will have more internal friction than the SMA mixture. This causes the dense graded mixture to be more difficult to compact at a given cycle than the SMA mixture

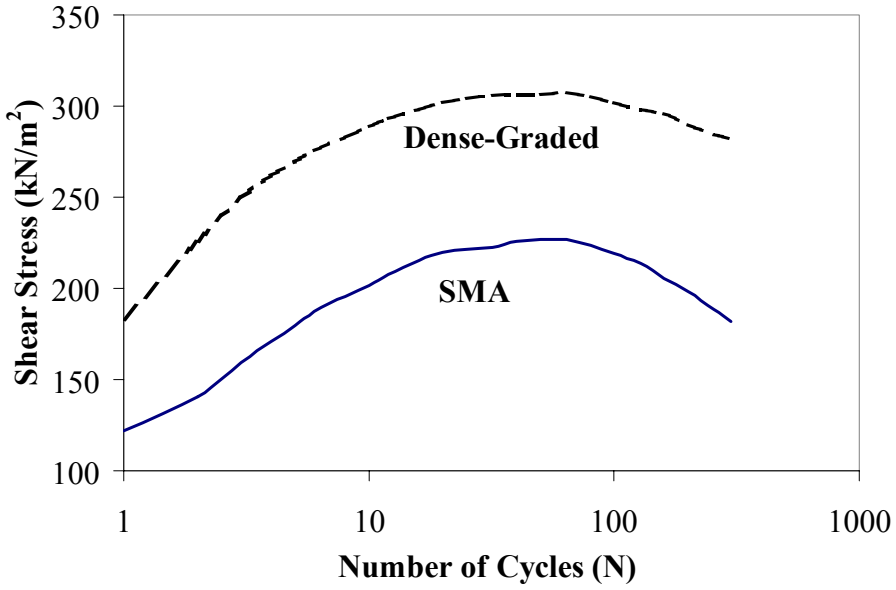

Figure 5.10 Shear Stress vs. Number of Cycles for PG52-34 Laboratory Mixtures

Figure 5.11 shows shear stress versus temperature relationships at 8 cycles for the laboratory mixtures. The shear stress reaches a minimum of about 300 kN/m^2 for the dense-graded mixture and is about 100 kN/m^2 less for the SMA mixture. Dense-graded and SMA gradations were also compared in mixtures containing PG 58-28 and 80/100 penetration binders. A comparison of shear stress vs. binder stiffness is somewhat analogous to the comparison of shear stress vs. aggregate type. Mixtures with a softer binder had greater initial compaction than those with a stiffer binder, and therefore showed higher shear stress throughout the compaction. It should be noted that most of the $N_{initial}$ density values for the dense-graded mixtures were at or above the 89 percent limit specified in Superpave. By Superpave standards this mixture would exhibit compaction characteristics of a tender mix during construction. The SMA density values were around 85 percent, well below the limit for $N_{initial}$.

As noted above, a minimum point can be identified on the shear stress vs. temperature curves. This corresponds to a point at which maximum compaction can occur. A comparison of Figure 5.9 and Figure 5.10 indicates that mixtures with the highest rate of compaction also have the lowest shear stress during compaction in the laboratory. There may also be an optimum compaction temperature range corresponding to minimum shear stress. This temperature range is between 105°C to 120°C for most of the laboratory fabricated mixtures.

Field Mixtures

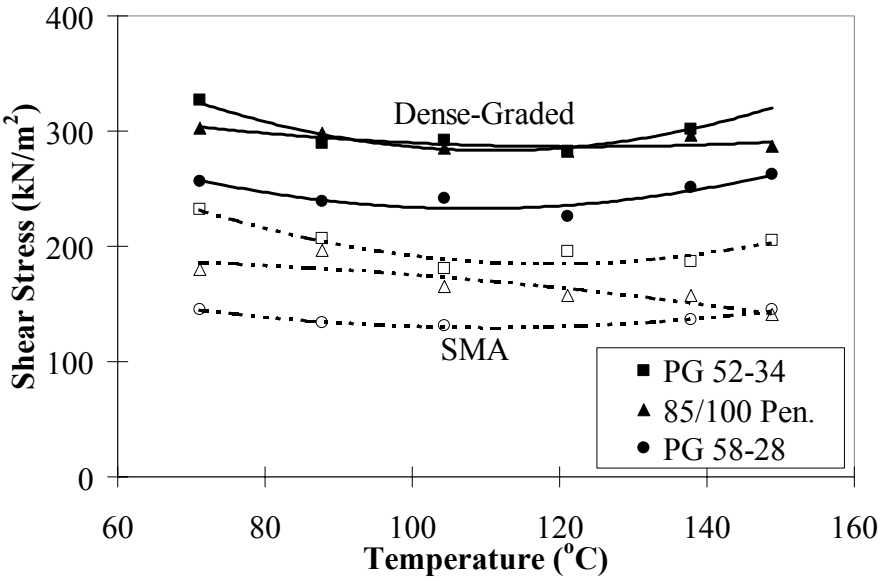

Figure 5.11 Shear Stress at $N_{initial}$ vs. Temperature for Laboratory Mixtures

The first five field mixtures presented were projects completed in the summer of 1996. The samples produced from these mixtures were 100-mm diameter samples. These are not the standard Superpave dimensions due to equipment limitations at the time of compaction. The results from these samples were used to determine the shear stress and power during compaction. These results of these field mixtures were then compared to one another, but not to the other five field mixtures due to the difference in sample geometry. The data can still, however, be used to determine optimum compaction temperature ranges.

Mixtures from five 1996 paving projects (two dense-graded and three Superpave) were compacted in the laboratory and analyzed for density and shear stress properties. Figure 5.12 shows the results of this analysis for the dense-graded mixtures. Figure 5.13 shows the results for the Superpave mixtures. Once again, the dense-graded mixtures exhibited higher shear stresses than the coarse mixtures. The density at $N_{initial}$ for the dense-graded mixtures was between 88.5 and 91 percent of the maximum density. By Superpave standards this mixture would exhibit compaction characteristics of a tender mix during construction. The percent of maximum density for the three Superpave mixtures was in the range of 84 to 87 percent of maximum.

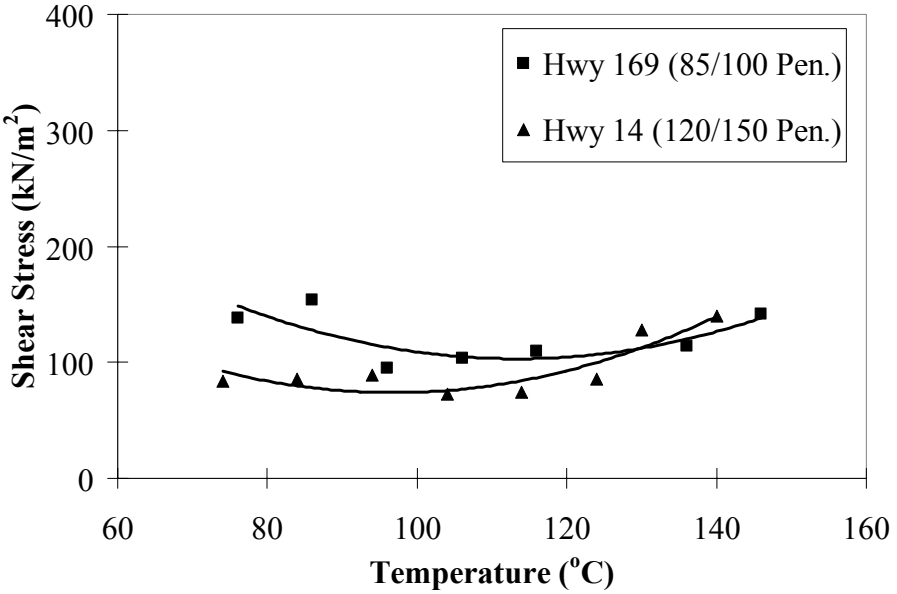

Figure 5.12 Shear Stress at N initial vs. Temperature for 1996 Dense-Graded Projects

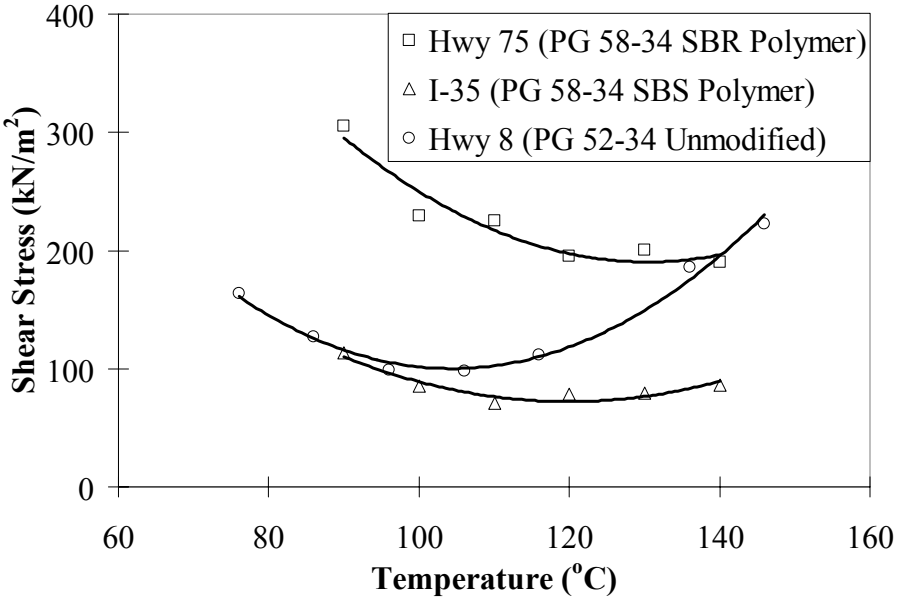

Figure 5.13 Shear Stress at $N_{initial}$ vs. Temperature for 1996 Superpave Projects

As with the laboratory mixtures, the minimum of shear stress typically occurred in a temperature range of 105°C to 120°C. A large difference is seen in the temperature at which the minimum shear stress occurs for the mixture used on Highway 75. The binder used in this project was a styrene butadiene rubber (SBR) modified PG58-34 binder. The type of modifier used in this project may be the reason why the minimum shear stress occurs at a much higher temperature (130°C) than the rest of the mixtures.

Mixtures from five field projects in 1997 were also analyzed (Figure 5.14). These samples were produced in the standard Superpave size of 150 mm diameter. The compaction results of these projects cannot be directly compared to the results from the 1996 field projects due to the difference in sample size. All mixtures from 1997 were designed to Superpave standards and meet the requirement of a maximum 89 percent of maximum density at $N_{initial}$ of 8 cycles.

Mn/ROAD Mixture A has a gradation that falls below the restricted zone and Mixture B has a denser gradation that falls through the restricted zone. Even though Mix B has a denser gradation, the difference was not sufficient to make the large differences in shear stress that were seen in the laboratory and 1996 mixtures. Interstate 494 had a coarser aggregate gradation than Mn/ROAD Mixture A. This is reflected in the lower shear stress values for Interstate 494.

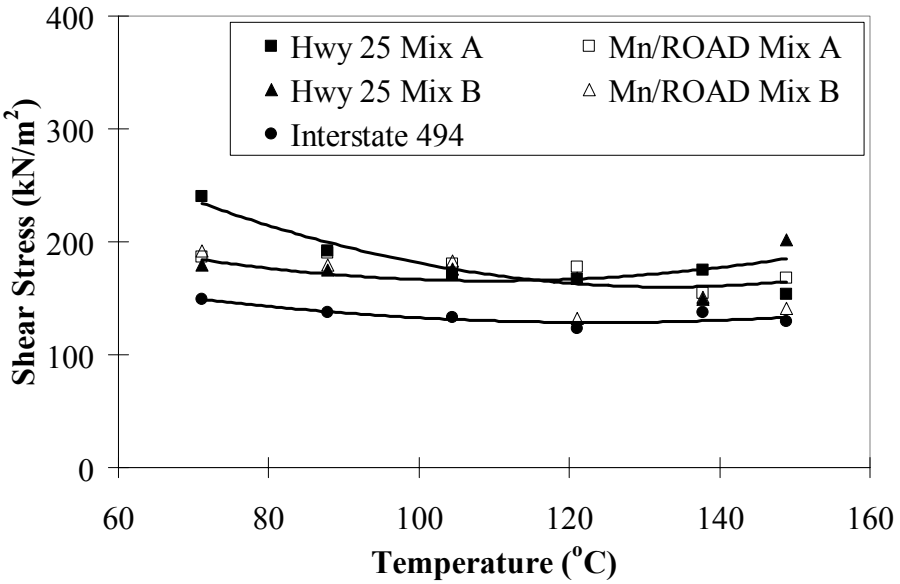

Figure 5.14 Shear Stress at $N_{initial}$ vs. Temperature for 1997 Projects

Power

Laboratory Mixtures

The power required to compact a sample during laboratory compaction was also used to quantify the workability or compactibility of hot-mix asphalt concrete. The power is equal to the work done during compaction divided by the amount of time required to compact the mixture to a specified density. The results of this calculation are shown in Figure 5.15 for all of the laboratory fabricated mixtures. The power was calculated at 4 percent air voids for all mixtures. The results show that less power is required to compact the dense graded mixtures than the SMA mixtures. More power is required to compact the SMA mixtures because the blocky, angular shape of the aggregate prevents the mixture from initially compacting under its own weight and reduces the amount the mixture can be compacted under the initial application of force by the gyratory compactor.

The type of asphalt used in each mixture also has an effect on the amount of power required to compact an asphalt concrete sample in the laboratory. This can be seen in the results for the dense graded mixtures in Figure 5.15. The softest grade of asphalt, the PG 52-34 has the lowest power requirement, while the stiffest asphalt, the PG 58-28 has the greatest power requirement of the three dense graded mixtures. Stiffer asphalts decrease the rate of compaction, increasing the amount of power required to compact a mixture.

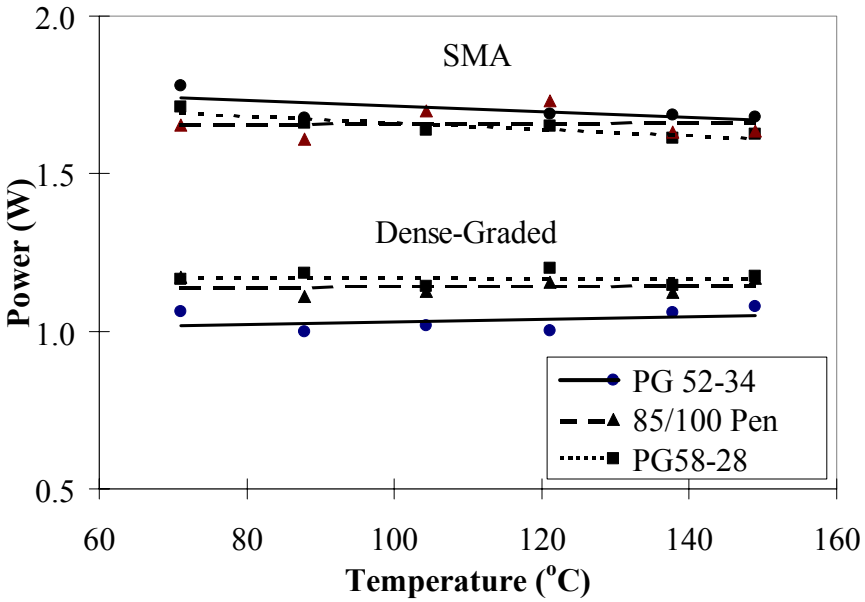

Figure 5.15 Power at N_{design} vs. Temperature for Laboratory Mixtures

Field Mixtures

Figure 5.16 shows the results of calculating power versus number of cycles for the field mixtures from 1996. The results are very similar to those seen for the laboratory mixtures with the exception that the power values are scaled down due the smaller sample size used in the samples from 1996. The very clear difference that was seen between the two aggregate gradations used in the laboratory samples is also seen in the field samples. The mixtures that were designed

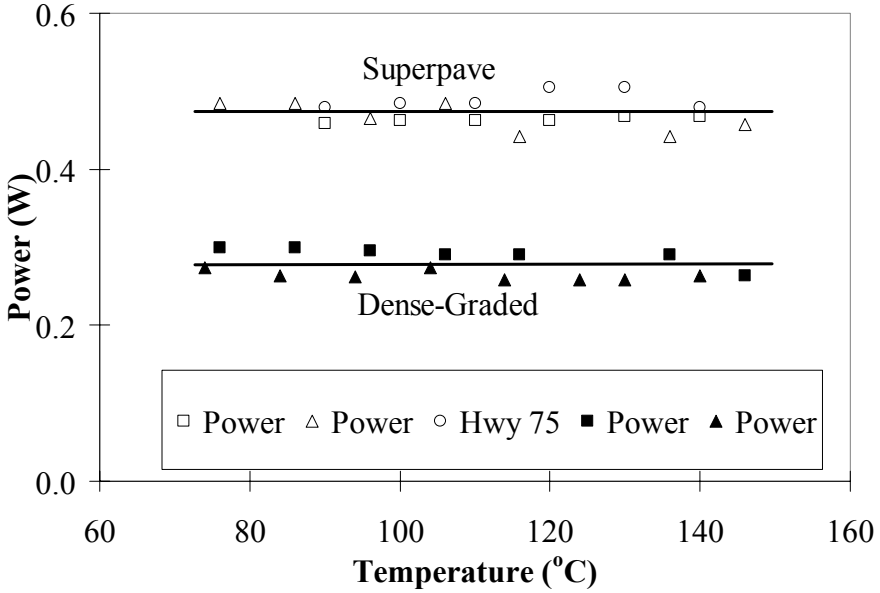

Figure 5.16 Power at N_{design} vs. Temperature in 1996 Field Mixtures

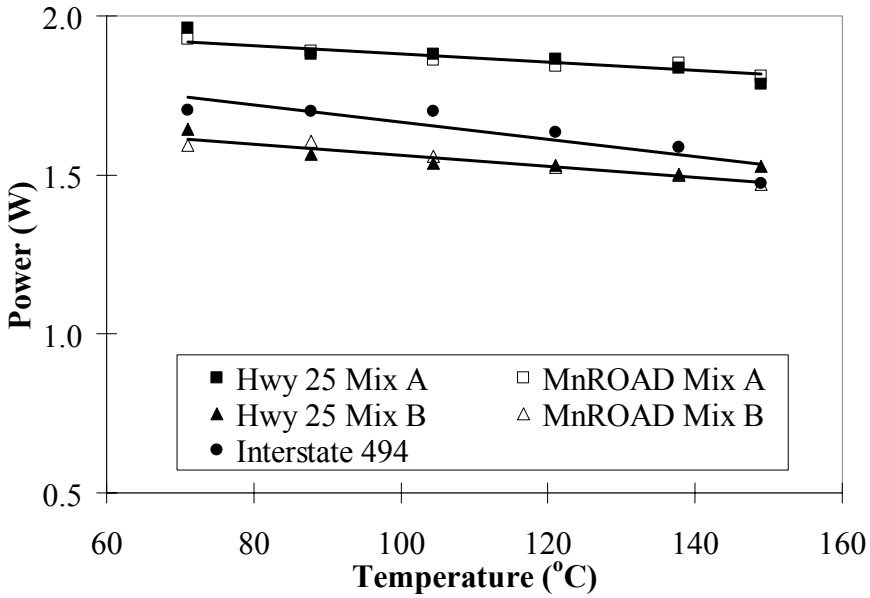

Figure 5.17 Power at N_{design} vs. Temperature in 1997 Field Mixtures

using Superpave aggregate requirements have distinctively higher power requirement than the mixtures that were designed as typical dense graded mixtures from Minnesota. The difference is due to the compaction rates that were discussed earlier in the chapter. The power results from the projects from 1997 are shown in Figure 5.17. These results are also similar to the previously discussed power results, but due to the similarities in aggregate gradations for these mixtures, the differences in the results are not as distinct as those for 1996.

Optimal Compaction Temperature

The shear stress curves for most of the mixtures tested reach a minimum in the 105 to 120 °C range. The temperature at which the shear stress curve reaches a minimum corresponds to the optimum compaction temperature described above. This interpretation appears to fit with typical field compaction temperatures. In order to use minimum shear stress as a means of determining the optimum compaction temperature range, one must assume that at minimum shear stress the mat can still support the weight of the roller. There may be issues of mixture tenderness due to low shear stress that this report does not address.

The optimum compaction temperature represents the point at which the binder acts as a lubricant between the aggregate particles. As the temperature increases from the optimum, the binder viscosity drops, and inter-particle friction increases the shear stress. As the temperature drops below the optimum, the increasing binder viscosity increases the shear stress. Figure 5.18 shows the optimum temperatures for mixtures tested in this study (excluding those which did not exhibit a minimum shear stress). The mixtures are arranged by binder grade ranging from softest on the left to hardest on the right. Although there is variation within each binder grade, there is a general trend towards higher optimum compaction temperatures for stiffer binders. The results of this analysis were used to determine the recommended temperatures to start compaction in the PaveCool program. The range of binder grades analyzed in this study limited the recommendations to two temperatures: 110 °C for PG grades of 52 and below, and 120 °C for PG grades of 58 and above. However, these recommended temperatures may not be applicable to all situations. Judgement must be used in order to achieve a properly compacted surface.

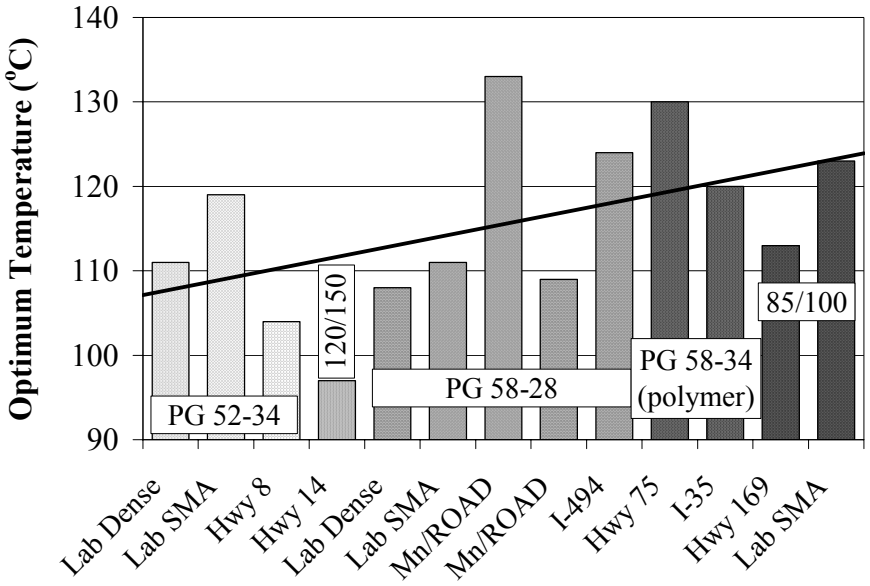

Figure 5.18 Optimum Compaction Temperatures Based on Shear Stress Curves

CHAPTER 6
ASPHALT PAVEMENT COOLING TOOL

DESCRIPTION

A computer program has been developed to predict cooling rates for asphalt mixtures based upon mixture temperature, air temperature, lift thickness, wind speed, type of existing base, and mixture type. The temperature related compaction data from this study would be used along with the cooling rates to determine the time period in which the maximum amount of compaction can occur. The user interface is shown in Figure 6.1. This program can then be used by personnel during the construction of an asphalt concrete pavement to determine the starting and ending times for compaction. The optimum compaction temperature is determined from the shear stress data and is then used along with the cooling rates to determine the time for compaction to begin. This is especially useful for late season paving in Minnesota when cooling times are greatly reduced due to inclement weather conditions.

The latest edition of PaveCool is Version 2.0. Improvements over previous versions include corrections to the thermal properties of "wet" aggregates, a plot that can be viewed from the

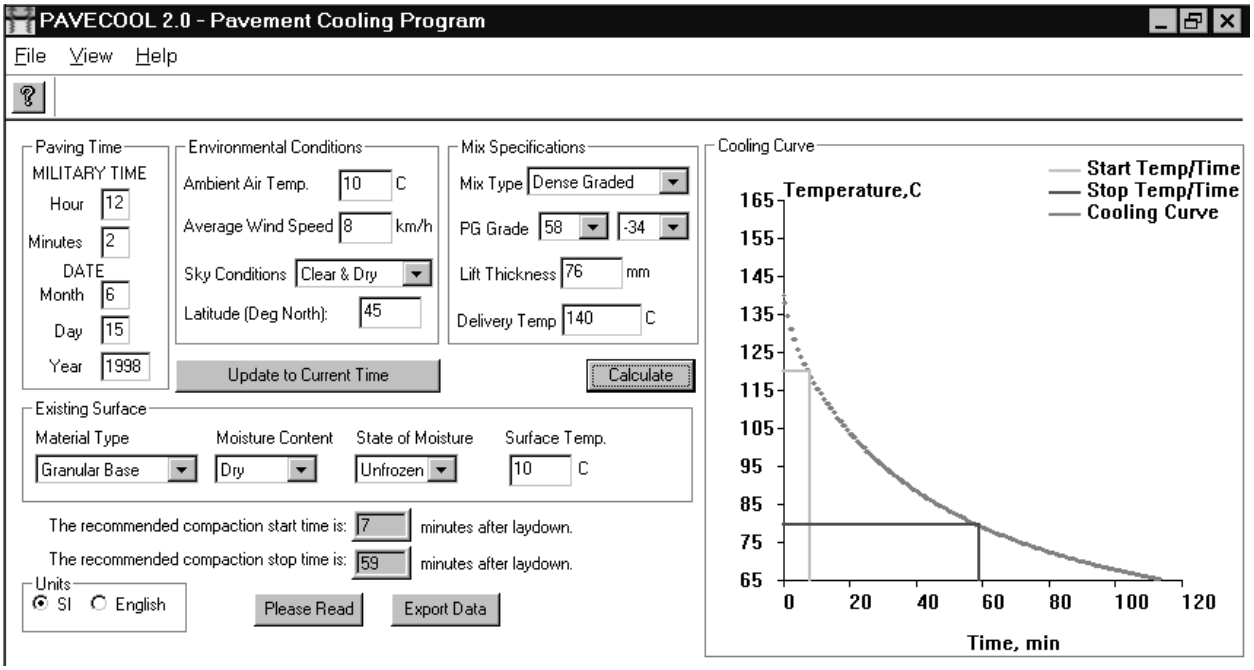

Figure 6.1 PaveCool 2.0 Input Screen

input window, and the recommended start compaction time/temperature. The thermal property corrections were necessary because the water content used to calculate the previous thermal values for the wet condition was discovered to be unreasonably high. The cooling curve appears to the right of the input screen. Recommended start and stop times are displayed as colored lines on the plot. The Performance Grade (PG) of the asphalt dictates the recommended start compaction temperature. The user must specify the high and low temperatures which make up the grading system.

THERMAL PROPERTIES

Unless otherwise specified, the thermal properties used in the PaveCool program are those recommended by Corlew and Dickson [16]. The results of the thermal conductivity tests described in Chapter 4 were used for hot-mix asphalt. Kersten [17] developed the following equations to estimate the thermal conductivity of fine and coarse granular materials:

Fine Unfrozen	$k = (0.9 \log(\omega)-0.2)\ 10^{0.01\gamma_d}$	for $\omega \geq 7$	(6.1)
Fine Frozen	$k = 0.01\ (10)^{0.022\gamma_d} + 0.085\ (10)^{0.008\gamma_d}\ \omega$	for $\omega \geq 7$	(6.2)
Coarse Unfrozen	$k = (0.07 \log(\omega) + 0.4)\ 10^{0.01\gamma_d}$	for $\omega \geq 1$	(6.3)
Coarse Frozen	$k = 0.076\ (10)^{0.013\gamma_d} + 0.032\ (10)^{0.0146\gamma_d}\ \omega$	for $\omega \geq 1$	(6.4)

Where:

k = thermal conductivity, $Btu \cdot in/ft^2 \cdot h \cdot °F$

γ_d = dry unit weight, pcf

ω = gravimetric moisture content, %

The values in Table 6.1 were calculated for materials at different moisture contents Based on typical densities and optimum moisture contents described by Atkins [35]. Values in bold represent the thermal conductivity at optimum moisture content, and those in bold italic represent dry and wet conditions. Table 6.2 shows the calculated specific heat for granular materials.

Table 6.1 Calculated Thermal Conductivity of Granular Materials

Thermal Conductivity, W/m·K									
	γ_d	Gravimetric Moisture Content, %							
Material	**kg/m^3**	**4**	**5**	**6**	**7**	**8**	**10**	**15**	**20**
Fine Unfrozen	1800				1.08	1.18	***1.35***	**1.65**	***1.87***
Fine Frozen	1800				1.11	1.21	***1.40***	**1.89**	***2.38***
Coarse Unfrozen	2000	1.14	***1.16***	1.18	**1.19**	1.20	***1.22***		
Coarse Frozen	2000	1.70	***2.00***	2.31	**2.62**	2.93	***3.55***		

Farouki [36] described the following equations for specific heat of granular materials:

$$c_U = \left(0.18 + 1.0\frac{\omega}{100}\right)c_w \tag{6.5}$$

$$c_F = \left(0.18 + 0.5\frac{\omega}{100}\right)c_w \tag{6.6}$$

Where:

c_U, c_F = specific heat of unfrozen and frozen granular materials

γ_w = unit weight of water

c_w = specific heat of water = 4187 J/kg·K

Table 6.2 Calculated Specific Heat of Granular Materials

Specific Heat, J/kg·K									
	γ_d	Gravimetric Moisture Content, %							
Material	**kg/m^3**	**4**	**5**	**6**	**7**	**8**	**10**	**15**	**20**
Fine Unfrozen	1800				1047	1089	***1172***	**1382**	***1591***
Fine Frozen	1800				900	921	***963***	**1068**	***1172***
Coarse Unfrozen	2000	921	***963***	1005	**1047**	1089	***1172***		
Coarse Frozen	2000	837	***858***	879	**900**	921	***963***		

FIELD VERIFICATION

Temperature readings were taken behind the paver for several projects from 1995 to 1997. The method used is outlined in Chapter 5. Density values were available only for the Highway 52 project. Figure 6.2 shows the temperature and density readings for the Highway 52 project. It also indicates how compaction diminishes as the mix cools off. The agreement between simulated and measured temperatures is typical of most of the projects in this study.

Results for the other projects are shown in Appendix F. Some projects were omitted because not enough temperature data was available due to broken probes. In general, the agreement was best in simulations where the measured lift thickness rather than the design thickness was used. Temperature measurements were more variable in coarse mixtures due to greater inhomogeneity relative to the dense-graded mixtures. Errors were also introduced with each roller pass, which tended to change the orientation of the probe. A limitation is the lack of temperature data for lifts placed on wet or dry subgrade soil. Thermal properties for these materials were calculated using well-documented algorithms, but extra care should be used when simulating temperatures for this type of project.

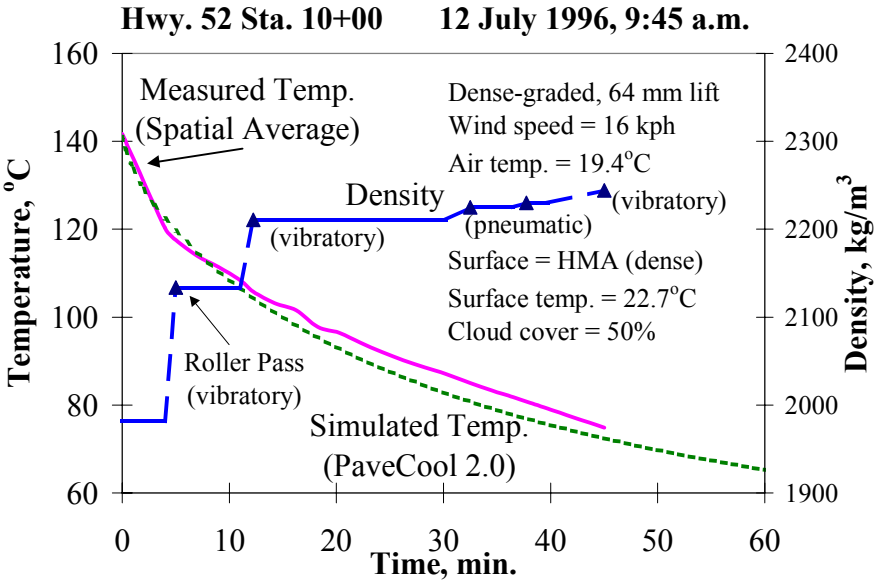

Figure 6.2 Temperature and Density Data for Highway 52, Rosemount, MN

CHAPTER 7
CONCLUSIONS AND RECOMMENDATIONS

CONCLUSIONS

1. PaveCool has proven to be a useful tool for simulating pavement cooling in a wide range of weather conditions.
2. The range of thermal diffusivity values determined by the slab cooling method (0.5 x 10^{-6} to 1.3 x 10^{-6} m^2/s) agrees with the range of values reported in the literature (0.37 x 10^{-6} to 1.44 x 10^{-6} m^2/s).
3. The range of thermal conductivity values determined by the thermal probe method (0.6 to 2.5 W/m·K) agrees with the range of values reported in the literature (0.76 to 2.88 W/m·K).
4. Thermal conductivity values calculated from the measured thermal diffusivity values and assumed values of density (2000 kg/m^3) and specific heat (900 J/kg·K) agree with the measured thermal conductivity values.
5. Mixtures with coarse, angular aggregate structures have a higher rate of compaction because there is relatively little initial compaction under its own weight and the initial application of force by the compactor.
6. Shear stress decreases as the coarseness and angularity of the aggregate gradation increases due to the lower amount of initial compaction of this type of mixture.
7. Shear stress typically comes to a minimum at 105°C to 120°C for mixtures in this study.
8. The power required to compact a given asphalt mixture mainly depends upon the aggregate type and gradation used.
9. The asphalt grades and temperatures examined play a small part in the amount of power required for compaction for some mixtures.

RECOMMENDATIONS

The following steps should be taken to verify the effects of asphalt material and thermal properties on hot-mix asphalt pavement cooling rates and to further the development of PaveCool.

1. Continue field verification, particularly with projects paved on wet or dry subgrade soil.
2. Develop an improved small slab specimen compaction method.
3. Conduct a complete test program to determine the variation in hot-mix asphalt thermal conductivity, thermal diffusivity, and specific heat values resulting from the temperature and density changes that occur throughout the compaction process.
4. Develop a method for determining the minimum temperature for effective compaction.
5. Test a more diverse battery of mixture types including different aggregate gradations and asphalt grades.
6. Determine the relationship between the power requirement and number of roller passes required for adequate field compaction
7. Establish a correlation between field compaction and laboratory compaction.

REFERENCES

1. Sowers, G.B., and Sowers, G.F., Introductory Soil Mechanics and Foundations, Macmillen, Third Edition, New York, 1970, pp. 306-307.
2. Kari, W.J., "Mix Properties as They Affect Compaction," Asphalt Paving Technology 1967, Proceedings: Association of Asphalt Paving Technologists Technical Sessions, Vol. 36, pp. 295-309.
3. Schmidt, R.J., Kari W.J., Bower, H.C., and Hein, T.C., "Behavior of Hot Asphaltic Concrete Under Steel-Wheel Rollers," Highway Research Bulletin No. 251, Highway Research Board, Washington, D.C., 1959, pp. 18-37.
4. Cabrera, J.G., "Assessment of the Workability of Bituminous Mixtures," Highways and Transportation, November 1991, pp. 17-23.
5. McLeod, N.W., "Influence of Viscosity of Asphalt Cements on Compaction of Paving Mixtures in the Field," Highway Research Record No. 158, Highway Research Board, National Academy of Sciences--National Research Council, Washington, D.C., 1967, pp. 76-115.
6. Parker, C.F., "Steel-Tired Rollers," Highway Research Bulletin No. 246, Highway Research Board, Washington, D.C., 1960.
7. Santucci, L.E., and Schmidt, R.J., "Setting Rate of Asphalt Concrete," Highway Research Bulletin No. 333, Highway Research Board, Washington, D.C., 1962, pp. 1-9.
8. Heukelom, W., "The Role of Filler in Bituminous Mixtures," Asphalt Paving Technology 1965, Proceedings: Association of Asphalt Paving Technologists Technical Sessions, Vol. 34, pp.396-429.
9. Tegeler, P.A. and Dempsey, B.J., "A Method of Predicting Compaction Time for Hot-Mix Bituminous Concrete," Asphalt Paving Technology 1973, Proceedings: Association of Asphalt Paving Technologists Technical Sessions, Vol. 42, pp. 499-523.
10. Dellert, R.B., "Vibratory Compaction of Thin Lift Asphalt Resurfacing," Asphalt Paving Technology 1977, Proceedings: Association of Asphalt Paving Technologists Technical Sessions, Vol. 46, pp. 287-309.
11. Geller, M., "Compaction Equipment for Asphalt Mixtures," Placement and Compaction of Asphalt Mixtures, ASTM STP 829, F.T. Wagner, Ed., American Society for Testing and Materials, 1984, pp. 28-47.

12. Goldberg, L.F. and Wang, W., An Improved Thermal Conductivity Probe, Underground Space Center, Department of Civil and Mineral Engineering, Institute of Technology, University of Minnesota, June 1991.
13. Turner, William C. and Malloy, John F., Thermal Insulation Handbook, Robert E. Krieger Publishing Company, Malabar, Florida, 1981, p. 549.
14. Kavianipour, A., "Thermal Property Estimation Utilizing the Laplace Transform with Application to Asphaltic Pavement," International Journal of Heat and Mass Transfer, Vol. 20, 1967, pp. 259-267.
15. Jordan, P.G. and Thomas, M.E., "Prediction of Cooling Curves for Hot-Mix Paving Materials by a Computer Program," Transport and Road Research Laboratory Report 729, 1976.
16. Corlew, J.S. and Dickson, P.F., "Methods for Calculating Temperature Profiles of Hot-Mix Asphalt Concrete as Related to the Construction of Asphalt Pavements," Asphalt Paving Technology 1968, Proceedings: Association of Asphalt Paving Technologists Technical Sessions, Vol. 37, pp. 101-140.
17. Kersten, M.S., "Thermal Properties of Soils," Bulletin No. 28, University of Minnesota Institute of Technology Engineering Experiment Station, Vol. 52, n. 21, June 1, 1949.
18. Raznjevic, K., Handbook of Thermodynamic Tables and Charts, Hemisphere, 1976.
19. Saal, R.N.J., "Physical Properties of Asphalt Bitumen," The Properties of Asphaltic Bitumen, ed. J.P. Pfeiffer, Elsevier Publishing Company, Inc., 1950, pp. 93-96.
20. Ozisik, M.N., Basic Heat Transfer, McGraw-Hill Book Company, New York.
21. Consuegra, A., Little, D.N., Von Quintus, H., and Burati, J., “Comparative Evaluation of Laboratory Compaction Devices Based on Their Ability to Produce Mixtures with Engineering Properties Similar to Those Produced in the Field,” Asphalt Mixtures and Asphalt Chemistry, Transportation Research Record 1228, Transportation Research Board, National Research Council, Washington, D.C., 1989, pp. 80-87.
22. Cabrera, J.G., “Assessment of the Workability of Bituminous Mixtures,” Highways and Transportation, Vol. 38, No. 11, November 1991, pp. 17-23.

23. Bissada, A.F., "Resistance to Compaction of Asphalt Paving Mixtures and Its Relationship to Stiffness," Placement and Compaction of Asphalt Mixtures, ASTM STP 829, F.T. Wagner, Ed., American Society for Testing and Materials, 1984, pp. 131-145.
24. Marvillet, J., and Bougualt, P. "Workability of Bituminous Mixes--Development of a Workability Meter," Asphalt Paving Technology 1979, Proceedings: Association of Asphalt Paving Technologists, Vol. 48, pp. 49.
25. ---, Superpave Mix Design: Superpave Series No. 2 (SP-2), Asphalt Institute, Lexington, KY, 1996.
26. Fwa, T F. Low, B H. Tan, S A., "Laboratory Determination of Thermal Properties of Asphalt Mixtures by Transient Heat Conduction Method," Transportation Research Record, No. 1492, Jul 1995, pp. 118-128.
27. Luoma, J.A., Allen, B., Voller, V.R., and Newcomb, D.E., "Modeling of Heat Transfer During Asphalt Paving," Proceedings, 9th International Conference on Numerical Methods in Thermal Problems, R.W. Lewis and P. Durbetaki, eds., Pineridge Press, Swansea, UK, July 1995, pp. 1125-1135.
28. Kreith, F. and Black, W.Z., Basic Heat Transfer, Harper & Row, New York, 1980.
29. Alford, J.S., Ryan, J.E., and Urban, F.O., "Effect of Heat Storage and Variation in Outdoor Temperature and Solar Intensity on Heat Transfer Through Walls," Transactions: American Society of Heating and Ventilating Engineers, Vol. 45, 1939, pp. 369-396.
30. Patankar, S.V., Computation of Conduction and Duct Flow Heat Transfer, Innovative Research Inc, Maple Grove, MN, 1991.
31. Patankar, S.V., Numerical Heat Transfer and Fluid Flow, McGraw-Hill, 1981.
32. Nicholls, J.C. and Daines, M.E., "Acceptable Weather Conditions for Laying Bituminous Materials," Department of Transport, Transport Research Laboratory Project Report 13, 1993.
33. Chadbourn, B., Luoma, J.A., Newcomb D.E., and Voller, V.R., "Consideration of Hot-Mix Asphalt Thermal Properties During Compaction," Quality Management of Hot-Mix Asphalt, ASTM1299, Dale S. Decker, ed., American Society for Testing and Materials, 1996, pp. 127-141.

34. Scholz, T.V., Allen, W.L., Terrel, R.L., and Hicks, R.G., "Preparation of Asphalt Concrete Test Specimens Using Rolling Wheel Compaction," Transportation Research Record 1417, Transportation Research Board, National Research Council, Washington, D.C., 1993, pp. 150-157.

35, Atkins, H.N., Highway Materials, Soils, and Concretes, Third Edition, Prentice-Hall, Columbus, Ohio, 1997.

36. Farouki, O.T., Thermal Properties of Soils, Trans Tech Publications, 1986.

37. Hunter, R. and McGuire, G.R., "A Fast and Efficient Method for Predicting Cooling Profiles in Bituminous Materials," Civil Engineering, London, June 1986, pp. 24-25.

38. Guttman, N.B. and Matthews, J.D., "Computation of Extraterrestrial Solar Radiation, Solar Elevation Angle, and True Solar Time of Sunrise and Sunset," SOLMET Vol. 2 -- Final Report, National Climatic Center, U.S. Department of Commerce, 1979, pp. 49-52.

39. Schmetz, J., "Relationship between Solar Net Radiative Fluxes at the Top of the Atmosphere and at the Surface," Journal of the Atmospheric Sciences, Vol. 50, No. 8, 15 April 1993, pp. 1125.

40. Alford, J.S., Ryan, J.E., and Urban, F.O., "Effect of Heat Storage and Variation in Outdoor Temperature and Solar Intensity on Heat Transfer Through Walls," Transactions: American Society of Heating and Ventilating Engineers, Vol. 45, 1939, pp. 369-396.

41. Barber, E.S., "Calculation of Maximum Pavement Temperatures from Weather Reports," Highway Research Board Bulletin 168, 1957, pp. 1-8.

APPENDIX A
PAVEMENT COOLING MODELS

CORLEW AND DICKSON [16]

The purpose of the Corlew and Dickson study was to develop a model which could predict pavement temperatures as a function of time and depth from the time the hot-mix leaves the paver to the final pass of the compactor. They developed an explicit finite difference algorithm to predict pavement temperature profiles and cooling rates.

Equation for first layer:

$$T_{1(t+\Delta t)} = T_{1(t)}\left[1 - \frac{2\alpha\Delta t}{\Delta z^2}(N_{Bi} + 1)\right] + \frac{2\alpha\Delta t}{\Delta z^2}(T_{2(t)} + N_{Bi}T_a) + \frac{2\alpha\Delta t}{k_m\Delta z}(\alpha H_s - \varepsilon\sigma T_{1(t)}^4) \qquad (A.1)$$

Where:

T_1 = temperature of the first layer

α = the thermal diffusivity of layer 1

Δt = time increment

Δz = space increment

N_{Bi} = Biot number = $\frac{h\Delta z}{k_m}$

T_a = atmospheric temperature

H_s = solar radiant energy incident on pavement

a = total absorptance

ε = total emittance

σ = Stefan-Boltzmann constant

Equation for intermediate layers:

$$T_{n(t+\Delta t)} = T_{n(t)} + \left(\frac{\alpha\Delta t}{\Delta z^2}\right)(T_{n+1(t)} - 2T_{n(t)} + T_{n+1(t+\Delta t)}) \qquad (A.2)$$

Where α is the thermal diffusivity of layer n.

JORDAN AND THOMAS [15]

Jordan and Thomas presented a slightly different model, which they adapted from the Crank Nicolson method, which Hunter and McGuire [37] describe as an accurate and stable method of solving conduction equations. This model includes an implicit scheme in the first layer equation. This requires two or three iterations to achieve convergence at the first layer before calculating the remaining layers.

$$T_{1(t+\Delta t)} = T_{1(t)}\left(1-\frac{2k_1\Delta t}{\rho_1 c_1 \Delta z^2}-\frac{2h\Delta t}{\rho_1 c_1 \Delta z}\right)+T_{2(t)}\frac{2k_1\Delta t}{\rho_1 c_1 \Delta z^2}+\frac{2h\Delta T_A}{\rho_1 c_1 \Delta z}-\frac{2\varepsilon\sigma\Delta t}{\rho_1 c_1 \Delta z}(\overline{T}_{1(t)}^4-\overline{T}_A^4)+\frac{2aS_R\Delta t}{\rho_1 c_1 \Delta z}$$

$$T_{r(t+\Delta t)} = T_{r(t)}\left(1-\frac{2k_1\Delta t}{\rho_1 c_1 \Delta z^2}\right)+\frac{k_1\Delta t}{\rho_1 c_1 \Delta z^2}(T_{r-1(t)}+T_{r+1(t)}) \qquad \text{(A.3)}$$

$$T_{N(t+\Delta t)} = T_{N(t)}\left(1-\frac{2\Delta t(k_1+k_2)}{(\rho_1 c_1+\rho_2 c_2)\Delta z^2}\right)+T_{N-1(t)}\left(\frac{2k_1\Delta t}{(\rho_1 c_1+\rho_2 c_2)\Delta z^2}\right)+T_{N-1(t)}\left(\frac{2k_2\Delta t}{(\rho_1 c_1+\rho_2 c_2)\Delta z^2}\right)$$

Where:

$T_{i(t)}$ = temperatures of the node (i) at time t

T_A = ambient temperature

k_1 and k_2 = thermal conductivity of layers 1 and 2

ρ_1 and ρ_2 = density of layers 1 and 2

c_1 and c_2 = specific heat of layers 1 and 2

Δz and Δt = increments in depth and time

$\overline{T}_{1(t)}$ and $\overline{T}_A$ = node 1 and ambient temperature (°R or K)

HUNTER AND MCGUIRE [35]

The previous two methods utilized main frame computers to solve systems of equations. Hunter and McGuire further modified the Crank Nicolson approach to develop a matrix system of linear equations which could be efficiently solved on a microcomputer. They avoided the problems associated with iterative solutions by developing a method of solving the matrix system directly.

APPENDIX B
MATERIAL PROPERTIES

MATERIALS FOR THERMAL TESTING

Table B.1 Batch weights for standard dense-graded and SMA mix designs

Aggregate Type	Sieve Size		Dense-Graded		SMA	
			4.4 kg batch	24 kg batch	4.4 kg batch	24 kg batch
	mm	U.S.	g	g	g	g
Crushed Granite (Granite Falls)	12.70	1/2 in.	-----	-----	1750	12000
	9.525	3/8 in.	1113	6071	700	4800
River Gravel (Lakeland)	4.750	No. 4	710	3873	175	1200
	2.360	No. 8	571	3115	175	1200
	1.180	No. 16	655	3573	280	1920
	0.600	No. 30	923	5035	35	240
	0.300	No. 50	168	916	70	480
	0.150	No. 100	159	867	35	240
	0.075	No. 200	64	349	35	240
	PAN		37	202	245	1680
	TOTAL		4400	24000	3500	24000

Table B.2 Determination of slab weights for 8.0 percent air voids

Specimen Dimensions 381 x 381 x 64 mm			Specimen Volume 0.09218 m^3		
Lab Marshall Mix Designs (50 blows/side)					
Mix Type	AC% TWM	24 kg Mix W_{AC}, g	TMSG	BSG for 8% AV	Wt. Mix g
Dense	4.7	1184	2.408	2.215	20421
SMA	4.3	1078	2.506	2.306	21252

Table B.3 Theoretical weights for loose mix, mid-compaction, and full compaction slab specimens

Slab Mix Weights					
Mix Type	W_{mold}, g	$W_{mold+slab}$, g	W_{min}, g	$W_{50\%}$, g	W_{max}, g
Dense	6600	23880	17280	18851	20421
SMA	6600	22790	16190	18721	21252

Table B.4 Theoretical bulk specific gravity and air void values

Approximate BSG's and Air Voids						
Mix Type	BSG_{min}	AV_{min}, %	$BSG_{50\%}$	$AV_{50\%}$, %	BSG_{max}	AV_{max}, %
Dense	1.875	22.2	2.045	15.1	2.215	8.0
SMA	1.756	29.9	2.031	19.0	2.306	8.0

Table B.5 Properties of Granite Falls/Lakeland aggregate mixtures

Aggregate Type	Dense-Graded 9.5 mm	SMA 12.5 mm
Weight of oven-dry aggregate (A)	1780.0	2599.9
Saturate Surface Dry (SSD) weight (B)	1785.6	2611.8
Weight of SSD agg. under water (C)	1124.3	1589.1
Bulk Specific Gravity A/(B - C)	2.692	2.542
Bulk Specific Gravity, SSD B/(B - C)	2.700	2.554
Apparent Specific Gravity A/(A - C)	2.714	2.573
Absorption Capacity, % 100·(B - A)/A	0.32	0.46

Table B.6 Physical properties of Koch 120/150 penetration grade asphalt cement

Property	Value
Viscosity at 40 °C, Pa·s	84.6
Viscosity at 135 °C, Pa·s	27.1
Penetration at 25 °C, 0.1 mm	130
Ductility at 25 °, 5 cm/min.	120 +
Flash point, °C	318
Tests on Residue from Thin Film Oven Test	
Viscosity at 40 °C, Pa·s	188
Viscosity at 135 °C, Pa·s	43.9
Penetration at 25 °C, 0.1 mm	71
Ductility at 25 °C, 5 cm/min.	120 +

APPENDIX C
THERMAL TESTING PROCEDURES

SLAB COOLING METHOD FOR THERMAL DIFFUSIVITY

Test Apparatus

1. Insulated Box: A 510 x 510 x 130 mm steel box capable of supporting a 23 kg slab insulated on the sides and bottom with 64 mm rigid mineral fiber insulation should be used to approximate one-dimensional upward heat flow in the center of the slab. The insulation may be wrapped in of heavy paper to prevent it from sticking to the specimen.
2. Thermocouples with Teflon insulated 0.081 mm (No. 20) wires which can be plugged into a multi-channel thermocouple reader
3. Thermocouple reader accurate to ± 0.1 °C with at least four channels
4. Timer accurate to ± 0.1 sec.
5. Oven capable of maintaining 150 ± 5 °C and large enough to accommodate the insulated box

Specimen

A 380 x 380 x 64 mm slab should be used. Slab dimensions should be such that the height-to-length ratio is less than the maximum recommended value of 0.2 for approximating an infinite wall condition. Holes of a diameter sufficient to allow the insertion of thermocouples are drilled into the bottom of the slab at depths of 13, 25, 38, and 51 mm in a radial pattern 25 mm from the center of the slab (Figure C.1).

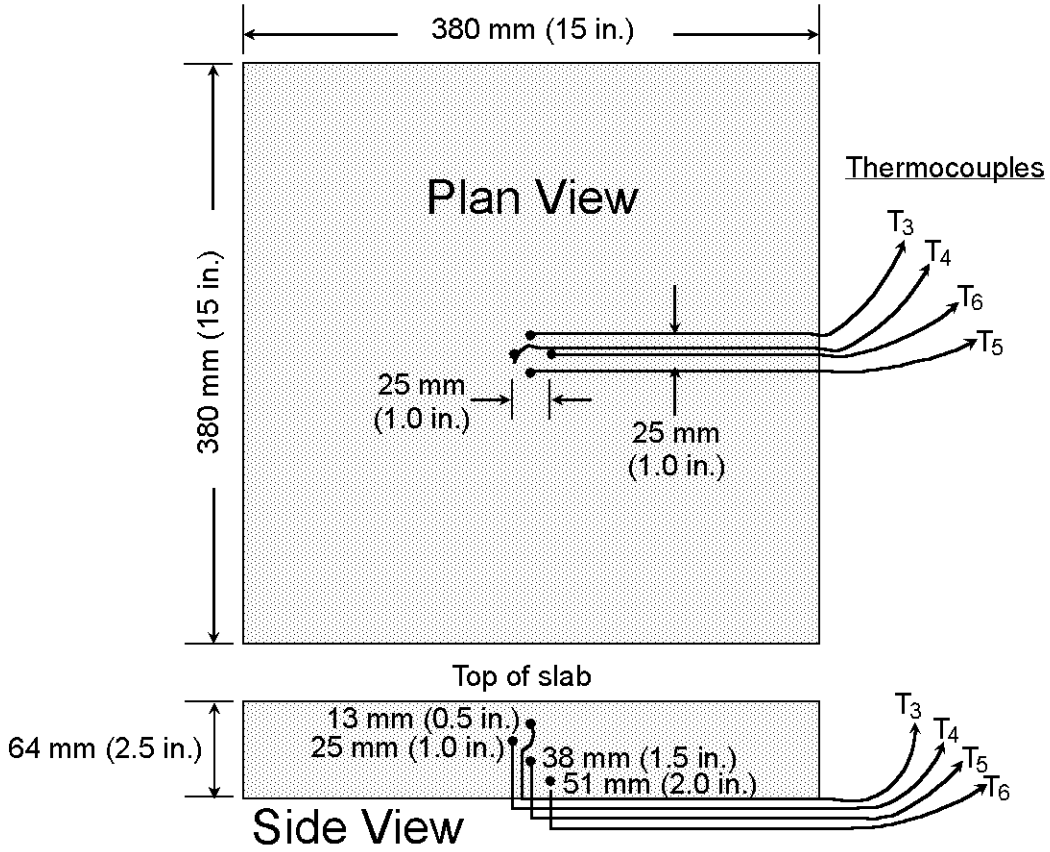

Figure C.1 Placement of thermocouples in slab specimen

Compaction Method

1. Use the mold volume, theoretical maximum specific gravity (TMSG), and the desired air void percent to determine the amount of mix to place in the mold.
2. Prepare the hot-mix according to ASTM mixing procedures.
3. Place the mixture in the compaction mold, taking care to avoid segregation and loss of material.
4. Compact the specimen to the height of the mold.
5. Allow the specimen to cool to room temperature, and remove from the mold.

Test Procedure

1. Label the thermocouple wires 1, 2, 3, and 4, corresponding to the 13, 25, 38, and 51 mm holes, respectively.

2. Coat the thermocouple junctions with silicone thermal grease and insert them into the four holes in the bottom of the slab, running the exposed wire along the bottom of the slab.
3. Heat a small amount of the asphalt binder used in the mix design until liquid and pour it around the wires to hold them in place while the slab is inverted and placed in the insulated box.
4. Invert the slab and place it in the insulated box so that only the upper surface is exposed to the air.
5. Place the box in a 150 °C oven and heat until the four thermocouple readings indicate a constant temperature in the slab. Record this temperature as T_o.
6. Remove the box from the oven and place it in a draft-free location. Record the four thermocouple readings at one minute intervals for the first 30 minutes, and then at 5 minute intervals for the next 150 minutes.

Calculations

1. Plot the temperature (° C) versus time (sec.) and divide the time scale into segments which are approximately linear (Figure 4.4).
2. For each time segment, plot the average of the four thermocouple readings (°C) versus time, and the average reading of each thermocouple over the time segment versus depth (m) in the slab.
3. Fit a first-order curve of the form $T = a_1 t + a_2$ to each time-temperature plot, and a second-order curve of the form $T = b_1 z^2 + b_2 z + b_3$ to each depth-temperature plot (Figure 3.8).
4. Calculate the thermal diffusivity using Eqs. (4.3) through (4.6):

$$\alpha \frac{d^2T}{dz^2} = \frac{dT}{dt}$$

$$\text{Substitute } \frac{d^2T}{dz^2} = 2a_1 \text{ and } \frac{dT}{dt} = b_1 \text{ ; then solve: } \alpha = \frac{b_1}{2a_1}$$

This value represents the thermal diffusivity at the midpoint of the temperature range corresponding to the given time segment.

CYLINDER THERMAL CONDUCTIVITY PROCEDURE

Test Apparatus

1. Thermal Probe (Figure 3.12)
2. Constant Current Source
3. Thermocouple reader accurate to ± 0.1C
4. Timer accurate to ± 0.1 sec.
5. Oven capable of maintaining 150 ± 5 °C

Specimen

A cylinder with minimum dimensions of 100 x 150 mm cylinder should be used. A hole of a depth and diameter sufficient to allow the insertion of the thermal probe should be drilled into the bottom of the cylinder or incorporated into the mold design. The specimen should be kept inside the mold and supported from the bottom to maintain its shape during high-temperature tests.

Procedure

1. Allow the specimen and thermal probe to come to equilibrium temperature.
2. Connect the heater wire leads to a constant current source.
3. Connect the thermocouple plug to a thermocouple reader.
4. Apply a known constant current to the heater wire such that the temperature change is less than 10 K in 1000 s.
5. Record the readings at 0, 5, 10, 15, 30, 45, and 60 s, then take readings at 30 s time intervals for a minimum of 1000 s.
6. Record the current and voltage readings.
7. Turn off constant current source.
8. Plot temperature, °C on the y-axis and log(time) on the x-axis.
9. Locate the linear portion (pseudo steady state portion) of the curve.

Calculations

1. Determine the values of T_1, T_2, t_1, and t_2 (Figure C.2).
2. Calculate the coefficient, c_1:

$$c_1 = \frac{(T_2 - T_1)}{\ln(t_2 / t_1)} \qquad \text{(C.1)}$$

3. Calculate the thermal conductivity, k:

$$k = \frac{EI}{4\pi L c_1} \qquad \text{(C.2)}$$

Where:

k = thermal conductivity, W/m·K

E = volts

I = amps

L = heated length of probe = 0.051 m

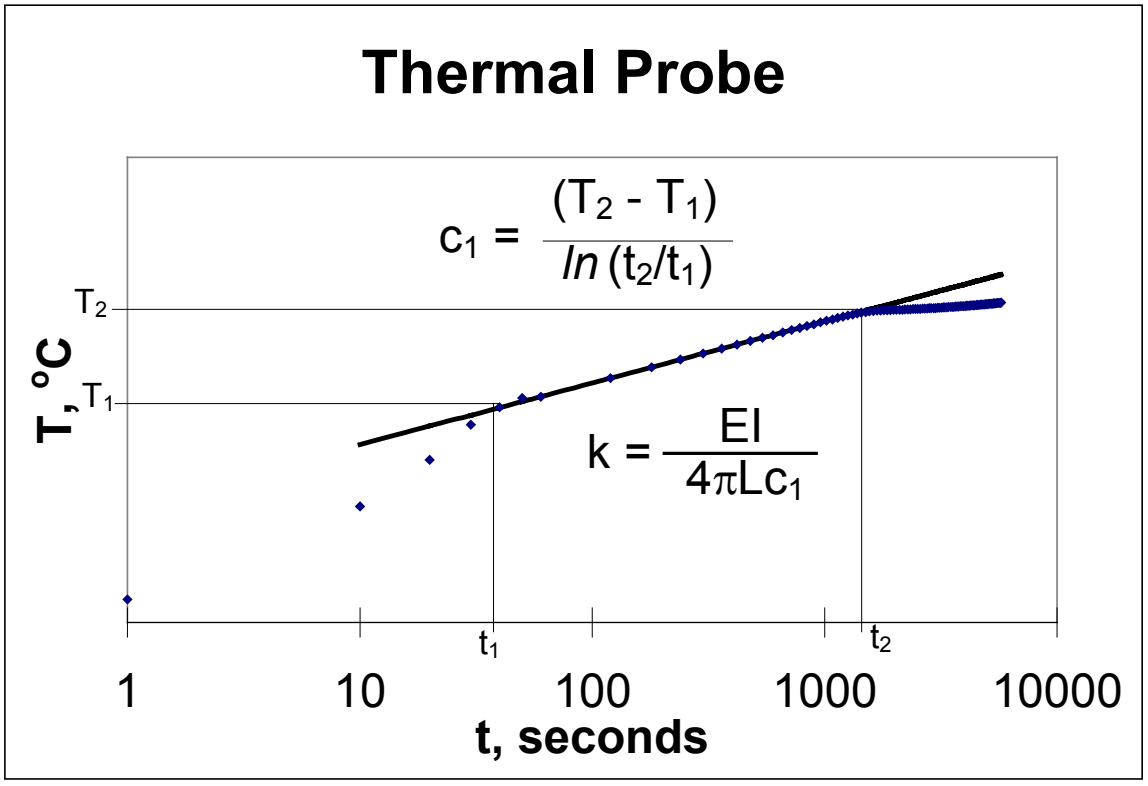

Figure C.2 Thermal probe time-temperature curve

APPENDIX D
ENVIRONMENTAL MODELS

A comprehensive pavement cooling model requires information on environmental conditions that may be difficult to measure directly and are not readily available from local weather reports. Values such as the net solar radiation at the surface, convection coefficient, and initial temperature profiles can be computed using more readily available weather data.

CALCULATION OF NET SOLAR FLUX ON A PAVEMENT SURFACE

Three models were combined to estimate the net solar flux (W/m^2) on a pavement surface given the following inputs:

ϕ = latitude, radians $\left(\text{radians} = \text{degrees} \times \frac{\pi}{180} \right)$

d = day of year ($1 \le d \le 365$)

t = time of day, hours ($0 < t \le 24$)

C_C = estimated cloud cover, percent ($0 \le C_C \le 100$)

Constants (from Guttman and Matthews [38]):

S (solar constant) = 1377 W/m^2

e = (ellipticity of the earth's orbit) = 0.0167238

Solar Flux At Top Of Atmosphere

Guttman and Matthews [36] the following model estimates the solar flux (W/m^2) at the top of the atmosphere based on location, day of year, and time of day.

Procedure

1. Calculate the earth's angular displacement from the major axis of orbit, θ (radians).

$$\theta = 2\pi \frac{d - 2}{365.242} \qquad 365 \le d \le 2 \qquad \text{(D.1)}$$

$$\theta = 2\pi \frac{d + 363}{365.242} \qquad 1 \le d \le 2 \qquad \text{(D.2)}$$

2. Calculate the angular fraction of a year represented by day number, ψ (radians).

$$\psi = 2\pi \frac{d - 1}{365.242} \qquad \text{(D.3)}$$

3. Calculate the solar declination, D (radians).

$$D = \arcsin\left[\sin(0.409172)\sin\sigma\right] \quad (D.4)$$

Where:

$$\sigma = 4.885784 + 3.342004 \times 10^{-2} \sin(\psi) - 1.3880 \times 10^{-3} \cos(\psi) + 3.4798 \times 10^{-4} \sin(2\psi) - 2.285 \times 10^{-5} \cos(2\psi) + \psi \text{ (radians)} \quad (D.5)$$

4. Calculate the equation of time, β (hours).

$$\beta = 0.12357\sin(\psi) - 0.004289\cos(\psi) + 0.153809\sin(2\psi) + 0.060783\cos(2\psi) \quad (D.6)$$

5. Calculate the solar hour angle, h (radians).

$$h = \frac{\pi}{12}(t - \beta - 12) \quad (D.7)$$

6. Calculate cos(Z).

$$\cos(Z) = \sin(\phi)\sin(D) + \cos(\phi)\cos(D)\cos(h) \quad (D.8)$$

Where:

Z = zenith angle of the sun (angle from the local vertical) in radians.

Calculate the instantaneous energy flux through an element of area parallel to the earth's surface at the top of the atmosphere, I ,W/m^2.

$$I = S\frac{\left[1 + e \times \cos(\theta)\right]^2}{1 - e^2}\cos(Z) \quad (D.9)$$

7. Calculate the average flux (t_1,t_2) at the top of the atmosphere, W/m^2.

$$\bar{I} = \frac{12S}{\pi(t_2 - t_1)}\frac{(1 + e \cdot \cos\theta)^2}{1 - e^2}\left[(\sin\phi \sin D)(h_2 - h_1) + (\cos\phi \cos D)(\sin(h_2) - \sin(h_1))\right] \quad (D.10)$$

Where:

(t_1,t_2) is the time interval (hours) during which temperature information is needed (ideally, t_1 would correspond to the time of sunrise)

h_1 and h_2 are the solar hour angles corresponding to times t_1 and t_2 (Equation D.7).

Net Surface Flux

The equation developed by Schmetz [39] is used to calculate the clear sky surface flux.

$$I_{clr} = 0.828I + b \quad (D.14)$$

Where:

b = intercept = -47.4 W/m^2

In order to take cloud cover into consideration, 100 percent cloud cover is assumed to block 100 percent of the solar radiation, and the C_C term is included to calculate the net surface flux.

$$I_s = (0.828I + b)\left(1 - \frac{C_C}{100}\right) \tag{D.15}$$

The average net surface flux over time interval (t_1,t_2) is calculated by substituting the average flux at the top of the atmosphere into Equation D.15.

$$\bar{I}_s = (0.828\bar{I} + b)\left(1 - \frac{C_C}{100}\right) \tag{D.16}$$

Convection Coefficient

Alford, et al [40] developed an equation that estimates the convection coefficient h, W/m^2K from the wind velocity.

$$h = r_{BB} + (h_o - r_{BB})\left(\frac{v}{v_o}\right)^{0.75} \tag{D.17}$$

Where:

v = wind velocity, m/s (mph)

h = convection coefficient for velocity v, W/m^2K

v_o = reference wind velocity = 6.7 m/s

h_o = convection coefficient for v_o = 34 W/m^2K

r_{BB} = black body radiation coefficient = 7.4 W/m^2K

The Alford, et al [38] stated that applying this algorithm required assuming that the surface is a black body, but that this method provided results of sufficient accuracy for practical purposes.

ESTIMATING TEMPERATURE PROFILES IN AN EXISTING PAVEMENT STRUCTURE

In 1957, Barber [41] presented a method for estimating temperature profiles in a pavement structure using information from weather reports. The model assumes the air temperature follows a 24-hour periodic cycle characterized by the following equation:

$$T_a = T_M + T_V \sin 0.262t \quad \text{(D.18)}$$

Where:

T_a = air temperature, ^oC

t = time from beginning of cycle, hours

T_M = mean effective air temperature, ^oC

$$T_M = T_A + R \quad \text{(D.19)}$$

Where:

T_A = average air temperature over time interval (t_1,t_2), ^oC

R = average net temperature loss from surface by long-wave radiation, ^oC

$$R = a.f_s.\bar{I}_s \quad \text{(D.20)}$$

Where:

a = absorptivity of surface to solar radiation (0.95 for asphalt concrete)

f_s = solar flux correction factor = 0.03200 $^oC \cdot m^2/W$

$\bar{I}_s$ = average solar flux at the surface over time interval (t_1,t_2), W/m^2 by Eq. D.16 (the C_C term in this case represents the average cloud cover over the time interval)

T_V = maximum variation of air temperature from mean, ^oC

$$T_V = 0.5T_R + 3R \quad \text{(D.21)}$$

Where:

T_R = daily range in air temperature, ^oC (from weather reports)

The temperature profile of the pavement structure can be calculated from measured air temperatures during time interval (t_1,t_2) as follows:

$$T_{(t,z)} = T_M + T_V \frac{He^{-zA}}{\sqrt{(H+A)^2 + A^2}} \sin\left(0.262t - zA - \arctan\frac{A}{H+A}\right) \quad (D.22)$$

Where:

$T_{(t,z)}$ = temperature at time t and depth z in pavement structure, ^oC

z = depth below surface, m

$$H = h / k \quad (D.23)$$

Where:

h = convection coefficient, $W/m^2 \cdot K$ (Equation D.17)

k = thermal conductivity of surface material, $W/m \cdot K$

$$A = \sqrt{f_t / \alpha} \quad (D.24)$$

Where:

α = thermal diffusivity of surface material, m^2/s

f_t = time conversion factor = 471.6 s

APPENDIX E
LABORATORY THERMAL DATA

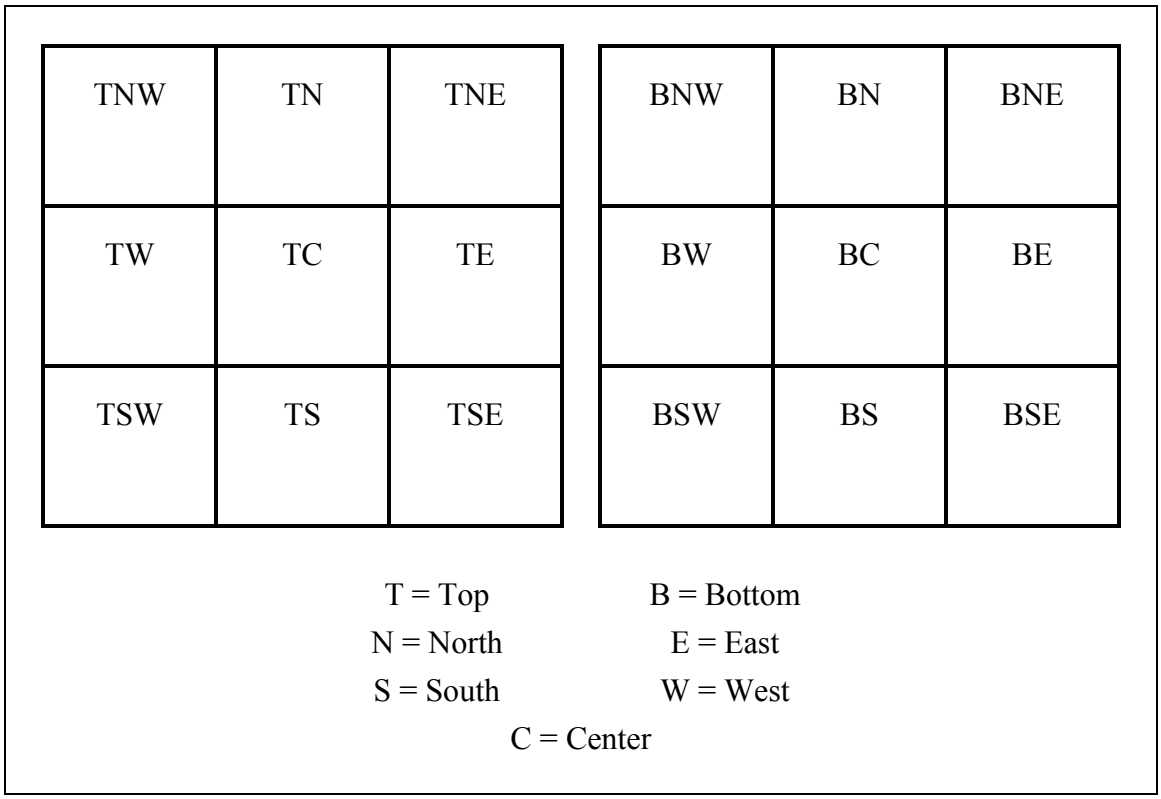

Figure E.1 Labeling Convention for Slab Sections

Bulk Specific Gravity
(Air Voids)

NW 1.980 (21.0)	N 1.945 (22.4)	NE 1.968 (21.5)
W 1.952 (22.1)	C 2.005 (20.0)	E 2.022 (19.3)
SW 1.993 (20.5)	S 1.964 (21.6)	SE 1.983 (20.9)

Dense-graded loose mix

TNW 2.105 (16.0)	TN 2.164 (13.6)	TNE 2.128 (15.1)	BNW 2.113 (15.7)	BN 2.183 (12.9)	BNE 2.114 (15.7)
TW 2.167 (13.5)	TC 2.184 (12.9)	TE 2.143 (14.5)	BW 2.178 (13.1)	BC 2.203 (12.1)	BE 2.139 (14.6)
BSW 2.116 (15.5)	BS 2.131 (15.0)	BSE 2.121 (15.3)	BSW 2.135 (14.8)	BS 2.132 (14.9)	BSE 2.120 (15.4)

Dense-graded mid-compaction

TNW 2.212 (11.7)	TN 2.195 (12.4)	TNE 2.201 (12.2)	BNW 2.215 (11.6)	BN 2.228 (11.1)	BNE 2.208 (11.9)
TW 2.243 (10.5)	TC 2.225 (11.2)	TE 2.191 (12.6)	BW 2.241 (10.6)	BC 2.259 (9.9)	BE 2.219 (11.5)
TSW 2.219 (11.4)	TS 2.239 (10.7)	TSE 2.386 (4.8)	BSW 2.180 (13.0)	BS 2.245 (10.4)	BSE 2.183 (12.9)

Dense-graded full compaction

Figure E.2 Bulk Specific Gravity and Air Voids for Dense-Graded Slab Specimens

Bulk Specific Gravity
(Air Voids)

NW 1.858 (26.5)	N 1.903 (24.7)	NE 1.875 (25.8)
W 1.846 (27.0)	C 1.930 (23.7)	E 1.885 (25.4)
SW 1.861 (26.4)	S 1.885 (25.4)	SE 1.816 (28.2)

SMA loose mix

TNW 2.029 (19.7)	TN 2.026 (19.9)	TNE 1.927 (23.8)	BNW 2.027 (19.8)	BN 2.068 (18.2)	BNE 2.066 (18.3)
TW 2.073 (18.0)	TC 2.020 (20.1)	TE 2.032 (19.6)	BW 2.108 (16.6)	BC 2.143 (15.2)	BE 2.051 (18.9)
TSW 1.958 (22.6)	TS 2.007 (20.6)	TSE 1.953 (22.7)	BSW 2.069 (18.2)	BS 2.034 (19.5)	BSE 2.039 (19.3)

SMA mid-compaction

TNW 1.974 (21.9)	TN 1.992 (21.2)	TNE 1.992 (23.2)	BNW 2.115 (16.3)	BN 2.233 (11.6)	BNE 2.182 (13.7)
TW 2.103 (16.8)	TC 2.105 (16.7)	TE 2.077 (17.8)	BW 2.220 (12.2)	BC 2.247 (11.1)	BE 2.195 (13.2)
TSW 2.051 (18.9)	TS 2.142 (15.3)	TSE 2.001 (20.8)	BSW 2.126 (15.9)	BS 2.154 (14.8)	BSE 2.061 (18.5)

SMA full compaction

Figure E.3 Bulk Specific Gravity and Air Voids for SMA Specimens

Table E.1 Copper-Constantan Thermocouple Calibration

4/13/95	Temperature, °C					
Mercury	Thermocouple Readings					
Therm.	T_1	T_2	T_3	T_4	T_5	T_6
22.8	22.8	22.7	22.8	22.8	22.7	22.7
59.2	57.8	57.8	57.8	57.8	57.8	57.8
101.0	99.3	99.4	99.3	99.5	99.4	99.3
134.9	134.3	134.3	134.3	134.3	134.3	134.2

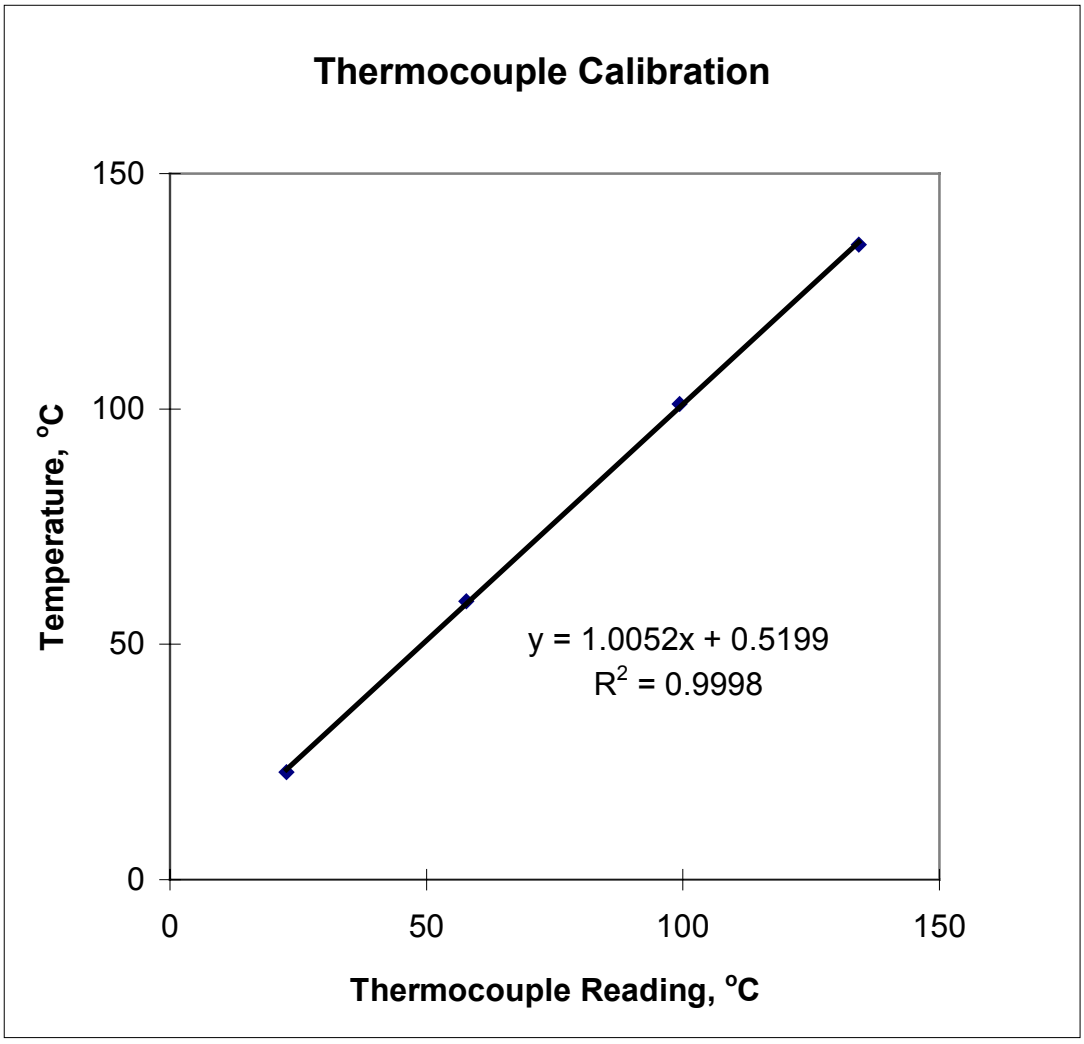

Figure E.4 Regression plot for thermocouple calibration

Table E.2 Slab specimen thermocouple readings: Dense-graded loose mix

	Thermocouple Readings, °C			
		4/28/95	Air Temp. =	22.7°C
time, minutes	T_1 13 mm	T_2 25 mm	T_3 38 mm	T_4 51 mm
0	147.4	147.1	147.2	147.1
1	146.1	146.4	146.6	146.6
2	145.1	146.7	147.1	147.2
3	144.2	147.2	147.5	147.7
4	143.2	146.7	148.0	148.1
5	142.0	146.7	148.1	148.5
6	141.1	146.3	148.1	148.4
7	140.3	145.8	148.0	148.5
8	139.2	144.9	147.7	148.4
9	138.2	144.6	147.3	148.4
10	137.4	144.0	146.9	148.2
11	136.6	143.4	146.5	147.9
12	135.7	142.7	146.1	147.6
13	134.8	141.9	145.6	147.1
14	134.1	141.4	145.0	146.8
15	133.3	140.7	144.5	146.4
16	132.6	140.0	143.9	145.8
17	131.7	139.3	143.4	145.4
18	131.2	138.7	142.8	144.8
19	130.4	138.0	142.2	144.4
20	129.9	137.5	141.7	143.7
21	129.2	136.8	141.1	143.3
22	128.6	136.1	140.6	142.8
23	127.9	135.5	139.8	142.1
24	127.3	134.8	139.3	141.5
25	126.7	134.4	138.6	140.8
26	125.9	133.6	138.1	140.3
27	125.4	133.2	137.6	139.8
28	124.6	132.2	136.8	139.0
29	124.2	131.8	136.3	138.7
30	123.7	131.2	135.7	138.1
35	120.8	128.2	132.6	135.0
40	118.3	125.3	129.7	132.0
45	115.8	122.5	126.7	128.9
50	113.2	119.7	123.7	126.3
55	110.9	117.2	121.0	123.2

Table E.2, continued

	Thermocouple Readings, °C			
		4/28/95	Air Temp. =	22.7°C
time, minutes	T_1 13 mm	T_2 25 mm	T_3 38 mm	T_4 51 mm
60	108.8	114.8	118.5	120.6
65	106.7	112.4	116.0	118.1
70	104.4	109.9	113.4	115.4
75	102.3	107.4	110.9	112.9
80	100.2	105.2	108.4	110.3
85	98.1	102.9	106.2	108.0
90	96.1	100.8	103.8	105.6
95	94.1	98.7	101.6	103.4
100	92.4	96.7	99.5	101.3
105	90.6	94.6	97.4	99.2
110	88.9	92.8	95.6	97.1
115	87.2	91.0	93.5	95.2
120	85.5	89.1	91.6	93.1
150	76.1	78.9	80.9	82.2
180	68.4	70.7	72.3	73.5

Table E.3 Slab specimen thermocouple readings: Dense-graded mid-compaction

	Thermocouple Readings, °C			
		4/29/95	Air Temp. =	22.9°C
time, minutes	T_1 13 mm	T_2 25 mm	T_3 38 mm	T_4 51 mm
0	148.4	148.2	148.3	148.2
1	147.9	148.1	148.3	148.4
2	147.2	148.5	148.8	148.8
3	146.4	148.5	148.8	149.2
4	145.5	148.2	149.2	149.4
5	144.5	147.8	149.0	149.3
6	143.5	147.2	148.8	149.1
7	142.7	146.7	148.6	148.9
8	141.7	146.3	148.2	148.8
9	141.0	145.6	147.9	148.8
10	140.1	145.0	147.4	148.5
11	139.3	144.4	147.1	148.2
12	138.5	143.8	146.6	147.7
13	137.7	143.1	146.1	147.4
14	136.9	142.4	145.5	146.9
15	136.2	141.8	145.0	146.4
16	135.6	141.3	144.4	145.9
17	134.8	140.6	143.8	145.2
18	134.2	139.9	143.3	144.8
19	133.4	139.2	142.7	144.1
20	132.8	138.7	142.2	143.7
21	132.2	138.1	141.6	143.3
22	131.6	137.4	141.0	142.7
23	131.0	136.9	140.3	142.1
24	130.3	136.3	139.8	141.6
25	129.7	135.6	139.2	140.9
26	129.1	135.1	138.7	140.3
27	128.6	134.5	137.9	139.7
28	127.9	133.8	137.3	139.1
29	127.3	133.2	136.8	138.4
30	126.7	132.7	136.0	137.7
35	124.1	129.9	133.3	135.0
40	121.5	127.0	130.3	131.9
45	119.0	124.3	127.4	129.1
50	116.5	121.6	124.4	126.2
55	114.2	119.0	121.6	123.6

Table E.3, continued

	Thermocouple Readings, °C			
		4/29/95	Air Temp. =	22.9°C
time, minutes	T_1 13 mm	T_2 25 mm	T_3 38 mm	T_4 51 mm
60	111.9	116.7	119.5	121.0
65	109.6	114.2	116.9	118.4
70	107.4	111.8	114.4	115.9
75	105.3	109.5	112.0	113.4
80	*	*	*	*
85	101.1	104.9	107.2	108.6
90	99.2	102.9	105.2	106.4
95	97.1	100.7	103.0	104.1
100	95.3	99.0	100.9	102.1
105	93.4	96.9	98.9	100.1
110	91.7	94.8	96.8	97.9
115	89.9	93.0	94.9	96.0
120	88.2	91.2	93.0	94.1
150	78.7	81.2	82.7	83.1
180	70.8	72.7	73.8	74.7

* No measurements taken

Table E.4 Slab specimen thermocouple readings: Dense-graded full compaction

	Thermocouple Readings, °C					
	5/11/95				Air Temp. =	23.4°C
time, minutes	T_1 6 mm	T_2 13 mm	T_3 19 mm	T_4 25 mm	T_5 38 mm	T_6 51 mm
0	144.8	144.4	144.8	144.8	144.9	144.8
1	143.7	143.9	144.4	144.5	144.6	144.4
2	141.9	143.4	144.7	144.6	144.9	144.7
3	140.7	142.7	144.2	144.4	145.0	144.9
4	139.6	141.7	143.7	144.5	145.3	145.1
5	138.3	141.1	143.0	144.3	145.3	145.2
6	137.4	140.4	142.5	143.9	145.2	145.2
7	136.4	139.5	141.7	143.1	145.0	145.1
8	135.5	138.7	141.1	143.1	144.7	144.9
9	134.6	137.9	140.3	142.5	144.4	144.6
10	133.7	137.2	139.6	142.0	144.0	144.4
11	132.9	136.4	138.9	141.2	143.7	144.0
12	132.2	135.7	138.2	140.9	143.2	143.8
13	131.3	135.0	137.5	140.3	142.8	143.3
14	130.7	134.3	136.9	139.8	142.4	143.2
15	130.0	133.6	136.3	139.3	141.9	142.8
16	129.3	133.1	135.3	138.7	141.4	142.5
17	128.7	132.4	135.0	138.2	140.9	141.8
18	128.0	131.7	134.4	137.6	140.5	141.5
19	127.4	131.2	133.8	137.1	140.0	141.0
20	126.8	130.6	133.3	136.4	139.3	140.4
21	126.4	129.9	132.7	135.9	138.8	140.1
22	125.8	129.4	132.2	135.4	138.3	139.6
23	125.2	129.0	131.3	134.8	137.8	139.1
24	124.7	128.3	131.0	134.0	137.4	138.7
25	124.1	127.7	130.4	133.7	136.7	137.9
26	123.6	127.2	129.9	133.3	136.3	137.6
27	123.0	126.7	129.4	132.5	135.8	137.1
28	122.4	126.2	129.0	132.2	135.2	136.5
29	121.9	125.6	128.2	131.7	134.7	135.9
30	121.3	124.8	127.7	130.9	134.0	135.2
35	118.8	122.3	124.9	128.3	131.5	132.7
40	116.4	119.8	122.3	125.6	128.6	129.9
45	114.2	117.4	119.8	123.0	125.9	127.1
50	111.9	115.1	117.5	120.6	123.4	124.7
55	109.7	112.8	115.2	118.1	120.8	121.9

Table E.4, continued

	Thermocouple Readings, °C					
	5/11/95				Air Temp. =	23.4°C
time, minutes	T_1 6 mm	T_2 13 mm	T_3 19 mm	T_4 25 mm	T_5 38 mm	T_6 51 mm
60	*	*	*	*	*	*
65	105.6	108.1	110.4	113.2	115.8	116.9
70	103.4	106.5	108.2	110.9	113.4	114.5
75	*	*	*	*	*	*
80	99.7	101.9	104.0	106.7	108.9	110.0
85	97.8	100.2	102.0	104.2	106.8	107.8
90	96.2	98.6	100.3	102.6	104.8	105.8
95	94.4	96.7	98.3	100.2	102.7	103.8
100	92.7	94.9	96.5	98.7	100.8	101.8
105	91.1	93.1	94.6	96.7	98.9	99.8
110	89.4	91.4	93.0	95.0	97.1	97.6
115	87.8	89.8	91.2	93.2	95.1	96.0
120	86.4	88.3	89.6	91.3	93.3	94.2
150	77.8	79.3	80.4	81.8	83.3	83.9
180	68.0	69.1	69.9	71.0	72.2	72.4

* No measurements taken

Table E.5 Slab specimen thermocouple readings: SMA loose mix

	Thermocouple Readings, C			
		4/26/95	Air Temp. =	23.8°C
time, minutes	T_1 13 mm	T_2 25 mm	T_3 38 mm	T_4 51 mm
0	149.9	150.2	150.5	150.2
1	148.1	149.8	150.3	149.9
2	146.3	149.4	150.0	149.9
3	146.6	149.0	150.2	150.1
4	142.7	148.2	150.1	150.1
5	141.3	147.3	149.7	149.8
6	140.1	146.6	149.3	149.6
7	138.7	145.4	148.8	149.3
8	137.5	144.8	148.3	148.9
9	136.3	143.8	147.7	148.7
10	135.2	142.9	147.0	148.1
11	134.3	142.1	146.4	147.8
12	133.2	141.3	145.8	147.2
13	132.2	140.3	145.0	146.6
14	131.2	139.5	144.3	145.8
15	130.2	138.6	143.5	145.2
16	129.4	137.9	142.8	144.6
17	128.5	137.1	142.1	143.9
18	127.8	136.3	141.3	143.2
19	126.9	135.5	140.7	142.5
20	126.2	134.8	139.9	141.8
21	125.5	134.0	139.1	141.0
22	124.6	133.1	138.1	140.2
23	124.1	132.6	137.7	139.6
24	123.4	131.8	136.9	138.8
25	122.7	131.0	136.1	138.1
26	122.0	130.3	135.5	137.4
27	121.1	129.6	134.7	136.7
28	120.6	128.8	134.0	135.9
29	120.0	128.2	133.4	135.2
30	119.3	127.5	132.6	134.5
35	116.2	123.9	128.9	130.7
40	113.2	120.7	125.4	127.2
45	110.4	117.6	122.1	123.7
50	107.4	114.3	118.6	120.1
55	105.1	111.6	115.8	117.2
60	102.2	108.3	112.3	113.5

Table E.5, continued

	Thermocouple Readings, °C			
		4/26/95	Air Temp. =	23.8°C
time, minutes	T_1 13 mm	T_2 25 mm	T_3 38 mm	T_4 51 mm
65	100.3	106.4	110.2	111.4
70	97.7	103.5	107.2	108.4
75	95.4	101.0	104.6	105.8
80	93.1	98.6	102.0	103.0
85	90.8	95.9	99.3	100.3
90	88.8	93.7	97.0	97.9
95	86.9	91.6	94.7	95.6
100	84.9	89.4	92.4	93.3
105	83.1	87.4	90.3	90.8
110	81.2	85.4	88.1	88.6
115	*	*	*	*
120	77.7	81.6	84.2	84.9
150	68.7	71.4	73.8	74.2
180	61.2	63.7	65.2	65.5

* No measurements taken

Table E.6 Slab specimen thermocouple readings: SMA full compaction

	Thermocouple Readings, °C			
		5/10/95	Air Temp. =	23.8°C
time, minutes	T_1 13 mm	T_2 25 mm	T_3 38 mm	T_4 51 mm
0	148.5	148.5	148.5	148.5
1	147.4	148.4	148.5	148.5
2	146.3	148.5	148.7	148.6
3	145.5	148.1	148.7	148.6
4	144.0	147.6	148.5	148.6
5	143.0	147.1	148.2	148.2
6	141.8	146.4	147.9	148.0
7	140.8	145.8	147.6	147.9
8	139.8	145.2	146.8	147.4
9	138.9	144.4	146.6	147.1
10	137.9	143.7	146.0	146.8
11	137.1	143.0	145.5	146.4
12	136.2	142.3	144.9	145.9
13	135.5	141.6	144.2	145.4
14	134.7	140.9	143.8	144.9
15	133.9	140.4	143.1	144.4
16	133.2	139.6	142.6	143.9
17	132.4	138.9	142.0	143.3
18	131.7	138.3	141.4	142.8
19	131.1	137.4	140.6	142.1
20	130.4	136.9	140.1	141.7
21	129.7	136.3	139.6	141.1
22	*	*	*	*
23	128.4	135.0	138.2	139.8
24	127.8	134.4	137.7	139.3
25	127.3	133.8	137.0	138.7
26	126.6	133.1	136.2	138.1
27	125.9	132.5	135.8	137.4
28	125.3	131.7	135.0	136.7
29	124.7	131.2	134.5	136.2
30	124.3	130.6	133.9	135.6
35	121.4	127.5	130.8	132.5
40	118.7	124.6	127.8	129.4
45	116.1	121.6	124.7	126.2
50	113.5	118.9	121.9	123.5
55	111.1	116.4	119.2	120.7

* No measurements taken

Table E.6, continued

	Thermocouple Readings, °C			
		5/10/95	Air Temp. =	23.8°C
time, minutes	T_1 13 mm	T_2 25 mm	T_3 38 mm	T_4 51 mm
60	108.8	113.8	116.7	118.0
65	106.6	111.3	114.0	115.4
70	104.3	108.9	111.6	112.9
75	*	*	*	*
80	100.1	104.2	106.8	108.0
85	98.0	102.1	104.3	105.6
90	95.9	99.8	102.2	103.2
95	93.9	97.6	99.9	100.9
100	91.9	95.4	97.6	98.7
105	90.1	93.5	95.6	96.6
110	88.2	91.4	93.3	94.3
115	86.6	89.6	91.6	92.6
120	84.4	87.4	89.3	90.3
150	75.3	77.7	79.4	79.9
180	67.7	69.4	70.7	71.2

* No measurements taken

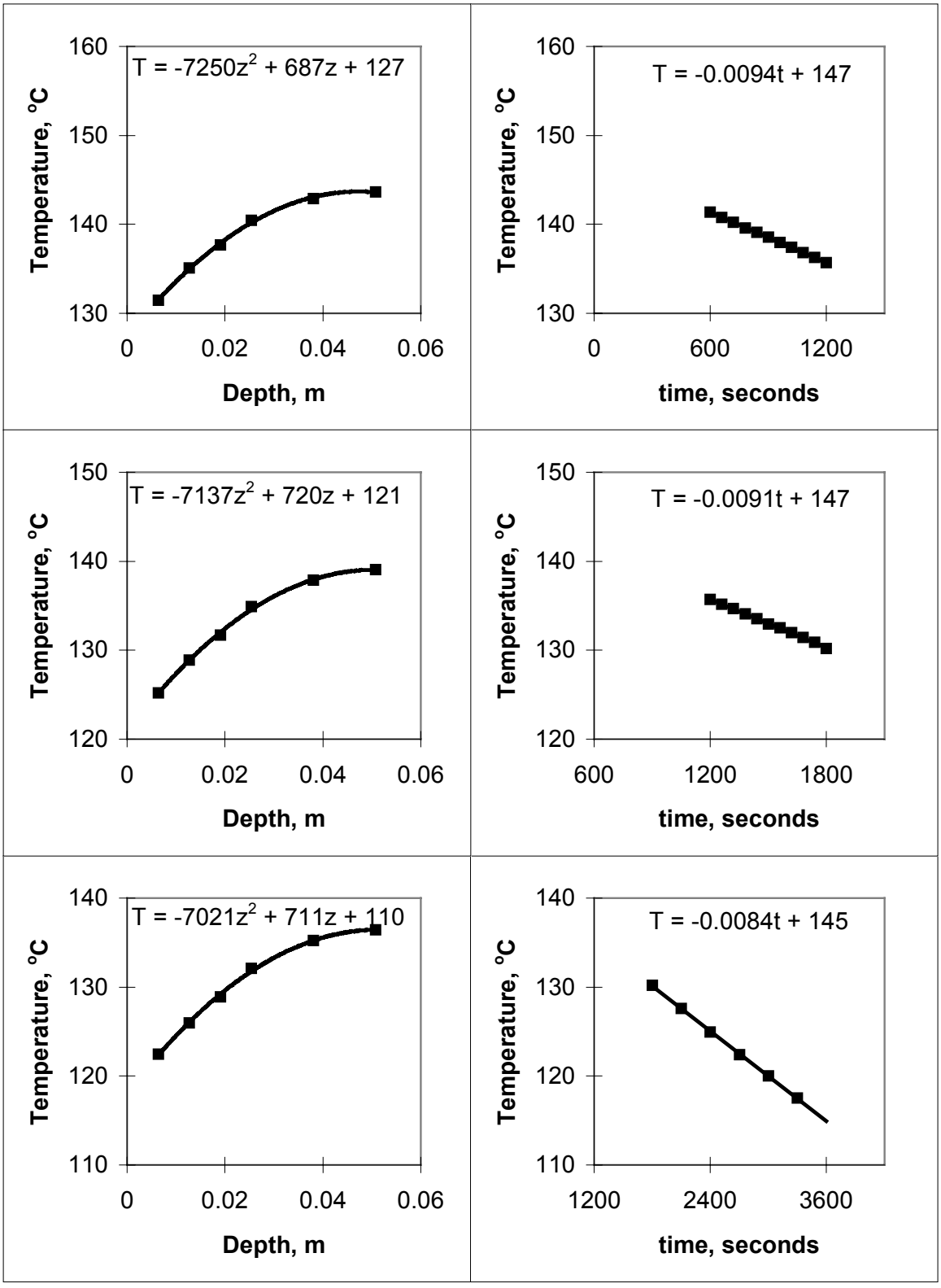

Figure E.5 Temperature Curves for Dense-Graded Full Compaction Slab Specimen

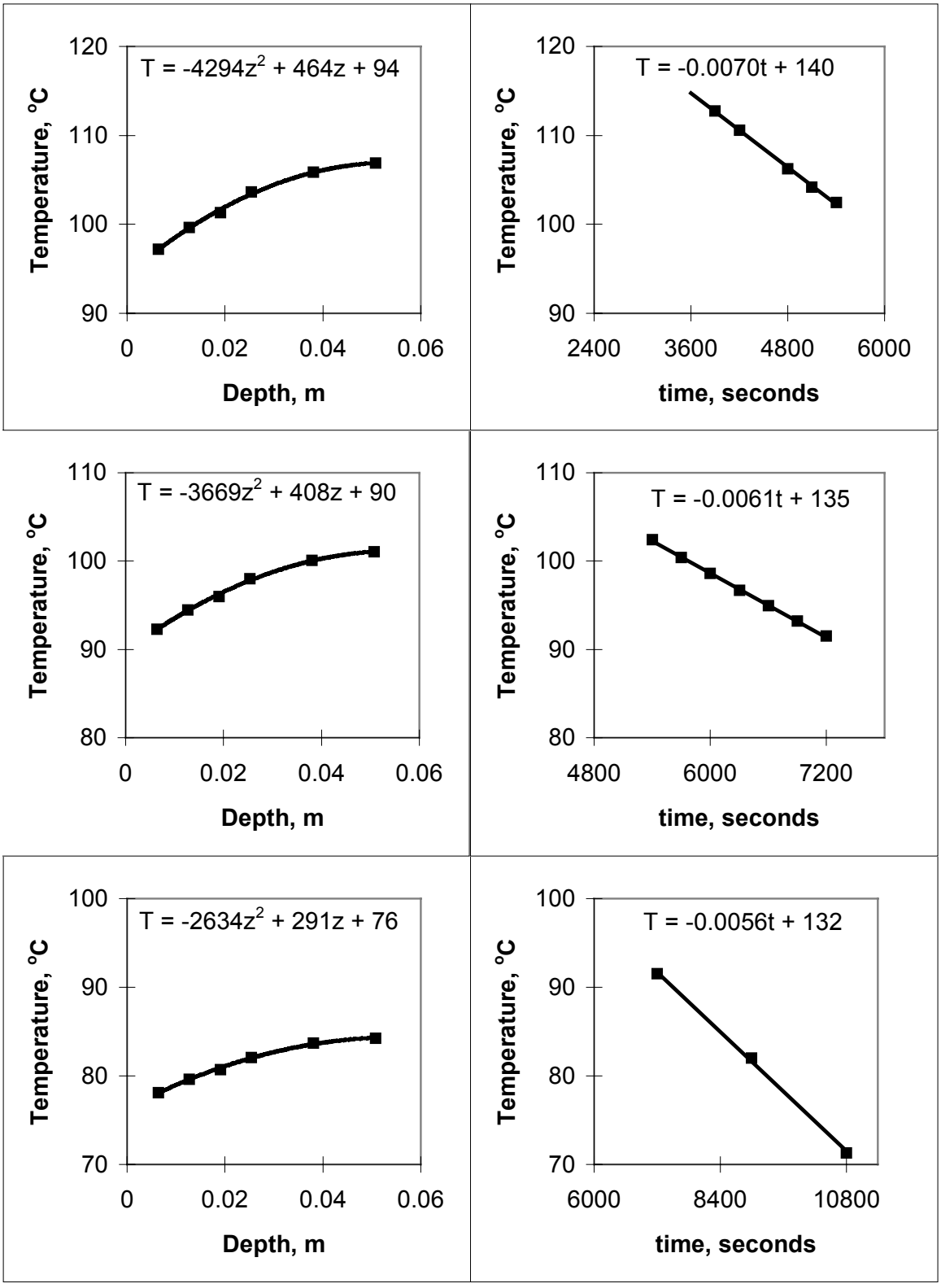

Figure E.5, continued

Table E.7 Thermal probe temperature readings, 24°C (75°F)

5/22/95	DG Loose	DG Full	SMA L	SMA Full
Amps	1.0 A	1.0 A	1.0 A	1.0 A
Volts	3.5 V	3.5 V	3.5 V	3.8 V
time, s	Temperature, °C			
1	24.2	24.1	24.1	23.9
5	31.9	30.0	47.2	33.1
10	34.3	31.5	52.1	*
15	34.6	32.7	54.9	37.0
30	37.2	34.1	61.1	39.0
45	*	35.0	64.0	38.6
60	37.6	35.5	66.0	39.4
90	38.9	36.4	68.1	40.6
120	39.3	37.0	69.4	41.2
150	39.8	37.3	70.2	41.5
180	40.3	37.6	71.0	41.8
210	40.6	38.1	71.6	42.0
240	40.8	38.5	72.1	42.2
270	40.8	38.7	72.3	42.5
300	40.8	38.8	72.5	42.7
330	40.9	39.0	72.7	42.8
360	41.0	39.2	73.0	43.0
390	41.4	39.3	73.2	43.2
420	41.7	39.5	73.3	43.3
450	41.2	39.6	73.5	43.4
480	40.3	39.6	73.5	43.5
510	40.2	39.7	73.6	43.6
540	40.1	39.8	73.7	43.7
570	40.1	39.8	73.7	43.8
600	40.1	39.9	73.8	44.0
630	40.1	40.1	74.0	44.1
660	40.2	40.2	74.1	44.1
690	40.2	40.2	74.2	44.2
720	40.2	40.2	74.2	44.2
750	40.2	40.2	74.2	44.3
780	40.3	40.3	74.3	44.3
810	40.3	40.4	74.3	44.4
840	40.3	40.4	74.5	44.4
870	40.3	40.5	74.5	44.5
900	40.3	40.5	74.6	44.6

Table E.7, continued

5/22/95	DG Loose	DG Full	SMA L	SMA Full
Amps	1.0 A	1.0 A	1.0 A	1.0 A
Volts	3.5 V	3.5 V	3.5 V	3.8 V
time, s	Temperature, °C			
930	40.4	40.6	74.6	44.7
960	40.5	40.6	74.6	44.7
990	40.5	40.6	74.7	44.8
1020	40.5	40.7	74.8	44.8
1050	40.5	40.7	74.8	44.9
1080	40.6	40.8	75.0	44.9
1110	40.6	40.8	75.0	44.9
1140	40.6	40.9	75.0	45.0
1170	40.7	40.9	75.1	45.0
1200	40.7	41.0	75.1	45.0
1230	40.7	41.0	74.9	45.0
1260	40.7	41.0	75.0	45.0
1290	40.7	41.0	75.0	45.1
1320	40.7	41.0	75.0	45.1
1350	40.8	41.0	75.1	45.1
1380	40.8	41.1	75.1	45.2
1410	40.8	41.1	75.1	45.2
1440	40.8	41.1	75.1	45.2
1470	40.9	41.1	75.2	45.2
1500	40.9	41.2	75.2	45.3

Table E.8 Thermal probe temperature readings, 72°C (162°F)

5/24/95	DG Loose	DG Full	SMA L	SMA Full
Amps	1.5 A	1.5 A	1.5 A	1.5 A
Volts	4.9 V	5.1 V	5.0 V	5.0 V
time, s	Temperature, °C			
1	72.2	73.3	71.8	73.7
5	84.9	86.7	98.2	98.8
10	87.7	91.0	114.7	112.0
15	89.1	92.3	127.8	118.8
30	94.1	94.9	142.3	125.5
45	95.8	96.7	150.3	129.0
60	97.4	98.2	154.1	130.8
90	100.2	100.3	159.1	133.3
120	101.8	101.7	162.1	135.1
150	103.2	103.0	164.5	136.4
180	104.2	103.7	166.2	137.2
210	104.8	104.5	167.7	137.9
240	105.3	105.2	168.8	138.5
270	105.6	105.9	169.7	139.1
300	105.6	106.4	170.5	139.6
330	105.9	106.8	171.2	140.0
360	107.2	107.2	171.9	140.2
390	107.7	107.6	172.5	140.4
420	108.1	108.0	173.0	140.7
450	108.5	108.3	173.5	141.1
480	108.8	108.5	173.9	141.1
510	109.1	108.7	174.2	141.2
540	109.5	109.0	174.6	141.3
570	109.7	109.1	174.8	141.5
600	110.1	109.2	175.1	141.7
630	110.3	109.5	175.3	141.9
660	110.5	109.6	175.6	142.0
690	110.7	109.8	175.8	142.2
720	110.9	109.9	176.0	142.3
750	111.1	110.1	176.2	142.4
780	111.2	110.1	176.4	142.5
810	111.4	110.3	176.6	142.6
840	111.7	110.4	176.8	142.7
870	111.8	110.5	177.0	142.8
900	112.0	110.6	177.2	142.8

Table E.8 , continued

5/24/95	DG Loose	DG Full	SMA L	SMA Full
Amps	1.5 A	1.5 A	1.5 A	1.5 A
Volts	4.9 V	5.1 V	5.0 V	5.0 V
time, s	Temperature, °C			
930	112.2	110.7	177.3	142.8
960	112.3	110.7	177.5	142.8
990	112.5	110.8	177.6	142.8
1020	112.7	110.8	177.7	142.8
1050	112.8	110.9	177.9	143.0
1080	112.8	111.0	178.0	143.0
1110	112.9	111.0	178.0	143.2
1140	113.1	111.1	178.1	143.3
1170	113.2	111.1	178.1	143.3
1200	113.3	111.2	178.2	143.3
1230	113.4	111.2	178.3	143.4
1260	113.5	111.3	178.3	143.6
1290	113.6	111.4	178.4	143.6
1320	113.6	111.4	178.5	143.6
1350	113.6	111.5	178.6	143.7
1380	113.7	111.5	178.7	143.7
1410	113.8	111.5	178.8	143.6
1440	113.9	111.5	178.8	143.5
1470	114.0	111.5	178.9	143.5
1500	114.1	111.6	179.1	143.5
1530	114.2	111.6	179.1	143.5
1560	114.3	111.6	179.1	143.6
1590	114.3	111.6	179.1	143.6
1620	114.3	111.7	179.2	143.6
1650	114.5	111.8	179.3	143.7
1680	114.4	111.8	179.3	143.7
1710	114.5	111.8	179.3	143.7
1740	114.6	111.9	179.4	143.7
1770	114.6	112.0	179.4	143.8
1800	114.7	112.0	179.5	143.8
1830	114.7	112.1	179.5	143.8
1860	114.8	112.1	179.6	143.8
1890	114.8	112.1	179.6	143.7
1920	115.0	112.1	179.7	143.7
1950	115.0	112.1	179.7	143.8

Table E.8, continued

5/24/95	DG Loose	DG Full	SMA L	SMA Full
Amps	1.5 A	1.5 A	1.5 A	1.5 A
Volts	4.9 V	5.1 V	5.0 V	5.0 V
time, s	Temperature, °C			
1980	115.1	112.1	179.8	144.1
2010	115.1	112.1	179.8	144.3
2040	115.2	112.2	179.8	144.6
2070	115.2	112.2	179.9	144.7
2100	115.3	112.3	180.0	144.8
2130	115.3	112.3	180.0	145.0
2160	115.3	112.3	180.0	145.0
2190	115.3	112.3	180.0	145.0
2220	115.4	112.4	180.0	145.1
2250	115.5	112.4	180.0	145.1
2280	115.5	112.4	180.1	145.1
2310	115.6	112.5	180.1	145.2
2340	115.6	112.5	180.2	145.2
2370	115.7	112.5	180.2	145.3
2400	115.7	112.5	180.3	145.3
2430	115.8	112.5	180.3	145.4
2460	115.8	112.5	180.3	145.4
2490	115.8	112.5	180.4	145.5
2520	115.8	112.5	180.5	145.5
2550	115.9	112.5	180.5	145.4
2580	115.9	112.5	180.5	145.4
2610	115.9	112.5	180.5	145.3
2640	115.9	112.6	180.5	145.2
2670	115.9	112.6	180.5	145.1
2700	116.0	112.6	180.5	145.1
2730	116.0	112.6	180.5	145.1
2760	116.1	112.6	180.5	145.1
2790	116.1	112.6	180.6	145.1
2820	116.1	112.6	180.7	145.1
2850	116.2	112.6	180.7	145.1
2880	116.2	112.6	180.7	145.1
2910	116.2	112.6	180.8	145.1
2940	116.2	112.6	180.8	145.1
2970	116.3	112.6	180.8	145.1
3000	116.3	112.6	180.9	145.2

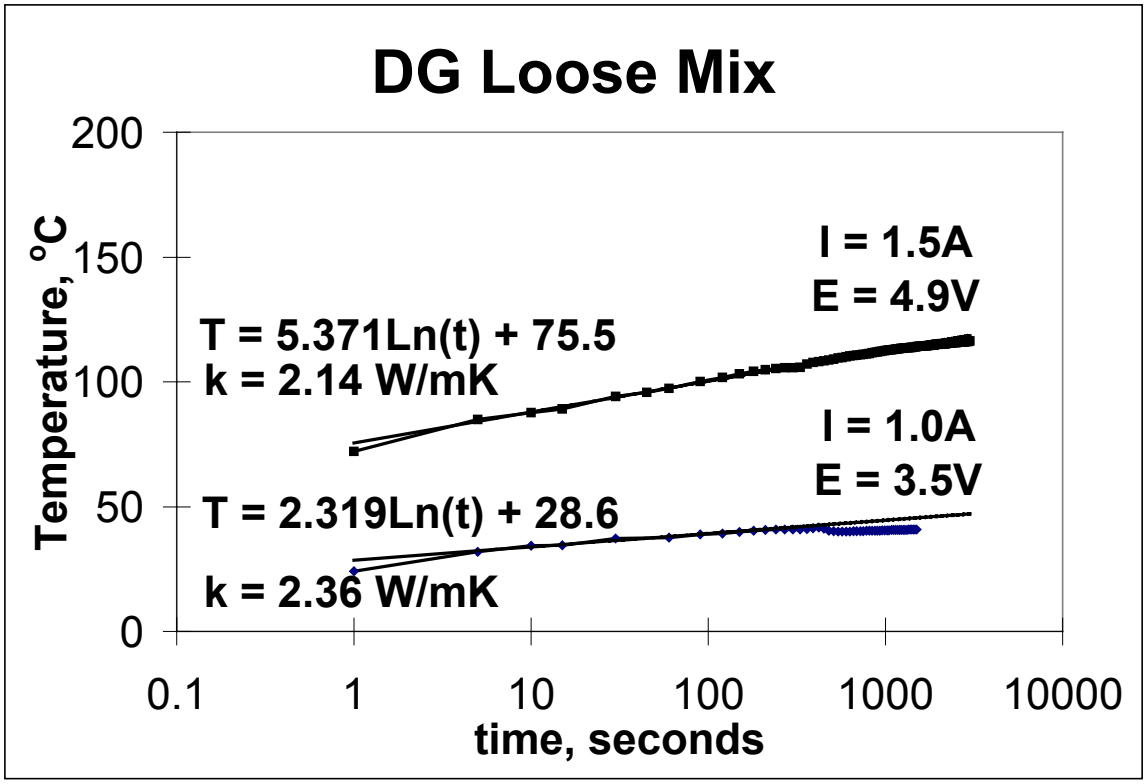

Figure E.6 Thermal probe time-temperature curves, dense-graded loose mix

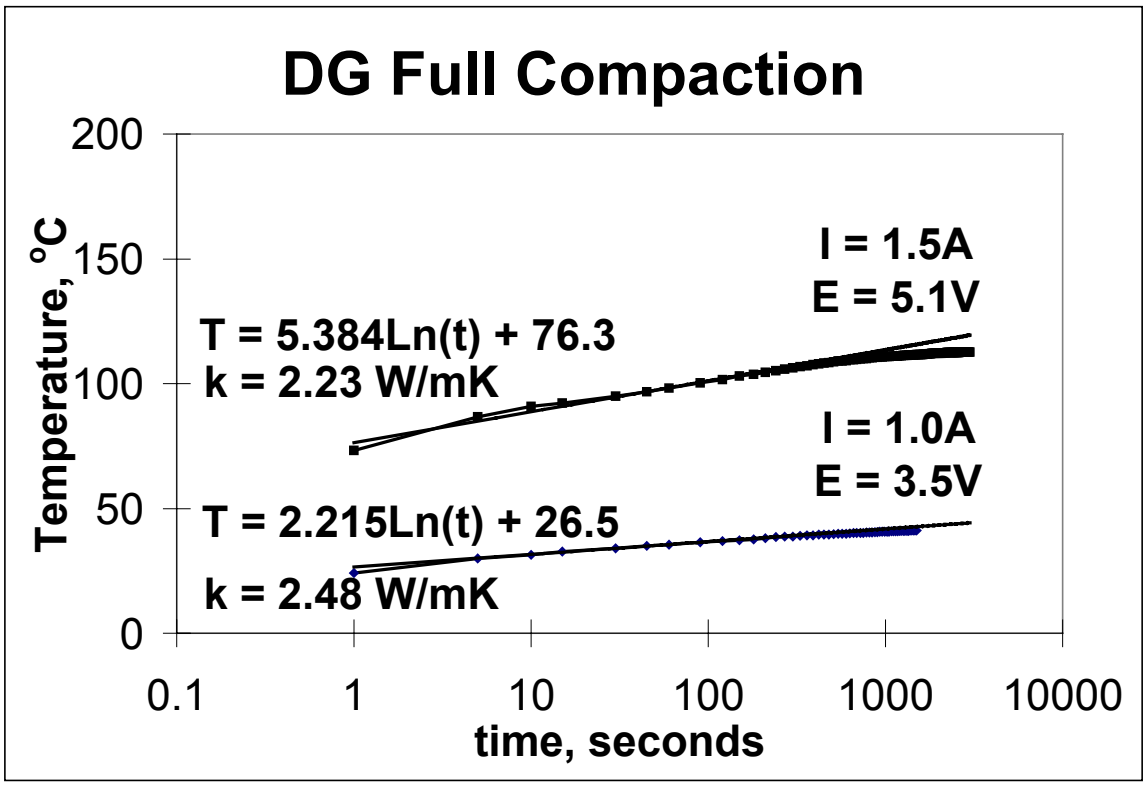

Figure E.7 Thermal probe time-temperature curves, dense-graded full compaction

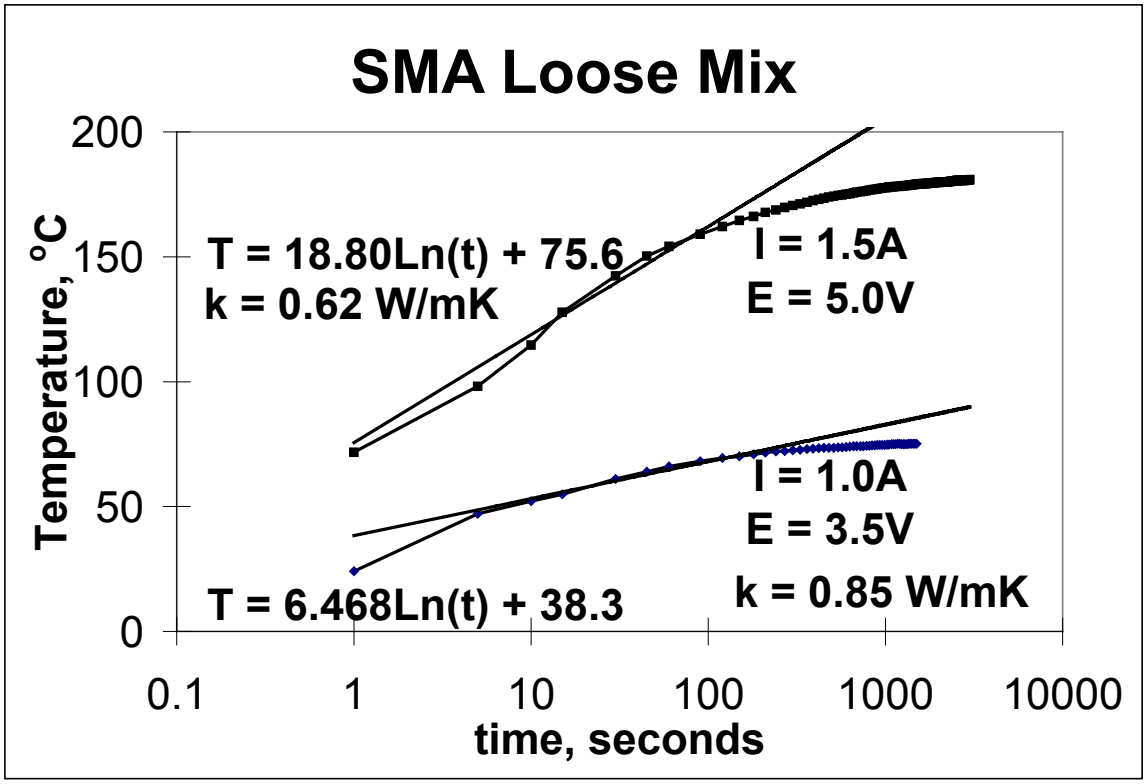

Figure E.8 Thermal probe time-temperature curves, SMA loose mix

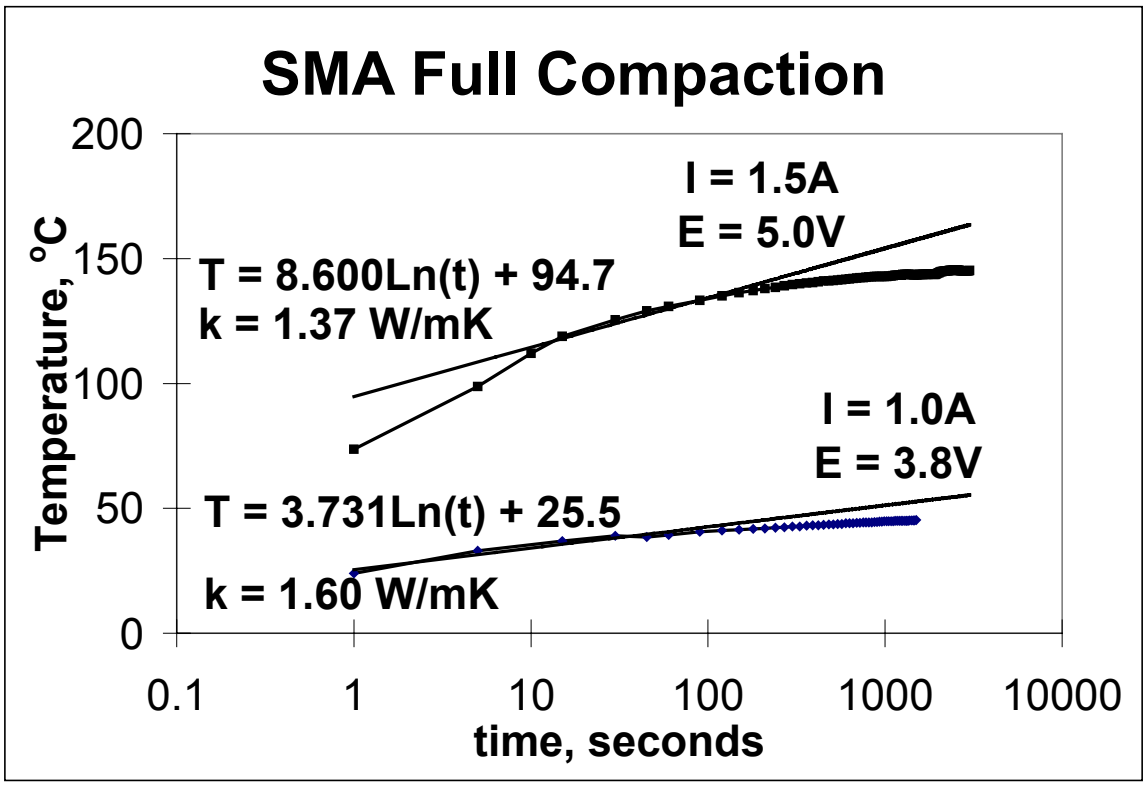

Figure E.9 Thermal probe time-temperature curves, SMA full compaction

APPENDIX F
FIELD VERIFICATION

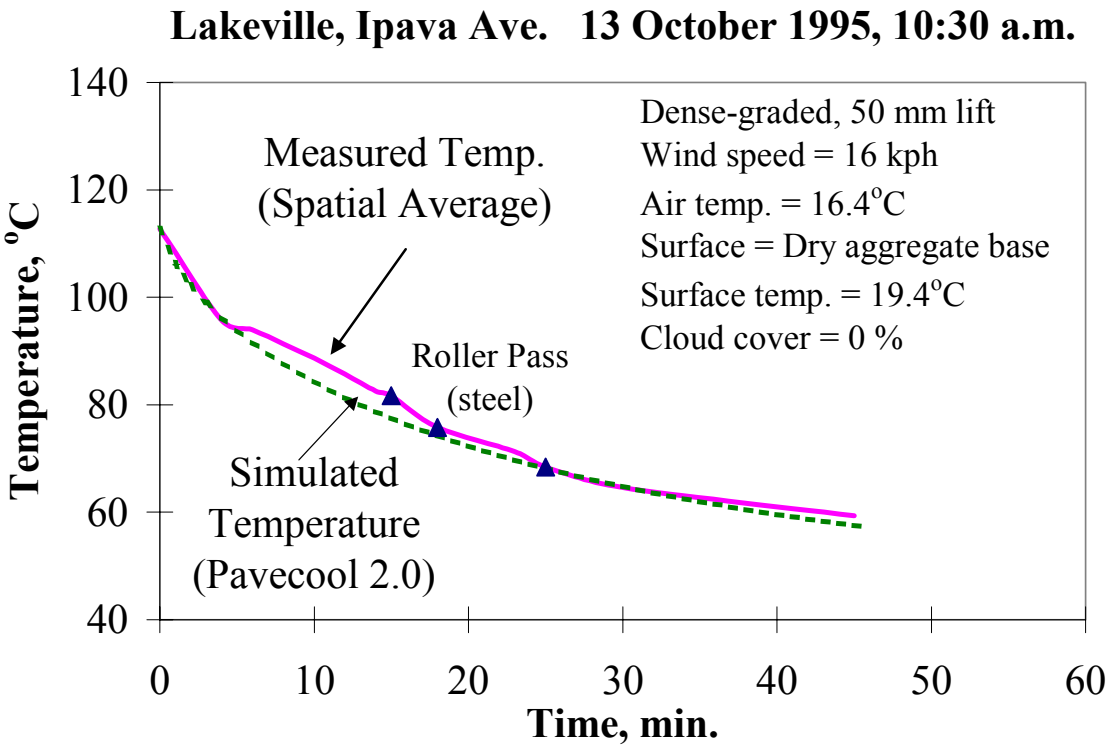

Figure F.1 Temperature Data for Ipava Avenue in Lakeville, MN

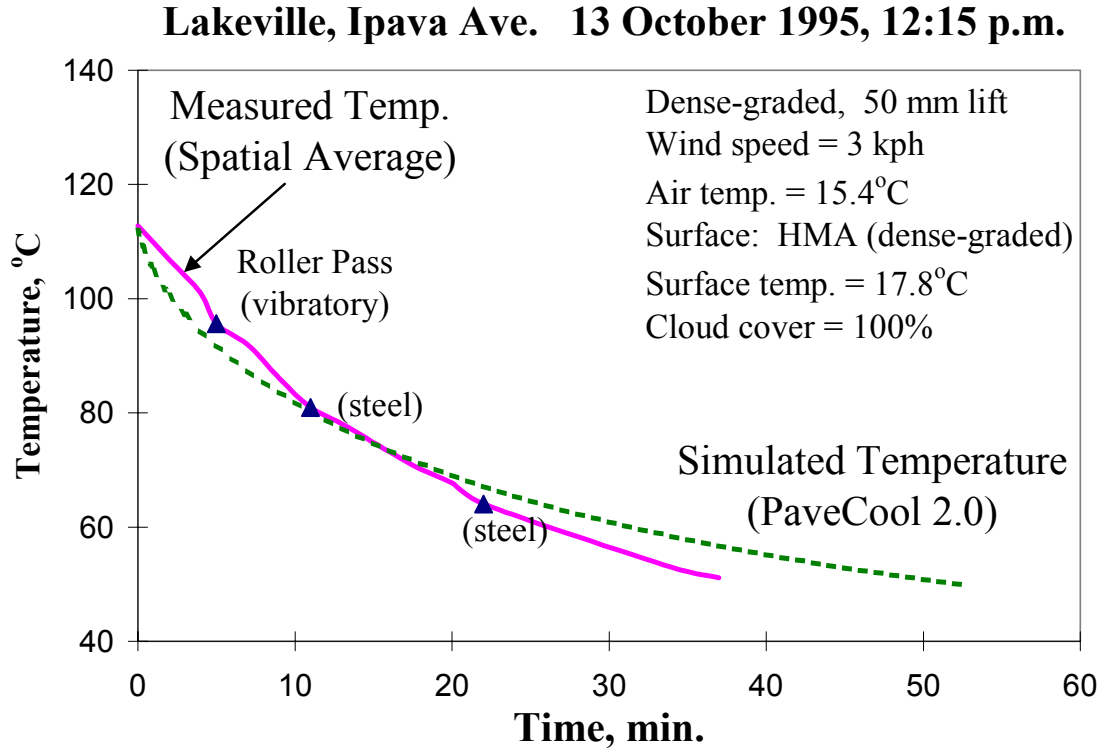

Figure F.2 Temperature Data for Ipava Avenue in Lakeville, MN

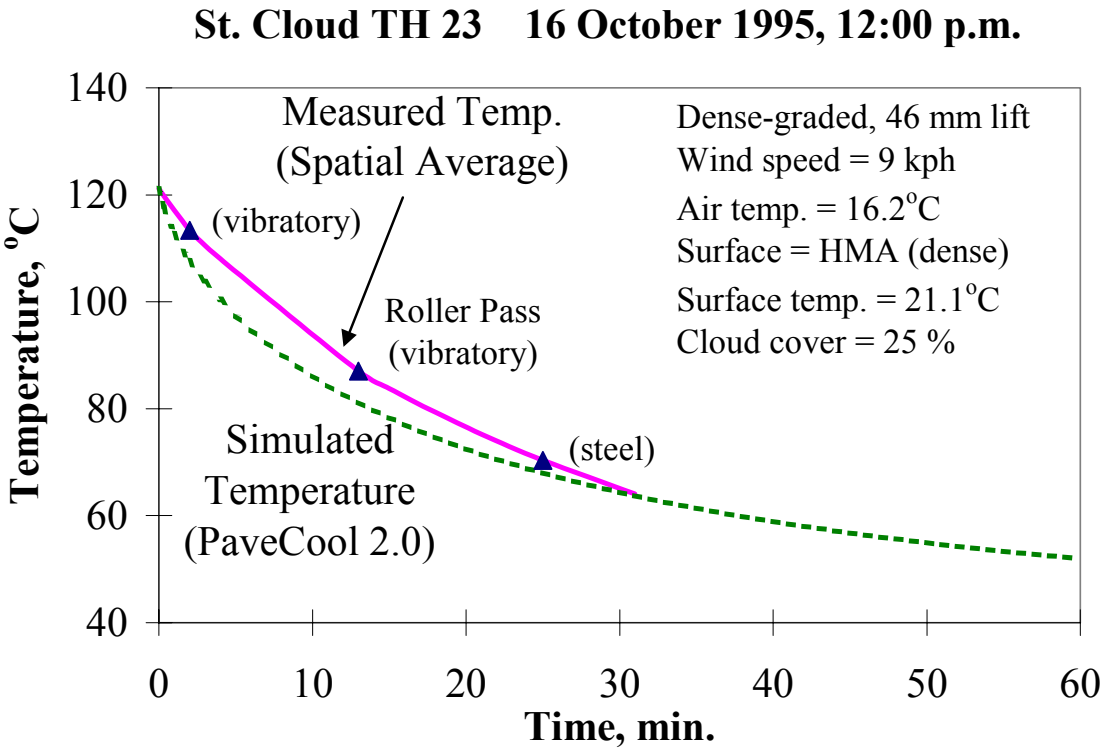

Figure F.3 Temperature Data for Highway 23, St. Cloud, MN

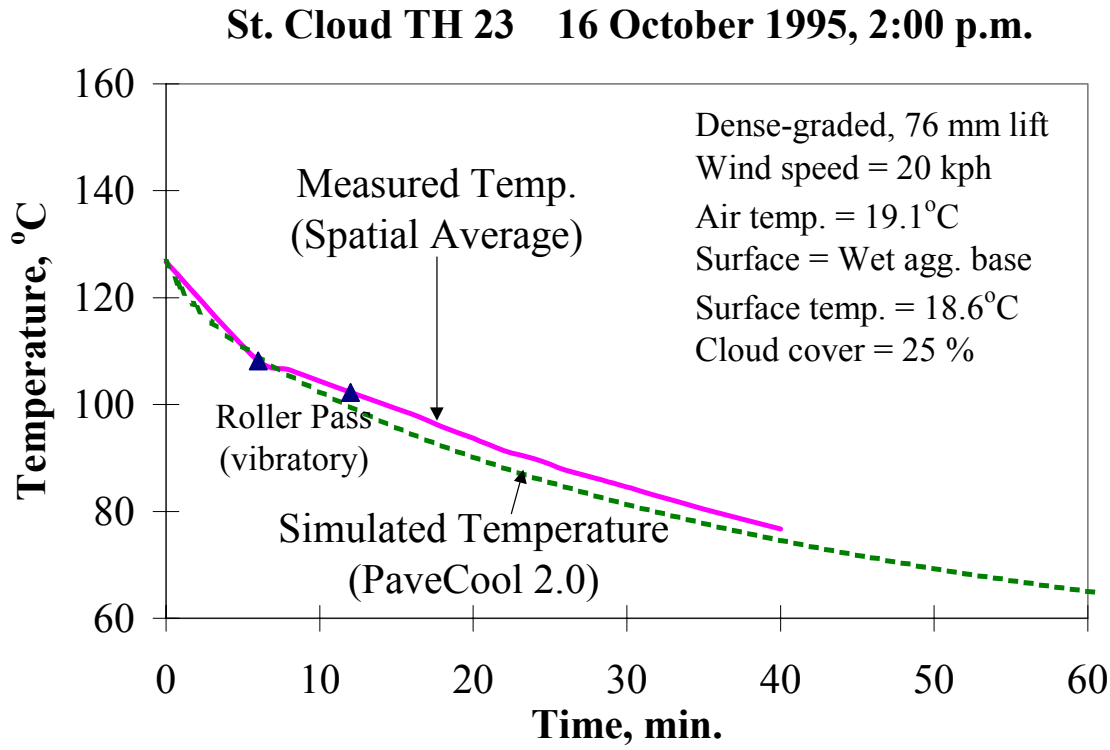

Figure F.4 Temperature Data for Highway 23, St. Cloud, MN

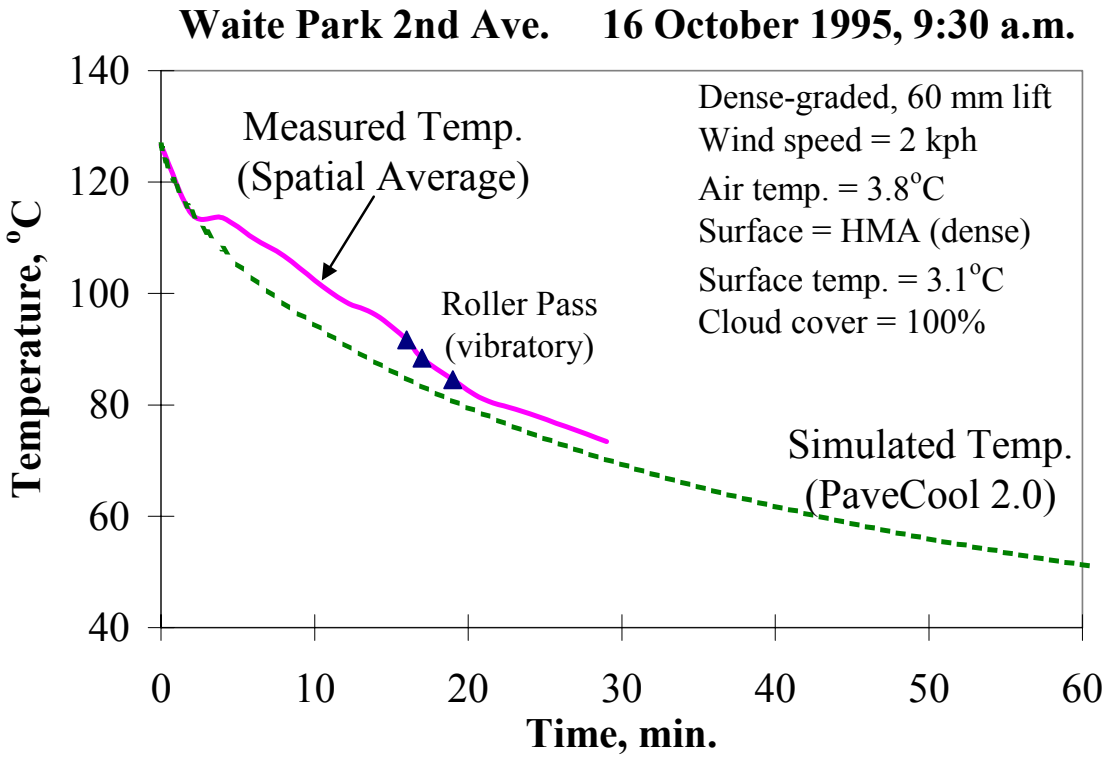

Figure F.5 Temperature Data for 2nd Avenue, Waite Park, MN

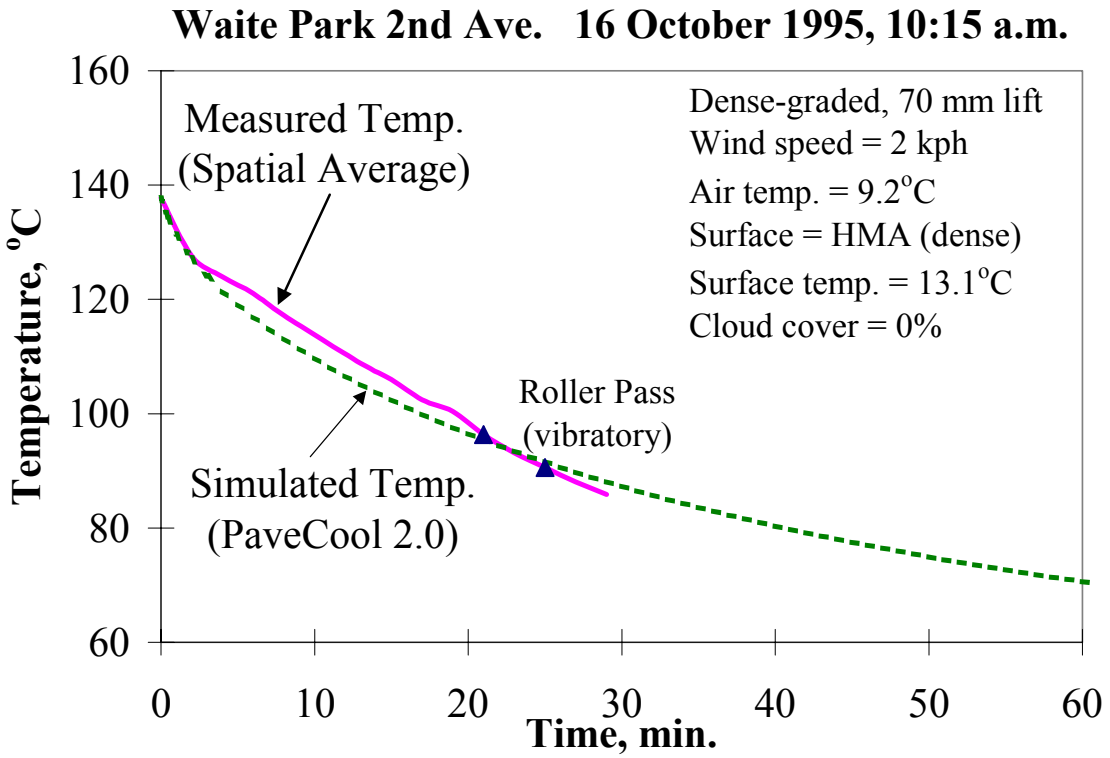

Figure F.6 Temperature Data for 2nd Avenue, Waite Park, MN

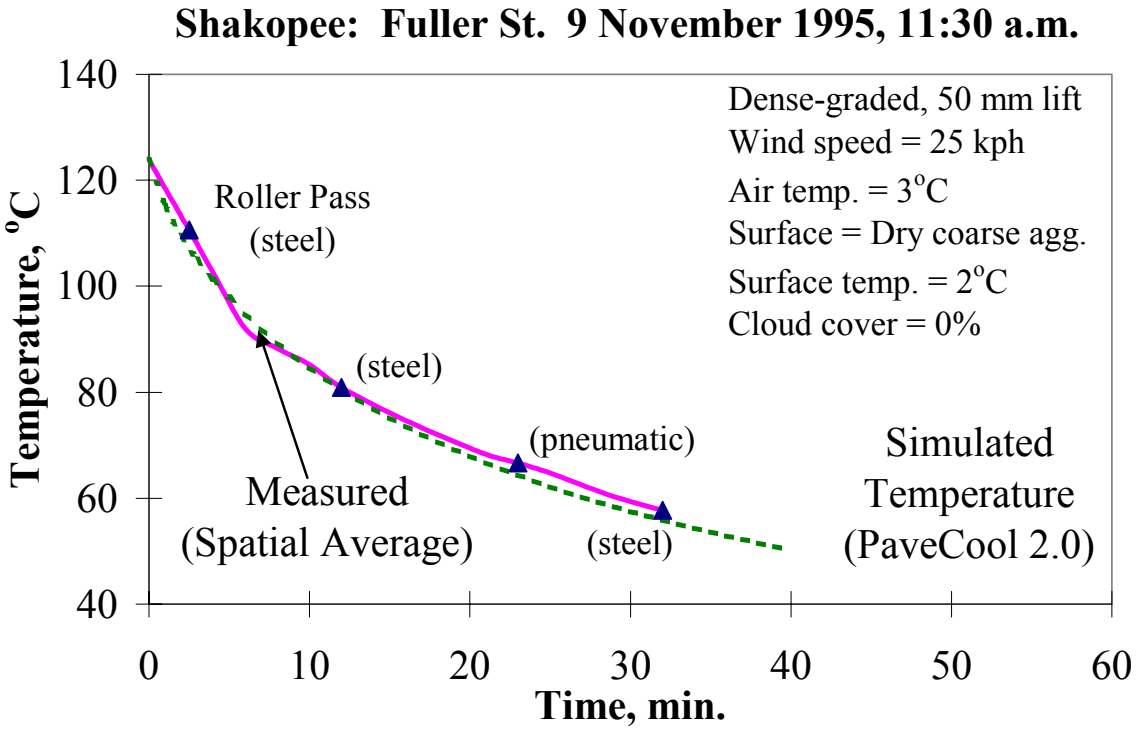

Figure F.7 Temperature Data for Fuller Street, Shakopee, MN

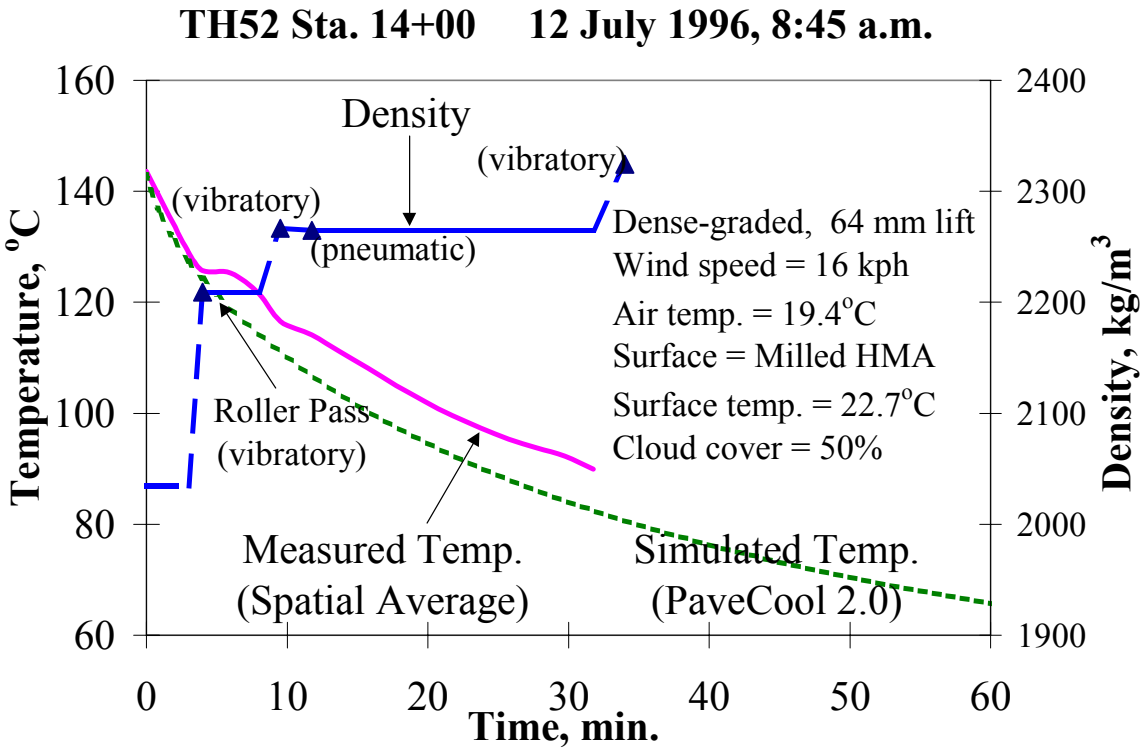

Figure F.8 Temperature and Density Data for Highway 52, Rosemount, MN

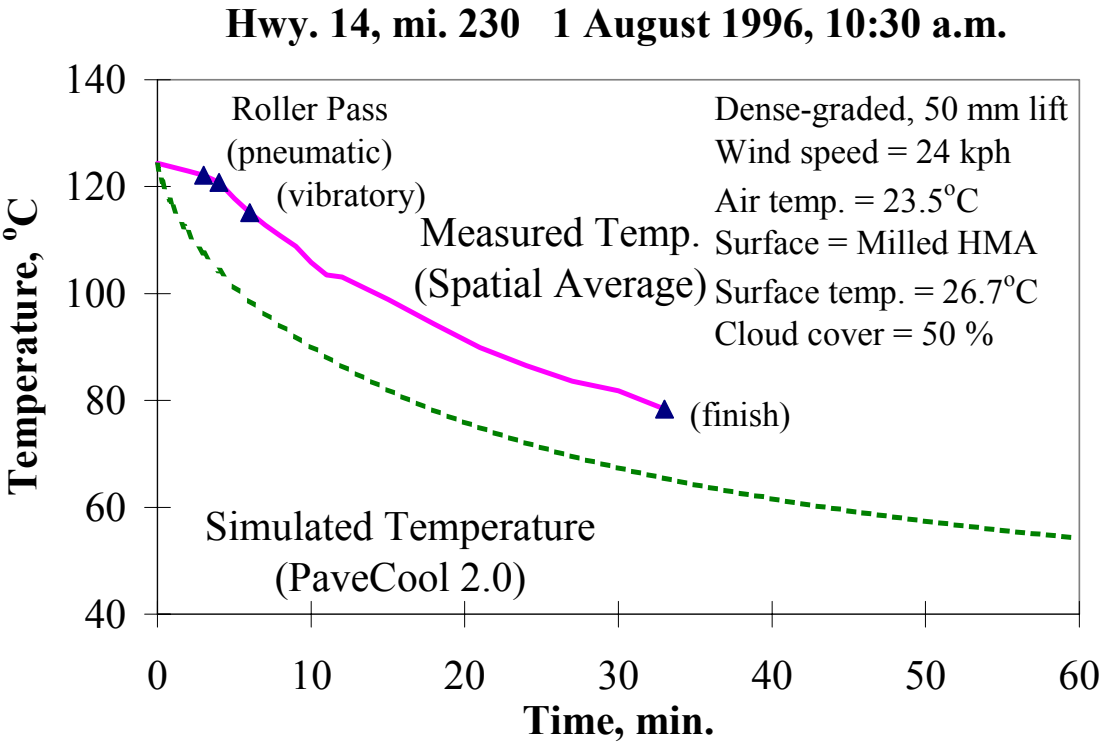

Figure F.9 Temperature Data for Highway 14, Rochester, MN

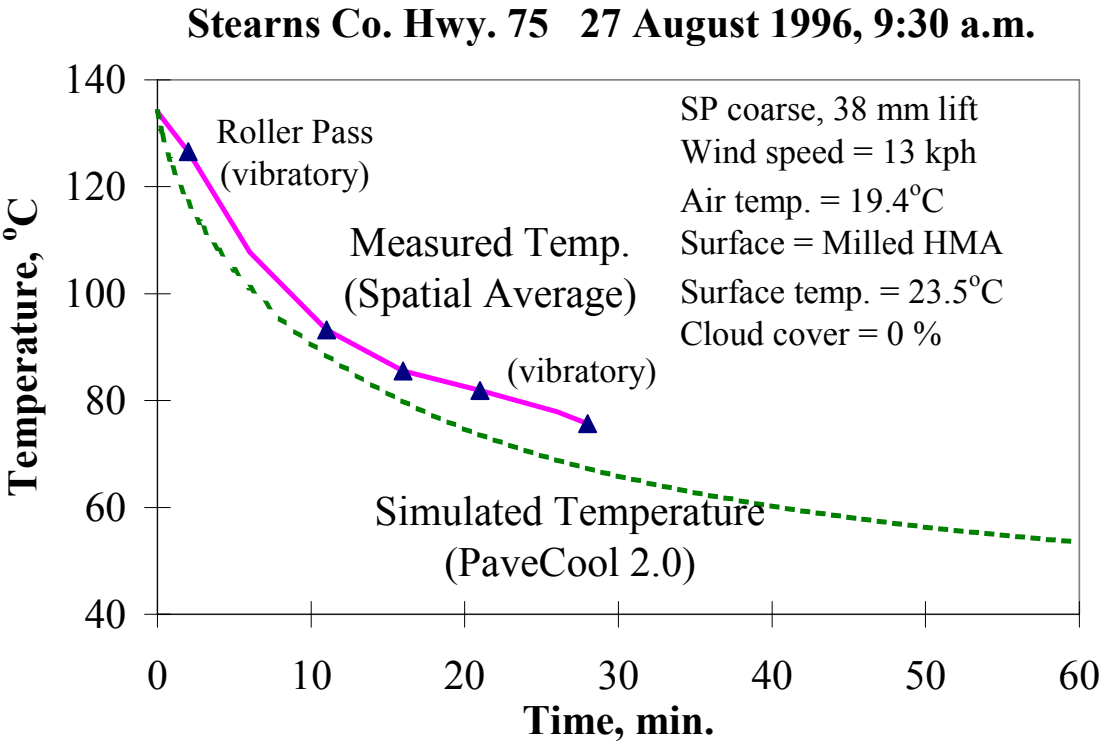

Figure F.10 Temperature Data for Highway 75, Stearns County, MN

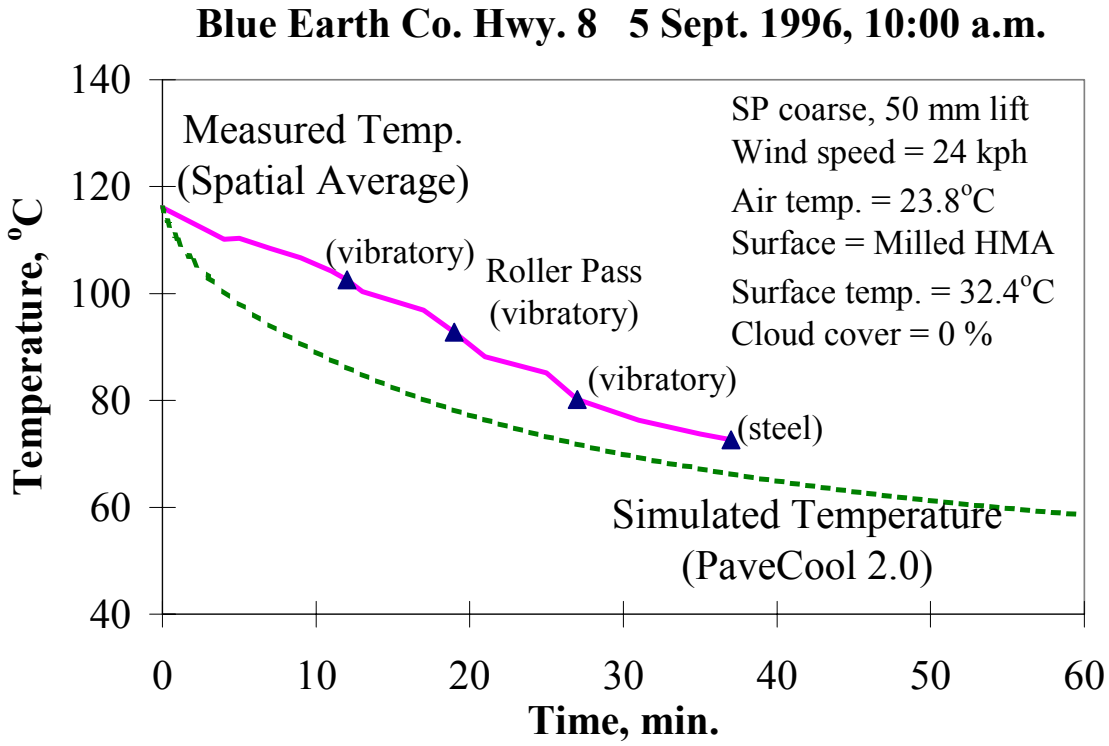

Figure F.11 Temperature Data for Highway 8, Blue Earth County, MN

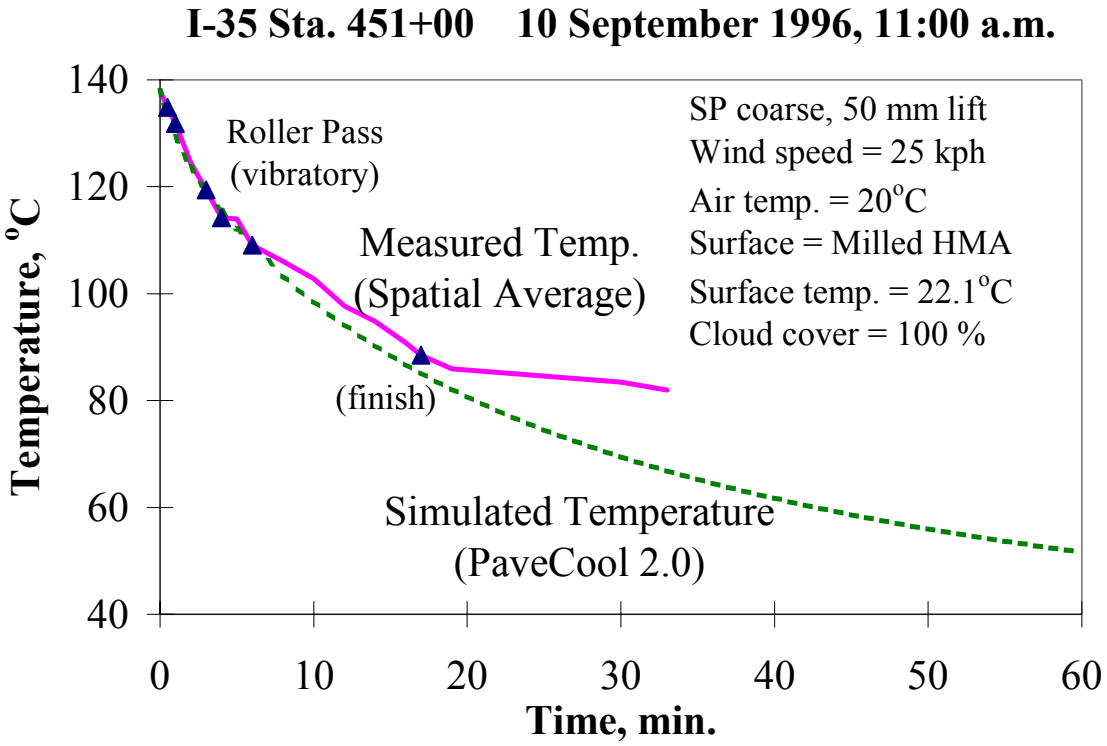

Figure F.12 Temperature Data for Minnesota Interstate 35

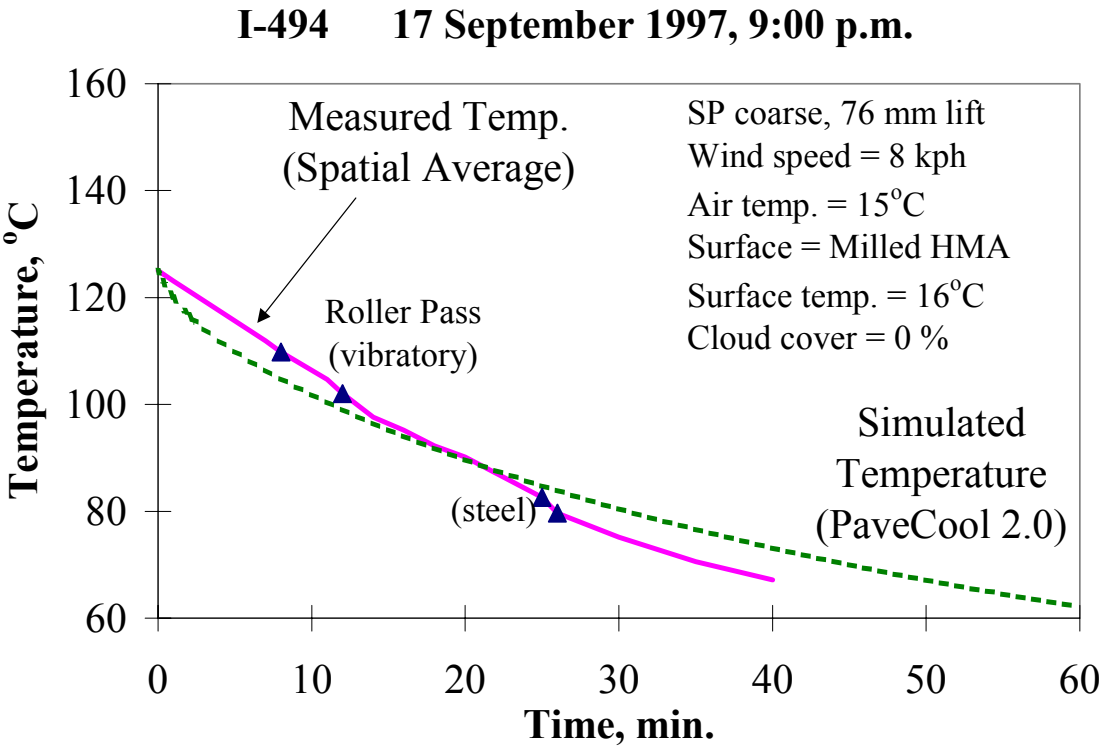

Figure F.13 Temperature Data for Minnesota Interstate 494

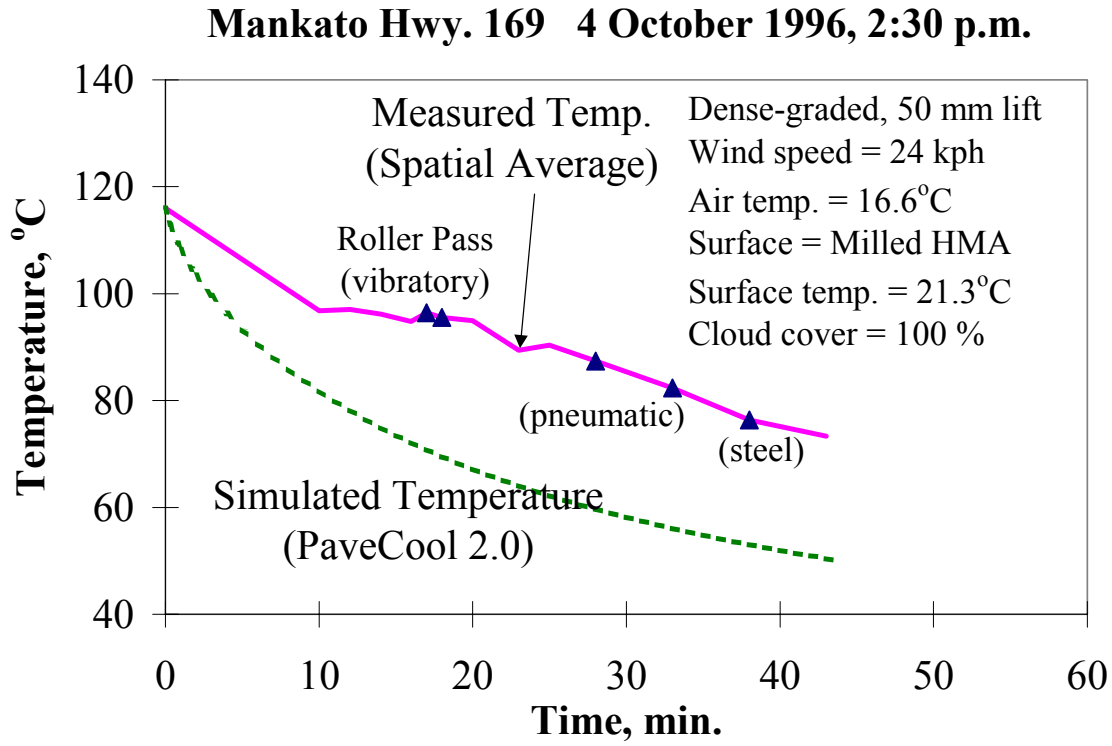

Figure F.14 Temperature Data for Highway 169, Mankato, MN

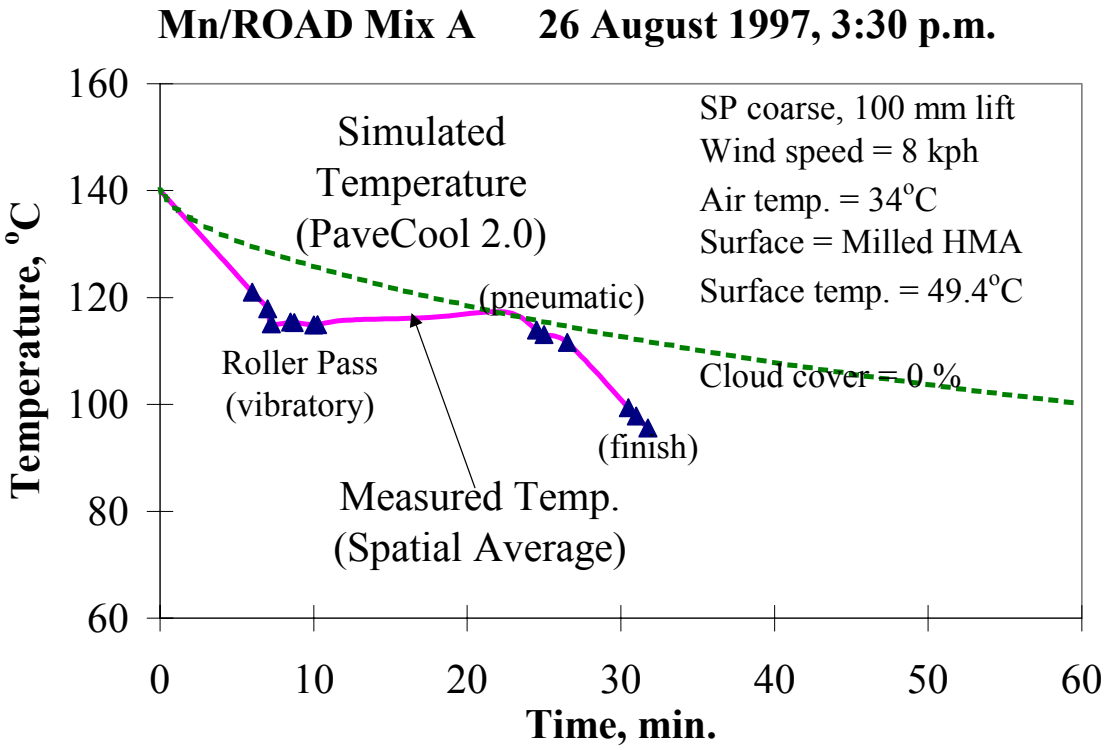

Figure F.15 Temperature Data for Mn/ROAD Transition, Mix A

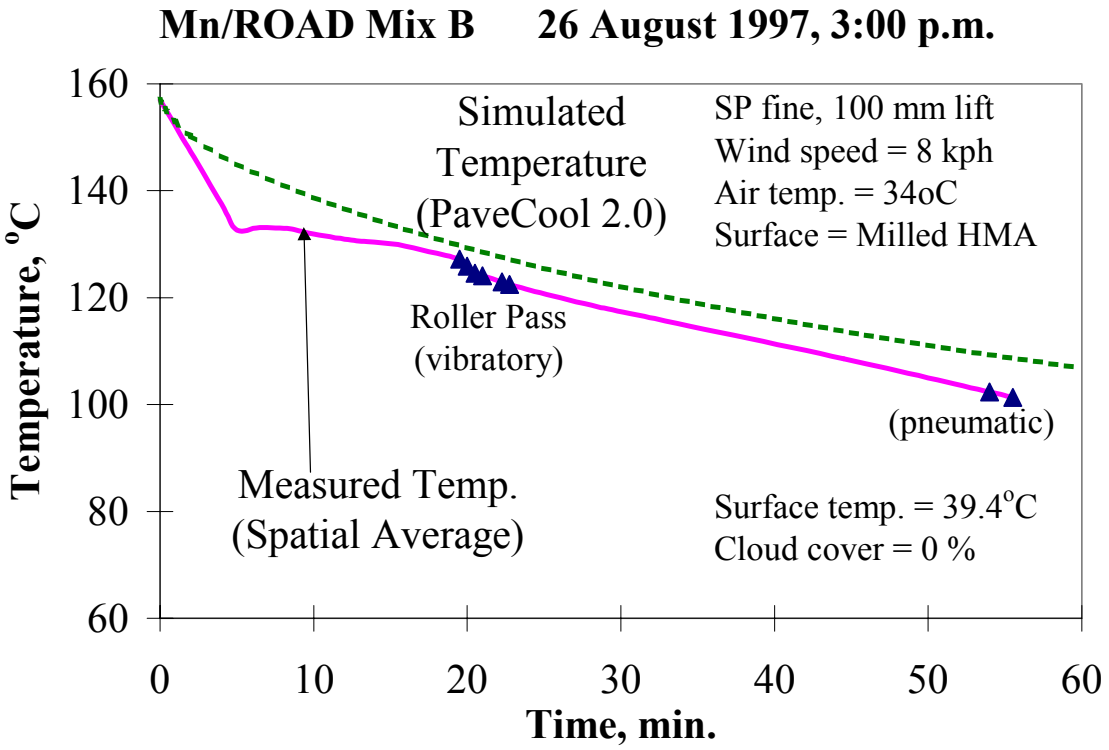

Figure F.16 Temperature Data for Mn/ROAD Transition, Mix B

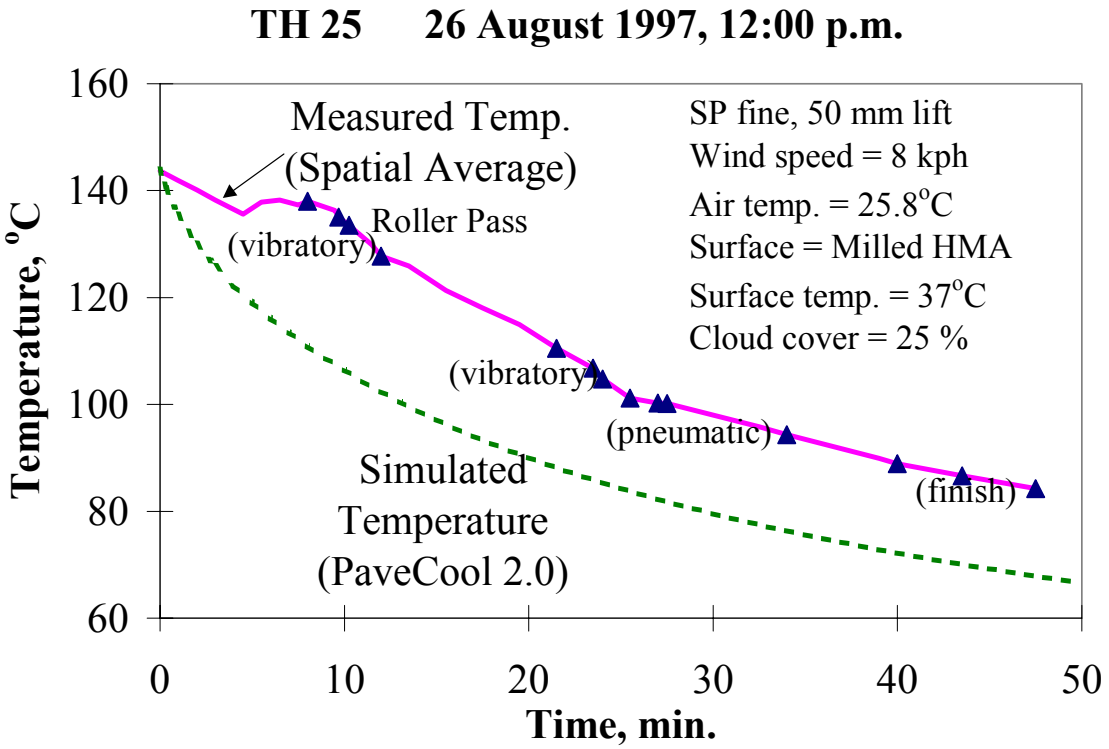

Figure F.17 Temperature Data for Highway 25 Mix B. St. Cloud, MN